# ON THE STRESS DISTRIBUTION IN CYLINDRICAL SHELLS WEAKENED BY A CIRCULAR HOLE

PROEFSCHRIFT
TER VERKRIJGING VAN DE GRAAD VAN DOCTOR IN DE TECHNISCHE WETENSCHAPPEN AAN DE TECHNISCHE HOGESCHOOL TE DELFT, OP GEZAG VAN DE RECTOR MAGNIFICUS IR. H. J. DE WIJS, HOOGLERAAR IN DE AFDELING DER MIJNBOUWKUNDE, TE VERDEDIGEN OP WOENSDAG 10 FEBRUARI 1965 DES NAMIDDAGS TE 4 UUR

DOOR

JOHANNES GERRIT LEKKERKERKER
werktuigkundig ingenieur

geboren te Veldhuizen



UITGEVERIJ WALTMAN - DELFT

DIT PROEFSCHRIFT IS GOEDGEKEURD DOOR DE PROMOTOR

PROF. DR. IR. W. T. KOITER

*Aan Nel*

*Aan Gonneke en Edith*

Mijn erkentelijkheid gaat uit naar de leiding van het laboratorium voor technische mechanica te Delft, die mij in de gelegenheid stelde het in dit proefschrift vermelde experimentele onderzoek te doen uitvoeren, en tevens naar alle medewerkers die aan dit onderzoek hebben deelgenomen.
De leiding van het laboratorium voor metaalkunde dank ik voor haar toestemming, gebruik te maken van de 200-tons trekbank.
Grote dank ben ik verschuldigd aan de directie van het instituut T.N.O. voor werktuigkundige constructies, die mij toestond de in dit proefschrift opgenomen numerieke berekeningen uit te voeren op haar „Elliott 803" rekentuig.
In dit verband dank ik ook de heer J. de Vries voor zijn vele adviezen bij het programmeren en bij de bediening van de apparatuur.

CONTENTS

# CHAPTER 1

# INTRODUCTION

## 1.1 Statement of problem

In a cylindrical shell or tube, weakened by a hole, the stress distribution, caused by some load applied to the shell, will differ considerably from that in an unweakened shell. For example, if a long tube is loaded in axial tension, we may expect that the maximum stress will be much larger if there is a circular hole in the shell than in the case that there is no cut-out. This conjecture is suggested immediately by the similar problem in the limiting case of a flat plate. The latter classical problem has been solved by Kirsch [ref. 4] [1]) and the result is that the maximum stress is 3 times the maximum stress in the solid plate. This factor 3 is known as the *stress concentration factor*.

There is no reason to expect that this factor is 3 in our case of a tube. In fact it should be expected that it depends on the geometry of the tube. This geometry may be described by two parameters. One is the ratio between the wall thickness and the radius of the middle-surface of the cylinder. The other one is the ratio between the diameter of the hole and the radius of the middle-surface. The most essential feature, however, is that *bending stresses* will also occur in the shell, although in the unweakened shell only membrane stresses are present.

At first sight it seems that we must distinguish several types of loading conditions, such as free hole boundary and loaded hole boundary, the load having some resultant force or moment. It can be shown that all types can be reduced to the one type of a *self-equilibrating loading* at the edge of the hole, the shell being unloaded outside the hole.

A first type of problems is met if the shell is loaded but the hole boundary is free. An example is the case, mentioned above, of the tube in axial tension. The method of solving problems of this type may be described as follows. First the stress distribution in the unweakened shell is determined. The stress system acting on the edge of the hole is then known, say $S_0$. We next solve the problem of the weakened shell loaded only by edge stresses $-S_0$, which constitute a self-equilibrating loading system. We finally add the stress distribution so obtained to the first one.

A second type is that where the hole boundary is loaded by a stress system,

[1]) See bibliography on pages 95.

say $S_1$. If this load has a resultant force or moment, we first determine the stress distribution in the unweakened shell loaded by some load statically equivalent to $S_1$ and applied in the region within the edge of the hole. The stress system on the edge belonging to this loading may be denoted by $S_2$. Of course, also $S_2$ is statically equivalent to $S_1$. We next solve the problem of the shell loaded on the edge of the hole by $S_1 - S_2$.

Both $-S_0$ and $S_1 - S_2$ have no resultant force or moment. So we only need to solve problems where the loading of the edge of the hole is self-equilibrating.

A quite different type of problems is met if we impose *geometric* boundary conditions, or boundary conditions *of mixed type*. The latter case occurs if a reinforcing ring or a transverse pipe is attached to the hole boundary. In general such problems can be solved in a straight-forward manner if appropriate *influence coefficients* for the displacements and the slope along the hole edge are available for suitably selected self-equilibrating unit load systems along this edge. Once these influence coefficients have been tabulated, it is merely a matter of solving a set of linear equations.

## 1.2 Survey of literature

The classical work on the subject is that by LUR'E [refs. 5 and 6]. He (like all investigators that will be mentioned here) based his analysis on the so-called theory of shallow shells, and he replaced the actual cylindrical shell by a hypothetical "spiral" shell where the azimuthal angle varies from $-\infty$ to $+\infty$. An error is introduced by the actual connection of the generators for which this angle is $-\pi$ and $+\pi$ respectively (the generators diametrically opposite to the hole centre).

In the theory of shallow shells all stresses and displacements can be written in terms of two functions, viz. the displacements normal to the shell surface and a stress function for the membrane stresses. LUR'E obtained the solution of the basic differential equations in terms of Bessel functions and exponentials (written as Krylov functions). In order to satisfy the boundary conditions and to determine the stresses in the shell, he expanded his solution in a formal power series in the only parameter involved, viz. $a^2/R\delta$ ($a$ being the radius of the hole, which is a circle in the developed shell surface, $R$ the radius of the middle-surface of the cylinder, and $\delta$ the wall thickness). The principal term in the series yields the solution for the flat plate. LUR'E retained the first additional term.

He dealt among others with the case of a long tube in axial tension. Apart from a formal error by which he overestimated the effect of his parameter by a factor 2, his results are correct. They are only valid, however, for small values of $a^2/R\delta$. Unfortunately this condition is not fulfilled in many cases encountered in practice.

SHEVLIAKOV and ZIGEL' dealt with the problem of the tube under torsion [ref. 14] and the case of prescribed normal displacements at the edge of the hole [ref. 15]. PIROGOV investigated the influence of a reinforcement of the hole boundary [ref. 11] and treated the problem of concentrated loads [ref. 12]. Both authors based their investigations on LUR'E's analysis and their results are therefore again valid only for small values of the parameter $a^2/R\delta$.

WITHUM [ref. 18] treated the problem of the tube under torsion in a different way. His method is not restricted to small values of the curvature parameter. Assuming a Fourier series expansion of the stresses and displacements he obtained a set of simultaneous ordinary differential equations, the independent variable being the polar coordinate $r$ in the developed shell surface. The unknown functions in these equations are the coefficients of $\sin 2\varphi$, $\sin 4\varphi$ etc. of the complex stress functions ($\varphi$ being the other polar coordinate in the developed shell surface). There appeared to be a coupling between adjacent coefficients. The strength of this coupling depends on the magnitude of the curvature parameter $a^2/R\delta$. In the case of a flat plate there is no coupling left. The author dealt with these equations by a perturbation method which, in a numerical example, appeared to converge rapidly.

During the completion of this thesis the author was informed that Mr. PETER VAN DYKE (Harvard University, Cambridge, Mass.) attacked the same problem in a different way. He apparently enforced dynamic boundary conditions along the hole circumference by a collocation method by means of which he obtained numerical results that are in agreement with ours. Furthermore he investigated the asymptotic behaviour if the magnitude of the curvature parameter $a^2/R\delta$ tends to infinity. It is hoped that the complete work, as yet unpublished, becomes soon available.

Essentially more complicated are the shell intersection problems, such as the determination of the stresses in the vicinity of a transverse pipe welded to a cylindrical shell. Such problems have been treated by REIDELBACH [ref. 13]. He solved similar differential equations as WITHUM but he neglected the coupling terms. In general this neglection must be considered as inadmissible. In most problems encountered in practice it will introduce large errors. It appeared to be very cumbersome to satisfy the boundary conditions. He gave a numerical example, concerning a shell geometry, however, that does not permit the neglections of shallow shell theory.

Also MYINT, RADOK and WOLFSON [ref. 8] have treated a shell intersection problem. They use a Ritz method. The three displacement components are written as linear combinations of suitably chosen functions, that satisfy the boundary conditions, and certain aspects of symmetry. The total potential energy is then minimized. It seems that in a general case of boundary conditions one has to choose rather complicated functions, which make the expression for the potential energy unwieldy. Therefore the authors make use of Lagrange multipliers for the purpose of enforcing the boundary conditions. This leads to a set of non-linear equations, which is solved by an iterative method. An example that is given bears on the case that the intersecting cylinder is undeformable. The boundary conditions are in consequence such that the edges of the hole in the main cylinder are fixed and clamped. Already in this relatively simple example the numerical work is cumbersome.

The world-wide interest in the type of problems under consideration might finally be underlined by drawing attention to the experimental work bearing on the subject. We mention only the experiments carried out by HOUGHTON and ROTHWELL [ref. 3] on tubes with circular and elliptic cut-outs both in tension and in torsion. The agreement between theory and experimental results reported in the literature is poor, and the validity of the analytical results has sometimes been questioned.

### 1.3 Summary of the present thesis

The scope of the present thesis is to evaluate an analysis of stresses and displacements in circular cylindrical shells, weakened by a circular hole. This analysis will be based on *shallow shell theory* and will *not* be restricted to small values of the curvature parameter $a^2/R\delta$. A restriction that originates from the shallow shell equations, however, is that $a/R$ must be comparatively small, e.g. smaller than $^1/_4$.

In none of the previous papers, mentioned in the foregoing section, an investigation has been undertaken of the theoretical aspects. Some aspects of the theory as a whole that will be investigated in the sequel are:

a. The completeness of the solution.
b. The possibility to deal with edge loads that have a resulting force or moment. Somewhat surprisingly it will appear that only one non-vanishing component of the moment vector can exist. In view of our previous observation that we may restrict our analysis to self-equilibrating loads along the hole boundary, the present limitation of our analysis is not too serious.
c. The uniqueness of the tangential displacements. This requirement leads to a simple condition that must be satisfied by the integration constants appearing in the solution.
d. The errors introduced by the approximative character of the solution. These errors arise from the replacement of the actual cylindrical shell by a spiral shell model and from the approximative character of the shallow shell equations.

Some numerical examples will be given, viz. the stress concentration around a circular hole both in a tube in tension and in torsion.

In order to be able to deal with boundary conditions that are geometric or of mixed type, a method will be developed to determine the tangential displacements. Then it is possible to calculate for distinct values of the parameter $a^2/R\delta$ the influence matrices of the hole boundary. With the aid of these influence matrices many types of boundary conditions can be dealt with. An example to be discussed is the case of a transverse pipe attached to the shell. The stresses due to internal pressure will be determined numerically.

The final chapter contains the results of careful experiments bearing on the cases of tension and torsion, which have been carried out in the laboratory of engineering mechanics of the Technological University, Delft. These results are compared with numerical results obtained from the present analysis. Agreement within test accuracy is found in general. We do not hesitate to conclude that the analytical results are now fully confirmed by experiments, at least in the range of our experimental investigation.

# CHAPTER 2

# THE BASIC EQUATIONS

## 2.1 The coordinate systems and the basic equations

We introduce geodetic coordinates in the shell surface, both Cartesian coordinates $\bar{x}, \bar{y}$ [1]), and polar coordinates $\bar{r}$, $\varphi$. The origin coincides with the centre of the circular hole of radius $a$. The $\bar{x}$-axis is parallel to the axis of the cylinder. The polar coordinates are such that the axis $\varphi = 0$ coincides with the positive $\bar{y}$-axis and $\varphi = \pi/2$ with the positive $\bar{x}$-axis (Fig. 2.1.1).

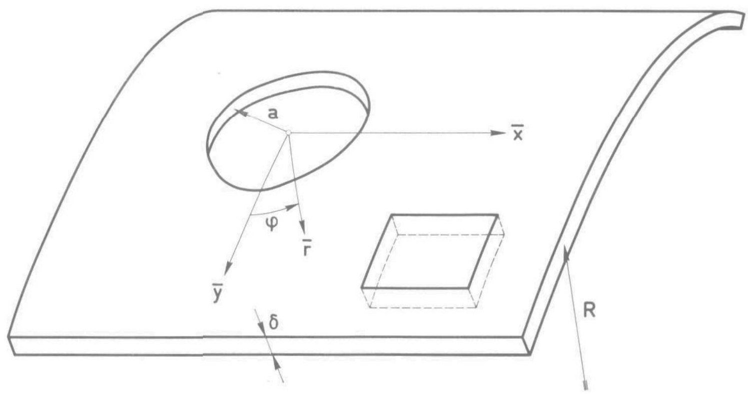


Fig. 2.1.1 The coordinates of the shell surface

Our analysis will be based on the assumption that the shell region is unbounded in the radial direction of our polar coordinates. This implies that our analysis is rigorous only for a hypothetical spiral cylindrical shell (Fig. 2.1.2). Its application to an actual cylindrical shell is permissible, if the effect of the connection between the generators $\vartheta = -\pi$ and $\vartheta = +\pi$ ($\vartheta$ is the circumferential angle) in the spiral shell is negligible in the vicinity of the hole. We shall return to the latter question in Chapter 6.

Our analysis will furthermore be of an approximate character through the underlying theory of shallow shells [2]). Accordingly all quantities concerning

[1]) Several quantities are barred or underlined in order to distinguish them from dimensionless quantities which will be introduced subsequently.

[2]) A general treatment of shallow shell theory is given among others by NOVOZHILOV [ref. 10, Chapter 1].

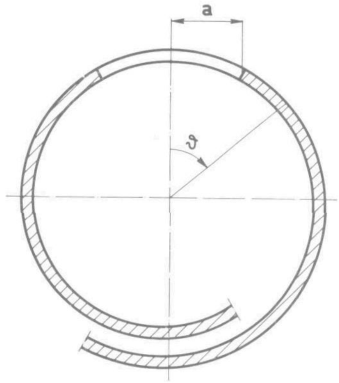


Fig. 2.1.2 Cross-section of the spiral shell $-\infty < \vartheta < \infty$

stresses and displacements may be expressed by the normal displacement $w$ and a stress function $\Phi$.

The stress resultants per unit length are indicated in Fig. 2.1.3 together with the displacement components $\bar{\xi}$ in $\bar{x}$-direction, $\bar{\eta}$ in $\bar{y}$-direction and $w$ in normal direction, *positive inward.* Fig. 2.1.4 shows the stress couples per unit length.

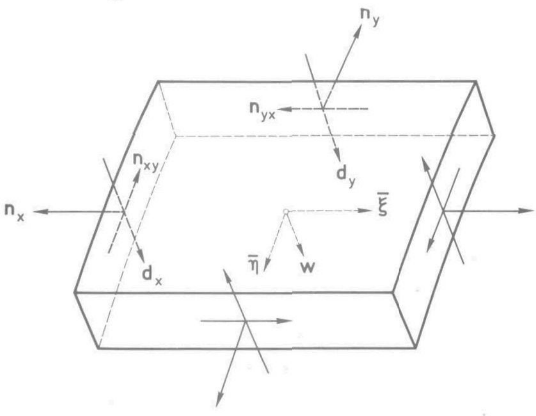


Fig. 2.1.3 Shell element with stress resultants per unit length and displacement components

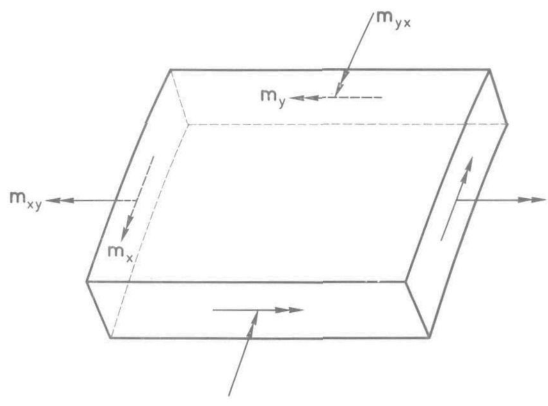


Fig. 2.1.4 Shell element and stress couples (right-handed screw rule)

We express the membrane forces by a stress function $\Phi$ as follows

$$\left.\begin{aligned} n_x &= \frac{\partial^2\Phi}{\partial\bar{y}^2} \\ n_y &= \frac{\partial^2\Phi}{\partial\bar{x}^2} \\ n_{xy} &= n_{yx} = -\frac{\partial^2\Phi}{\partial\bar{x}\,\partial\bar{y}} \end{aligned}\right\} \qquad (2.1.1)$$

It is evident that this procedure implies the equilibrium of a shell element, so far as the forces and moments acting in the shell surface are concerned, only approximately. In the complete equilibrium equation of the forces in $\bar{y}$-direction reading

$$\frac{\partial n_{xy}}{\partial \bar{x}} + \frac{\partial n_y}{\partial \bar{y}} + \frac{1}{R} d_y = 0 \quad \dots\dots\dots\dots\dots\dots \quad (2.1.2)$$

the last term containing the shear force $d_y$ has been neglected. Also in the equation that expresses the equilibrium of moments about the normal to the shell surface,

$$n_{yx} - n_{xy} + \frac{1}{R} m_{yx} = 0 \quad \dots\dots\dots\dots\dots\dots \quad (2.1.3)$$

again the last term of the left-hand side has been neglected.

If we assume that stresses arising from the membrane forces are at least comparable in magnitude with the stresses arising from the moments these neglections correspond to the neglection of $\delta/R$ with respect to 1.

According to Hooke's law the derivatives of the displacements $\bar{\xi}$ and $\bar{\eta}$ can be expressed as follows ($E$ is Young's modulus, $\nu$ is Poisson's ratio)

$$\left.\begin{aligned} \frac{\partial \bar{\xi}}{\partial \bar{x}} &= \frac{1}{E\delta}\left\{\frac{\partial^2 \Phi}{\partial \bar{y}^2} - \nu \frac{\partial^2 \Phi}{\partial \bar{x}^2}\right\} \\ \frac{\partial \bar{\eta}}{\partial \bar{y}} - \frac{w}{R} &= \frac{1}{E\delta}\left\{\frac{\partial^2 \Phi}{\partial \bar{x}^2} - \nu \frac{\partial^2 \Phi}{\partial \bar{y}^2}\right\} \\ \frac{\partial \bar{\xi}}{\partial \bar{y}} + \frac{\partial \bar{\eta}}{\partial \bar{x}} &= -\frac{2(1+\nu)}{E\delta} \frac{\partial^2 \Phi}{\partial \bar{x} \partial \bar{y}} \end{aligned}\right\} \quad \dots\dots\dots\dots \quad (2.1.4)$$

We eliminate $\bar{\xi}$ and $\bar{\eta}$ from these equations. This yields the *compatibility equation*

$$\Delta\Delta(\Phi) = -E\delta \frac{1}{R} \frac{\partial^2 w}{\partial \bar{x}^2} \quad \dots\dots\dots\dots\dots\dots \quad (2.1.5)$$

Here $\Delta$ denotes the Laplace operator $(\partial^2/\partial \bar{x}^2 + \partial^2/\partial \bar{y}^2)$.

A second differential equation for the unknown functions $\Phi$ and $w$ results from the equilibrium of a shell element in normal direction, and the equilibrium of the moments (Fig. 2.1.3). The latter requirements lead to

$$\left.\begin{aligned} d_x &= \frac{\partial m_x}{\partial \bar{x}} + \frac{\partial m_{yx}}{\partial \bar{y}} \\ d_y &= \frac{\partial m_{xy}}{\partial \bar{x}} + \frac{\partial m_y}{\partial \bar{y}} \end{aligned}\right\} \quad \dots\dots\dots\dots\dots\dots \quad (2.1.6)$$

The equilibrium equation of the forces in normal direction is

$$\frac{1}{R} n_y = \frac{\partial d_x}{\partial \bar{x}} + \frac{\partial d_y}{\partial \bar{y}} \quad \ldots \ldots \ldots \ldots \ldots \ldots \quad (2.1.7)$$

The expressions for the moments in terms of the displacements are [cf. FLÜGGE, ref. 2, p. 214].

$$\left.\begin{aligned} m_x &= \frac{E\delta^3}{12(1-\nu^2)} \left\{ \frac{\partial^2 w}{\partial \bar{x}^2} + \nu \frac{\partial^2 w}{\partial \bar{y}^2} + \underline{\frac{\nu}{R} \frac{\partial \bar{\eta}}{\partial \bar{y}} + \frac{1}{R} \frac{\partial \bar{\xi}}{\partial \bar{x}}} \right\} \\ m_{yx} &= \frac{E\delta^3}{12(1-\nu^2)} (1-\nu) \left\{ \frac{\partial^2 w}{\partial \bar{x} \partial \bar{y}} + \underline{\frac{1}{2R} \frac{\partial \bar{\eta}}{\partial \bar{x}} - \frac{1}{2R} \frac{\partial \bar{\xi}}{\partial \bar{y}}} \right\} \\ m_{xy} &= \frac{E\delta^3}{12(1-\nu^2)} (1-\nu) \left\{ \frac{\partial^2 w}{\partial \bar{x} \partial \bar{y}} + \underline{\frac{1}{R} \frac{\partial \bar{\eta}}{\partial \bar{x}}} \right\} \\ m_y &= \frac{E\delta^3}{12(1-\nu^2)} \left\{ \frac{\partial^2 w}{\partial \bar{y}^2} + \nu \frac{\partial^2 w}{\partial \bar{x}^2} + \underline{\frac{w}{R^2}} \right\} \end{aligned} \right\} \quad \ldots \quad (2.1.8)$$

Now the underlined terms will be neglected. If they would originate from in-plane strains the error introduced would be of the order $\delta/R$ with respect to 1 in the case that the membrane stresses and the bending stresses are comparable in magnitude. However, they contain unfortunately also terms that can be large when the membrane stresses are small, such as $(\nu/R)\partial\bar{\eta}/\partial\bar{y}$ (the actual strain $\varepsilon_y$ is equal to $\partial\bar{\eta}/\partial\bar{y} - w/R$) and the rotation in the plane of the shell surface. So it is not so easy to decide whether the approximation is good or not. A closer inspection reveals that it will be accurate when the functions involved are *rapidly changing functions* [1]. When the radius of the hole is comparatively small with respect to $R$ it can indeed be expected that the wave-length of the deformation pattern caused by the edge load will be small with respect to $R$.

After this neglection (2.1.6) becomes

$$\left.\begin{aligned} d_x &= \frac{E\delta^3}{12(1-\nu^2)} \frac{\partial}{\partial \bar{x}} (\Delta w) \\ d_y &= \frac{E\delta^3}{12(1-\nu^2)} \frac{\partial}{\partial \bar{y}} (\Delta w) \end{aligned} \right\} \quad \ldots \ldots \ldots \ldots \ldots \quad (2.1.9)$$

Inserting these expressions into the equilibrium equation (2.1.7) yields the second basic differential equation

$$\Delta\Delta(w) = \frac{12(1-\nu^2)}{E\delta^3} \frac{1}{R} \frac{\partial^2 \Phi}{\partial \bar{x}^2} \quad \ldots \ldots \ldots \ldots \ldots \quad (2.1.10)$$

[1] Cf. NOVOZHILOV loc. cit.

We established the equations of the so-called *theory of shallow shells* in the special case of cylindrical shells. We shall have to find solutions of these equations that satisfy given boundary conditions and give rise to single-valued displacements. The compatibility equation (2.1.5) does not imply the uniqueness of these displacements since we are dealing with a multiply-connected region. So this question must be investigated separately.

## 2.2 Dimensionless quantities

We shall now bring the basic formulae in a more convenient form by introducing the dimensionless coordinates

$$x = \bar{x}/a; \quad y = \bar{y}/a; \quad r = \bar{r}/a \qquad (2.2.1)$$

the dimensionless complex function

$$\Psi = \frac{12(1-\nu^2)}{E\delta^3}\Phi + i\frac{\sqrt{12(1-\nu^2)}}{\delta}w \qquad (2.2.2)$$

where $i$ is the imaginary unity, and the parameter $\mu$, given by

$$\mu = \frac{\sqrt[4]{12(1-\nu^2)}}{2}\frac{a}{\sqrt{\delta R}} \qquad (2.2.3)$$

Let $\Delta$ denote the Laplace operator in the dimensionless coördinates, so $\Delta = a^2\underline{\Delta}$. The set of simultaneous equations (2.1.5) and (2.1.10) is equivalent to one complex equation obtained by multiplying the former equation with $12(1-\nu^2)a^4/E\delta^3$ and the latter with $\sqrt{12(1-\nu^2)}ia^4/\delta$ and adding the two equations. The result is

$$\Delta\Delta\Psi - 4\mu^2 i\frac{\partial^2\Psi}{\partial x^2} = 0 \qquad (2.2.4)$$

The membrane forces, the moments and the shear forces, given by (2.1.1), (2.1.8) and (2.1.9) respectively, are in terms of the dimensionless quantities as follows.

The membrane forces are

$$\left.\begin{aligned} n_x &= \frac{E\delta^3}{12(1-\nu^2)a^2}\operatorname{Re}\frac{\partial^2\Psi}{\partial y^2} \\ n_y &= \frac{E\delta^3}{12(1-\nu^2)a^2}\operatorname{Re}\frac{\partial^2\Psi}{\partial x^2} \\ n_{xy} = n_{yx} &= -\frac{E\delta^3}{12(1-\nu^2)a^2}\operatorname{Re}\frac{\partial^2\Psi}{\partial x\partial y} \end{aligned}\right\} \qquad (2.2.5)$$

The moments are

$$\left.\begin{aligned}
m_x &= \frac{E\delta^4}{\{12(1-\nu^2)\}^{3/2}a^2}\,\mathrm{Im}\left\{\frac{\partial^2\Psi}{\partial x^2}+\nu\,\frac{\partial^2\Psi}{\partial y^2}\right\}\\
m_y &= \frac{E\delta^4}{\{12(1-\nu^2)\}^{3/2}a^2}\,\mathrm{Im}\left\{\frac{\partial^2\Psi}{\partial y^2}+\nu\,\frac{\partial^2\Psi}{\partial x^2}\right\}\\
m_{xy} = m_{yx} &= \frac{E\delta^4}{\{12(1-\nu^2)\}^{3/2}a^2}\,\mathrm{Im}\left\{(1-\nu)\,\frac{\partial^2\Psi}{\partial x\partial y}\right\}
\end{aligned}\right\} \quad \ldots\ldots \quad (2.2.6)$$

The shear forces are

$$\left.\begin{aligned}
d_x &= \frac{E\delta^4}{\{12(1-\nu^2)\}^{3/2}a^3}\,\mathrm{Im}\left\{\frac{\partial}{\partial x}\,(\Delta\Psi)\right\}\\
d_y &= \frac{E\delta^4}{\{12(1-\nu^2)\}^{3/2}a^3}\,\mathrm{Im}\left\{\frac{\partial}{\partial y}\,(\Delta\Psi)\right\}
\end{aligned}\right\} \quad \ldots\ldots\ldots \quad (2.2.7)$$

The normal displacement is

$$w = \frac{\delta}{\sqrt{12(1-\nu^2)}}\,\mathrm{Im}\,\Psi \quad \ldots\ldots\ldots\ldots\ldots \quad (2.2.8)$$

We finally introduce dimensionless displacements $\xi$ and $\eta$ by

$$\left.\begin{aligned}
\xi &= \frac{12(1-\nu^2)a}{\delta^2}\,\bar{\xi}\\
\eta &= \frac{12(1-\nu^2)a}{\delta^2}\,\bar{\eta}
\end{aligned}\right\} \quad \ldots\ldots\ldots\ldots\ldots \quad (2.2.9)$$

As a result the stress-strain relations (2.1.5) become

$$\left.\begin{aligned}
\frac{\partial\xi}{\partial x} &= \mathrm{Re}\left\{\frac{\partial^2\Psi}{\partial y^2}-\nu\,\frac{\partial^2\Psi}{\partial x^2}\right\}\\
\frac{\partial\eta}{\partial y} &= \mathrm{Re}\left\{\frac{\partial^2\Psi}{\partial x^2}-\nu\,\frac{\partial^2\Psi}{\partial y^2}\right\}+\mathrm{Im}\,(4\mu^2\Psi)\\
\frac{\partial\xi}{\partial y}+\frac{\partial\eta}{\partial x} &= -\,\mathrm{Re}\left\{2(1+\nu)\,\frac{\partial^2\Psi}{\partial x\partial y}\right\}
\end{aligned}\right\} \quad \ldots\ldots \quad (2.2.10)$$

It is interesting to note at this stage that $\mu$ is the only parameter appearing *explicitly* in the problem, although the geometry of the shell with the cut-out depends on two parameters. The distribution of bending stresses and membrane stresses depends only on $\mu$, while only the transverse shear stresses that are of the order of magnitude $d_x/\delta$ and $d_y/\delta$ contain an additional factor $\delta/a$.

# CHAPTER 3

# THE SOLUTION OF THE BASIC EQUATIONS

## 3.1 Solution in series of Bessel functions

The basic differential equation (2.2.4) is rewritten as

$$\left(\Delta + 2\mu\sqrt{i}\,\frac{\partial}{\partial x}\right)\left(\Delta - 2\mu\sqrt{i}\,\frac{\partial}{\partial x}\right)\Psi = 0 \qquad (3.1.1)$$

Each solution of either of the equations

$$\left(\Delta + 2\mu\sqrt{i}\,\frac{\partial}{\partial x}\right)\Psi = 0 \qquad (3.1.2)$$

and

$$\left(\Delta - 2\mu\sqrt{i}\,\frac{\partial}{\partial x}\right)\Psi = 0 \qquad (3.1.3)$$

is a solution of (3.1.1). It will be shown in Section 3.2 that these solutions together represent the complete solution of (3.1.1).

In order to solve (3.1.2) we substitute

$$\Psi = e^{\lambda x}\chi(x, y) \qquad (3.1.4)$$

and (3.1.2) becomes

$$\Delta\chi + 2(\lambda + \mu\sqrt{i})\,\frac{\partial\chi}{\partial x} + (\lambda^2 + 2\lambda\mu\sqrt{i})\chi = 0 \qquad (3.1.5)$$

Without loss in generality we can put

$$\lambda = -\mu\sqrt{i} \qquad (3.1.6)$$

which yields the wave equation

$$\Delta\chi - \mu^2 i\chi = 0 \qquad (3.1.7)$$

This equation can easily be solved, in polar coordinates, by Bernoulli's separation method. We assume that the solution can be written in the form

$$\chi = R(r)\Phi(\varphi) \qquad (3.1.8)$$

Then, by (3.1.7)

$$\Phi R'' + \Phi\,\frac{1}{r}\,R' + \Phi''\,\frac{1}{r^2}\,R - \mu^2 i\Phi R = 0 \qquad (3.1.9)$$

Or, separating the variables,

$$\frac{r^2R''}{R} + \frac{rR'}{R} - r^2\mu^2 i = -\frac{\Phi''}{\Phi} = \text{(say) } n^2 \quad \ldots\ldots\ldots \quad (3.1.10)$$

The ordinary differential equation for the function $R(r)$ can be recognized as Bessel's equation of order $n$. For our purpose it is convenient to write the solution in terms of Hankel functions, viz.

$$R = \tilde{A}_n H_n^{(2)}(\mu r\sqrt{-i}) + \tilde{A}_n{}^* H_n^{(1)}(\mu r\sqrt{-i}) \quad \ldots\ldots\ldots \quad (3.1.11)$$

We choose the root $\sqrt{-i} = e^{-i\pi/4}$. $\tilde{A}_n$ and $\tilde{A}_n{}^*$ are complex constants, and their value will depend on the boundary conditions. Since the function $\chi$ must be multiplied with the exponential $e^{\lambda x}$ where $\lambda$ is given by (3.1.6), the term containing $H_n^{(1)}(\mu r\sqrt{-i})$ must be omitted in view of its asymptotic behaviour. In fact we must require that $R$ decreases exponentially, when $r$ tends to infinity, as $e^{-\mu r/\sqrt{2}}$. And indeed the asymptotic expansion of the Hankel function of the second kind for $|z| \to \infty$ has a leading term [cf. for ex. ref. 7, Chapter 4.30]

$$H_n^{(2)}(z) = \sqrt{\frac{2}{\pi z}}\, e^{-iz+{}^1/_2 i\pi(n+{}^1/_2)} \quad \ldots\ldots\ldots \quad (3.1.12)$$

if $-{}^1/_2\pi \leqslant$ phase $z \leqslant {}^1/_2\pi$. This condition is fulfilled here. Hence it follows

$$H_n^{(2)}(\mu r\sqrt{-i}) = \sqrt{\frac{2}{\pi\mu r}}\, e^{i[(n/2+{}^3/_8)\pi - \mu r/\sqrt{2}]} e^{-\mu r/\sqrt{2}} \quad \ldots\ldots\ldots \quad (3.1.13)$$

The last factor ensures the boundedness of the solution. Furthermore (3.1.10) gives

$$\left.\begin{array}{l} \Phi = e^{\pm in\varphi} \text{ (if } n \neq 0) \\ \Phi = \text{const.} + \text{const. } \varphi \;\; (n = 0) \end{array}\right\} \quad \ldots\ldots\ldots \quad (3.1.14)$$

The imaginary part of the function $\Psi$, which is, apart from a constant factor, the normal displacement $w$ must be single-valued, so we can use only integral values of $n$, and for $n = 0$ the solution $\Phi =$ const. From (3.1.4), (3.1.6), (3.1.8), (3.1.11) and (3.1.14) we can now derive the solution of (3.1.2)

$$\Psi = e^{-\mu x\sqrt{i}} \sum_{n=-\infty}^{+\infty} \tilde{A}_n e^{in\varphi} H_n^{(2)}(\mu r\sqrt{-i}) \quad \ldots\ldots\ldots \quad (3.1.15)$$

In similar manner we find the solution of (3.1.3)

$$\Psi = e^{\mu x\sqrt{i}} \sum_{n=-\infty}^{+\infty} \tilde{B}_n e^{in\varphi} H_n^{(2)}(\mu r\sqrt{-i}) \quad \ldots\ldots\ldots \quad (3.1.16)$$

We can write our solution in another form if we make use of a well-known expansion in a Fourier series [ref. 17, Chapter 2.1]

$$e^{iz\sin\varphi} = \sum_{n=-\infty}^{+\infty} e^{in\varphi} J_n(z) \quad \ldots\ldots\ldots \quad (3.1.17)$$

daar $x = r\sin\varphi \to e^{-\mu x\sqrt{i}} = e^{-\sqrt{i}\mu r\sin\varphi}$

The sum of the solutions (3.1.15) and (3.1.16) may then be written as

$$\Psi = \sum_{k=-\infty}^{+\infty} e^{ik\varphi} J_k(-\mu r\sqrt{-i}) \sum_{n=-\infty}^{+\infty} \tilde{A}_n e^{in\varphi} H_n^{(2)}(\mu r\sqrt{-i}) +$$

$$+ \sum_{k=-\infty}^{+\infty} e^{ik\varphi} J_k(\mu r\sqrt{-i}) \sum_{n=-\infty}^{+\infty} \tilde{B}_n e^{in\varphi} H_n^{(2)}(\mu r\sqrt{-i}) \quad \ldots\ldots \quad (3.1.18)$$

Since $J_k(-z) = (-1)^k J_k(z)$ this can finally be transformed into

$$\Psi = \sum_{k=\text{even}} e^{ik\varphi} J_k(\mu r\sqrt{-i}) \sum_{n=-\infty}^{+\infty} (\tilde{A}_n + \tilde{B}_n) e^{in\varphi} H_n^{(2)}(\mu r\sqrt{-i}) +$$

$$+ \sum_{k=\text{odd}} e^{ik\varphi} J_k(\mu r\sqrt{-i}) \sum_{n=-\infty}^{+\infty} (-\tilde{A}_n + \tilde{B}_n) e^{in\varphi} H_n^{(2)}(\mu r\sqrt{-i}) \quad \ldots \quad (3.1.19)$$

It has to be kept in mind that $\sqrt{-i}$ means $e^{-i\pi/4}$.

### 3.2 Completeness of the solution

We denote the general solution of (3.1.2) by $\Phi$ and the general solution of (3.1.3) by $\Theta$. It is not an established fact as yet that $\Phi+\Theta$ is the general solution of (3.1.1). It will now be proved that this is the case.

It is clear that the general solution of (3.1.1) is given by $\Phi$ plus the *complete solution* of

$$\left(\Delta - 2\mu\sqrt{i}\,\frac{\partial}{\partial x}\right)\Psi = \Phi \quad \ldots\ldots \quad (3.2.1)$$

The statement is proved if we can show that a particular solution $\Phi_1$ of (3.2.1) exists that also satisfies (3.1.2). This system of two equations is equivalent to the system, obtained by adding respectively subtracting the two equations. Adding gives

$$\Delta\Phi_1 = {}^1/_2\Phi \quad \ldots\ldots \quad (3.2.2)$$

Subtracting gives

$$\frac{\partial\Phi_1}{\partial x} = -\frac{1}{4\mu\sqrt{i}}\,\Phi \quad \ldots\ldots \quad (3.2.3)$$

The solution $\Phi_1$ must satisfy these two equations.

First $\partial\Phi_1/\partial y$ is obtained as follows. We differentiate (3.2.3) with respect to $x$ and subtract it from (3.2.2), which gives

$$\frac{\partial^2\Phi_1}{\partial y^2} = \frac{1}{4\mu\sqrt{i}}\,\frac{\partial\Phi}{\partial x} + {}^1/_2\Phi \quad \ldots\ldots \quad (3.2.4)$$

and we differentiate (3.2.3) with respect to $y$, which gives

$$\frac{\partial^2\Phi_1}{\partial x\partial y} = -\frac{1}{4\mu\sqrt{i}}\,\frac{\partial\Phi}{\partial y} \quad \ldots\ldots \quad (3.2.5)$$

From these equations $\partial\Phi_1/\partial y$ can be determined by integrating, since the derivative of $\partial^2\Phi_1/\partial y^2$ with respect to $x$ is equal to the derivative of $\partial^2\Phi_1/\partial x\partial y$ with respect to $y$, in view of (3.1.2). Integrating from some point $A$ to a point $B$ gives

$$\left(\frac{\partial\Phi_1}{\partial y}\right)_B = \left(\frac{\partial\Phi_1}{\partial y}\right)_A +$$

$$+ \int_A^B \left\{ -\frac{1}{4\mu\sqrt{i}} \frac{\partial\Phi(x,y)}{\partial y} \mathrm{d}x + \left[ {}^1\!/_2\Phi(x,y) + \frac{1}{4\mu\sqrt{i}} \frac{\partial\Phi(x,y)}{\partial x} \right] \mathrm{d}y \right\} \quad (3.2.6)$$

Now also the derivative of $\partial\Phi_1/\partial x$ with respect to $y$ is equal to the derivative of $\partial\Phi_1/\partial y$ with respect to $x$, which can easily be verified. So we can indeed find a function $\Phi_1$ that satisfies both (3.2.2) and (3.2.3), and so it satisfies also both (3.1.2) and (3.1.3). This proves the statement that $\Psi = \Phi + \Theta$,

$$\Psi = e^{-\mu x\sqrt{i}} \sum_{n=-\infty}^{+\infty} \tilde{A}_n e^{in\varphi} H_n^{(2)}(\mu r\sqrt{-i}) +$$

$$+ e^{\mu x\sqrt{i}} \sum_{n=-\infty}^{+\infty} \tilde{B}_n e^{in\varphi} H_n^{(2)}(\mu r\sqrt{-i}) \quad \ldots\ldots\ldots\ldots \quad (3.2.7)$$

which can also be written in the form (3.1.19) is the complete solution of (3.1.1.), *when we restrict ourselves to single-valued functions* $\Psi$.

### 3.3 The resultant forces and moments of the edge load

In this section we shall determine the resulting force and the resulting moment of the edge load, belonging to any single-valued solution of (3.1.1). It will be shown that each of the three components of the resulting force (in $x$- and $y$-direction and in the direction normal to the shell surface respectively) is identically zero for each function $\Psi$ by which stress resultants and stress couples are determined according to (2.2.5), (2.2.6) and (2.2.7) if $\Psi$ is a solution of either (3.1.2) or (3.1.3) and is a single-valued function of the coordinates. This is also the case for the resulting moment, except for one component. Only the moment with respect to the $y$-axis can be different from zero.

In the introduction it has been shown that we only need to deal with loading systems along the edge of the hole, that are self-equilibrating. From the statement above it is evident that the present theory would in general have been uncapable of treating a load that is not self-equilibrating. The reason of this shortcoming of our analysis is not quite clear. It is not probable that it must be blamed to the fact that we based the analysis on shallow shell theory. In this connection we may, as a counter-example, mention the work of Yuan [ref. 19] who applied shallow shell equations in dealing with the problem of concentrated loads acting on cylindrical shells. It is more likely that the reason lies in the fact that we wrote the solution of the wave equation (3.1.7) in the form (3.1.8). This assumption lead to the following consequence. We had to require that the *imaginary* part of $\Psi$ is single-valued since it is proportional to the normal displacement component $w$, and this requirement implied also the uniqueness of the *real* part of $\Psi$ as a consequence of the assumption (3.1.8).

This uniqueness, however, is not required a priori. It is not excluded that also solutions of the basic differential equation exist with a multi-valued real part permitting the description of the stress distribution resulting from non self-equilibrating edge loads. In this thesis, however, no further investigation of this possibility has been undertaken.

In order to find the magnitude of the resulting forces and moments we determine the resultants of the stresses along an arbitrary contour surrounding the hole, in view of the fact that we satisfied the equilibrium equations (at least approximately) of each shell element. In Fig. 3.3.1 a shell element bounded by a part $\mathrm{d}s$ of such a contour and two line elements $\mathrm{d}x$ and $-\mathrm{d}y$ parallel to the $x$- and the $y$-axis respectively is given. We have already expressions for the stress resultants and the stress couples of the sides $\mathrm{d}x$ and $-\mathrm{d}y$. They are given by equations (2.2.5), (2.2.6) and (2.2.7). The stress resultants and the stress couples on the contour element $\mathrm{d}s$ can be expressed, if we make use of the equilibrium of the shell element of Fig. 3.3.1.

The equilibrium equations applied to this shell element yield

$$\left.\begin{aligned} p_x\,\mathrm{d}s &= n_{yx}\mathrm{d}x - n_x\,\mathrm{d}y \\ p_y\,\mathrm{d}s &= n_y\,\mathrm{d}x - n_{xy}\mathrm{d}y \\ D\,\mathrm{d}s &= d_y\,\mathrm{d}x - d_x\,\mathrm{d}y \\ M_x\,\mathrm{d}s &= m_y\,\mathrm{d}x - m_{xy}\mathrm{d}y \\ M_y\,\mathrm{d}s &= -m_{yx}\mathrm{d}x + m_x\,\mathrm{d}y \end{aligned}\right\} \quad \ldots\ldots\ldots\ldots \quad (3.3.1)$$

We are now in a position to determine the three resulting forces and the three resulting moments of the stresses on a closed contour, of which $\mathrm{d}s$ is a part, successively. It will appear that only the resulting moment about the $y$-axis is not identically zero.

*A. The resulting force in x-direction*

This force is given by the contour integral (note that $\mathrm{d}s$ is non-dimensional)

$$a\int_c p_x\,\mathrm{d}s = \frac{E\delta^3}{12(1-\nu^2)a}\,\mathrm{Re}\int_c\left\{-\frac{\partial^2\Psi}{\partial x\partial y}\,\mathrm{d}x - \frac{\partial^2\Psi}{\partial y^2}\,\mathrm{d}y\right\} =$$

$$= -\frac{E\delta^3}{12(1-\nu^2)a}\,\mathrm{Re}\int_c \mathrm{d}\left(\frac{\partial\Psi}{\partial y}\right) = 0 \quad \ldots\ldots\ldots \quad (3.3.2)$$

Since $\Psi$ is single-valued the exact differential $\mathrm{d}(\partial\Psi/\partial y)$ yields a value zero of the contour integral.

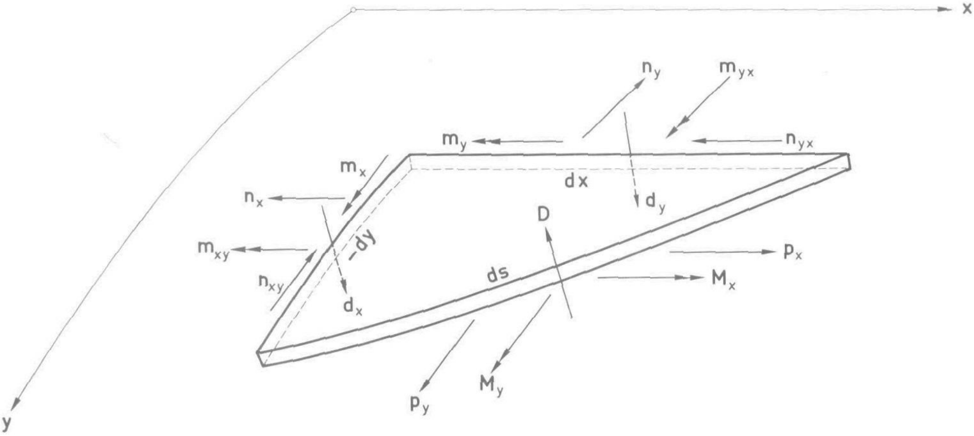


Fig. 3.3.1 Shell element bounded by a part d$s$ of an integration contour

*B. The resulting force in y-direction*

This force is

$$a \int_c p_y \,\mathrm{d}s = \frac{E\delta^3}{12(1-\nu^2)a} \operatorname{Re} \int_c \left\{ \frac{\partial^2 \Psi}{\partial x^2} \mathrm{d}x + \frac{\partial^2 \Psi}{\partial x \partial y} \mathrm{d}y \right\} =$$

$$= \frac{E\delta^3}{12(1-\nu^2)a} \operatorname{Re} \int_c \mathrm{d}\left(\frac{\partial \Psi}{\partial x}\right) = 0 \quad . \; . \; . \; . \; . \; . \; . \; . \; . \quad (3.3.3)$$

Here the contribution of the component of the shear force $D$ has been omitted since in the establishment of the equilibrium equations the corresponding term has been neglected (cf. (2.1.2)).

*C. The resulting normal force*

The total force in the direction normal to the shell surface is (neglecting terms that contain higher powers of $a/R$)

$$a \int_c \left\{ p_y \frac{ay}{R} - D \right\} \mathrm{d}s = \frac{E\delta^3}{12(1-\nu^2)R} \operatorname{Re} \int_c \left\{ \frac{\partial^2 \Psi}{\partial x^2} \mathrm{d}x + \frac{\partial^2 \Psi}{\partial x \partial y} \mathrm{d}y \right\} y +$$

$$+ \frac{E\delta^4}{\{12(1-\nu^2)\}^{3/2} a^2} \operatorname{Im} \int_c \left\{ \frac{\partial}{\partial x} (\Delta \Psi) \mathrm{d}y - \frac{\partial}{\partial y} (\Delta \Psi) \mathrm{d}x \right\} \quad . \; . \; . \; . \quad (3.3.4)$$

The first integral can be transformed by integration by parts into:

$$- \int_c \frac{\partial \Psi}{\partial x} \mathrm{d}y$$

The second integral is transformed using (3.1.2) or (3.1.3), $\Psi$ being a solution of either the former or the latter equation. So

$$\Delta\Psi = \mp\, 2\mu\sqrt{i}\,\frac{\partial\Psi}{\partial x} \quad \text{(3.3.5)}$$

The upper sign has to be used if $\Psi$ is a solution of (3.1.2), the lower sign if $\Psi$ is a solution of (3.1.3). It now follows

$$\int_c \left\{\frac{\partial}{\partial x}(\Delta\Psi)\,\mathrm{d}y - \frac{\partial}{\partial y}(\Delta\Psi)\,\mathrm{d}x\right\} =$$

$$= \int_c \left\{\mp\, 2\mu\sqrt{i}\,\frac{\partial^2\Psi}{\partial x^2}\,\mathrm{d}y \pm 2\mu\sqrt{i}\,\frac{\partial^2\Psi}{\partial x\partial y}\,\mathrm{d}x\right\} =$$

$$= \int_c \left\{4\mu^2 i\,\frac{\partial\Psi}{\partial x}\,\mathrm{d}y \pm 2\mu\sqrt{i}\,\mathrm{d}\left(\frac{\partial\Psi}{\partial y}\right)\right\} \quad \text{(3.3.6)}$$

The second term, being an exact differential, does not contribute to the value of the contour integral. So (3.3.4) becomes

$$-\frac{E\delta^3}{12(1-\nu^2)R}\,\mathrm{Re}\int_c \frac{\partial\Psi}{\partial x}\,\mathrm{d}y + \frac{E\delta^4}{\{12(1-\nu^2)\}^{3/2}a^2}\,\mathrm{Im}\int_c 4\mu^2 i\,\frac{\partial\Psi}{\partial x}\,\mathrm{d}y \quad \text{(3.3.7)}$$

And this is zero, taking into account the value of $\mu$, given by (2.2.3).

*D. The moment about the normal to the shell*

The moment of the stress resultants on the given contour with respect to the normal to the shell surface in the origin is

$$a\int_c \{p_y ax - p_x ay\}\,\mathrm{d}s = \frac{E\delta^3}{12(1-\nu^2)}\,\mathrm{Re}\int_c \left\{x\,\mathrm{d}\left(\frac{\partial\Psi}{\partial x}\right) + y\,\mathrm{d}\left(\frac{\partial\Psi}{\partial y}\right)\right\} \quad \text{(3.3.8)}$$

where the expressions of $p_x$ and $p_y$ have been treated as in (3.3.2) and (3.3.3) respectively. The contour integral in the right-hand side can be integrated by parts as follows,

$$\int_c \left\{x\,\mathrm{d}\left(\frac{\partial\Psi}{\partial x}\right) + y\,\mathrm{d}\left(\frac{\partial\Psi}{\partial y}\right)\right\} = -\int_c \left\{\frac{\partial\Psi}{\partial x}\,\mathrm{d}x + \frac{\partial\Psi}{\partial y}\,\mathrm{d}y\right\} = -\int_c \mathrm{d}\Psi = 0 \quad \text{(3.3.9)}$$

*E. The moment about the x-axis*

The total moment with respect to the $x$-axis is

$$a\int_c \left\{M_x\,\mathrm{d}s - ayD\,\mathrm{d}s + \frac{a^2y^2}{2R}\,p_y\,\mathrm{d}s\right\} =$$

$$= \frac{E\delta^4}{\{12(1-\nu^2)\}^{3/2} a} \left[\mathrm{Im} \int\limits_c \left\{-\frac{\partial^2 \Psi}{\partial x \partial y} \mathrm{d}y + \frac{\partial^2 \Psi}{\partial y^2} \mathrm{d}x - y \frac{\partial}{\partial y} (\Delta \Psi) \mathrm{d}x + y \frac{\partial}{\partial x} (\Delta \Psi) \mathrm{d}y \right\}\right] +$$

$$+ \frac{E\delta^3 a}{12(1-\nu^2) R} \left[\mathrm{Re} \int\limits_c {}^1/_2 y^2 \, \mathrm{d}\left(\frac{\partial \Psi}{\partial x}\right)\right] \quad \ldots \ldots \ldots \ldots \quad (3.3.10)$$

The first integral is written as follows

$$\int\limits_c \left\{-\frac{\partial^2 \Psi}{\partial x \partial y} \mathrm{d}y - \frac{\partial^2 \Psi}{\partial x^2} \mathrm{d}x + \Delta \Psi \, \mathrm{d}x - y \frac{\partial}{\partial y} (\Delta \Psi) \mathrm{d}x + y \frac{\partial}{\partial x} (\Delta \Psi) \mathrm{d}y \right\} =$$

$$= \int\limits_c \left\{-\mathrm{d}\left(\frac{\partial \Psi}{\partial x}\right) \mp 2\mu \sqrt{i} \frac{\partial \Psi}{\partial x} \mathrm{d}x \pm 2\mu \sqrt{i} y \frac{\partial^2 \Psi}{\partial x \partial y} \mathrm{d}x \mp 2\mu \sqrt{i} y \frac{\partial^2 \Psi}{\partial x^2} \mathrm{d}y \right\} =$$

$$= \int\limits_c \left\{\mp 2\mu \sqrt{i} \frac{\partial \Psi}{\partial x} \mathrm{d}x \pm 2\mu \sqrt{i} y \, \mathrm{d}\left(\frac{\partial \Psi}{\partial y}\right) \mp 2\mu \sqrt{i} y \, \Delta \Psi \, \mathrm{d}y \right\} =$$

$$= \int\limits_c \left\{\mp 2\mu \sqrt{i} \, \mathrm{d}\Psi + 4\mu^2 i y \frac{\partial \Psi}{\partial x} \mathrm{d}y \right\} =$$

$$= 4\mu^2 i \int\limits_c \frac{\partial \Psi}{\partial x} \mathrm{d}({}^1/_2 y^2) \quad \ldots \ldots \ldots \ldots \quad (3.3.11)$$

Here several times use has been made both of the circumstance that an exact differential of the single-valued function $\Psi$ or its derivatives does not contribute to a contour integration, and of the equation (3.3.5). Integrating finally the second integral of (3.3.10) by parts and taking into account the value of $\mu$ given by (2.2.3) it follows immediately that the moment about the $x$-axis is identically zero.

### *F. The moment about the y-axis*

The total moment with respect to the $y$-axis is

$$a \int\limits_c \left\{M_y \, \mathrm{d}s + axD \, \mathrm{d}s + \frac{a^2 y^2}{2R} p_x \, \mathrm{d}s - \frac{a^2 xy}{R} p_y \, \mathrm{d}s \right\} =$$

$$= \frac{E\delta^4}{\{12(1-\nu^2)\}^{3/2} a} \left[\mathrm{Im} \int\limits_c \left\{-\frac{\partial^2 \Psi}{\partial x \partial y} \mathrm{d}x + \frac{\partial^2 \Psi}{\partial x^2} \mathrm{d}y + x \frac{\partial}{\partial y} (\Delta \Psi) \mathrm{d}x - x \frac{\partial}{\partial x} (\Delta \Psi) \mathrm{d}y \right\} +\right.$$

$$\left. + 4\mu^2 \, \mathrm{Re} \int\limits_c \left\{-{}^1/_2 y^2 \frac{\partial^2 \Psi}{\partial y^2} \mathrm{d}y - {}^1/_2 y^2 \frac{\partial^2 \Psi}{\partial x \partial y} \mathrm{d}x - xy \frac{\partial^2 \Psi}{\partial x^2} \mathrm{d}x - xy \frac{\partial^2 \Psi}{\partial x \partial y} \mathrm{d}y \right\}\right] \quad (3.3.12)$$

Here we substituted already (2.2.3) in the coefficient of the second integral.

Now the first integral can be written as

$$\int\limits_c \left\{-\mathrm{d}\left(\frac{\partial \Psi}{\partial y}\right) \mp 2\mu\sqrt{i}\,\frac{\partial \Psi}{\partial x}\,\mathrm{d}y \mp 2\mu\sqrt{i}\,x\,\frac{\partial^2 \Psi}{\partial x \partial y}\,\mathrm{d}x \pm 2\mu\sqrt{i}\,x\,\frac{\partial^2 \Psi}{\partial x^2}\,\mathrm{d}y\right\} =$$

$$= \int\limits_c \left\{\mp 2\mu\sqrt{i}\,\frac{\partial \Psi}{\partial x}\,\mathrm{d}y \mp 2\mu\sqrt{i}\,x\,\mathrm{d}\left(\frac{\partial \Psi}{\partial y}\right) - 4\mu^2 i x\,\frac{\partial \Psi}{\partial x}\,\mathrm{d}y\right\} =$$

$$= \int\limits_c \left\{\mp 2\mu\sqrt{i}\,\frac{\partial \Psi}{\partial x}\,\mathrm{d}y \pm 2\mu\sqrt{i}\,\frac{\partial \Psi}{\partial y}\,\mathrm{d}x - \underline{4\mu^2 i x\,\frac{\partial \Psi}{\partial x}\,\mathrm{d}y}\right\} \quad . \; . \; . \quad (3.3.13)$$

The second integral can be written as

$$\int\limits_c \left\{-{}^1\!/_2\, y^2\,\mathrm{d}\left(\frac{\partial \Psi}{\partial y}\right) - xy\,\mathrm{d}\left(\frac{\partial \Psi}{\partial x}\right)\right\} =$$

$$= \int\limits_c \left\{y\,\frac{\partial \Psi}{\partial y}\,\mathrm{d}y + y\,\frac{\partial \Psi}{\partial x}\,\mathrm{d}x + x\,\frac{\partial \Psi}{\partial x}\,\mathrm{d}y\right\} =$$

$$= \int\limits_c \left\{-\Psi\,\mathrm{d}y + \underline{x\,\frac{\partial \Psi}{\partial x}\,\mathrm{d}y}\right\} \quad . \; . \; . \; . \; . \; . \; . \; . \; . \; . \; . \; . \; . \; . \; . \quad (3.3.14)$$

where we carried out integration by parts several times. Substituting the results (3.3.13) and (3.3.14) in the expression of the moment (3.3.12) the underlined terms cancel. The total moment about the $y$-axis appears not to be identically zero. We find

$$\frac{E\delta^4}{\{12(1-\nu^2)\}^{3/2} a}\,\mathrm{Im}\left[2\mu\sqrt{i}\int\limits_c \left\{\mp \frac{\partial \Psi}{\partial x}\,\mathrm{d}y \pm \frac{\partial \Psi}{\partial y}\,\mathrm{d}x - 2\mu\sqrt{i}\,\Psi\,\mathrm{d}y\right\}\right] \quad (3.3.15)$$

This seems to be an unwieldy expression. We shall meet the expression in brackets again in the next section in discussing the uniqueness of the tangential displacements. We shall postpone a further treatment of this expression until then.

## 3.4 Uniqueness of the displacements

The equations (2.2.10) that express the strains of the shell surface do not necessarily give rise to single-valued tangential displacements, although the compatibility conditions have been satisfied. The restriction to single-valued functions $\Psi$ (in order that the *normal* displacements are single-valued) is insufficient. The reason is that we are dealing with a multiply connected region.

We shall now try to determine the displacement components $\xi$ and $\eta$ from the three equations (2.2.10). It will appear that only $\eta$ gives rise to difficulties and is single-valued only if the function $\Psi$ satisfies a certain condition, that will be established in the sequel. In order to determine $\xi$, we first eliminate $\eta$ from the equations (2.2.10). We subtract the derivative with respect to $x$ of the second equation from the derivative with respect to $y$ of the third equation. The result is

$$\frac{\partial^2 \xi}{\partial y^2} = -2(1+\nu)\,\mathrm{Re}\,\frac{\partial^3 \Psi}{\partial x \partial y^2} - \mathrm{Re}\left\{\frac{\partial^3 \Psi}{\partial x^3} - \nu\,\frac{\partial^3 \Psi}{\partial x \partial y^2}\right\} - 4\mu^2\,\mathrm{Im}\,\frac{\partial \Psi}{\partial x} \tag{3.4.1}$$

After some computation, using (3.3.5), we find

$$\frac{\partial^2 \xi}{\partial y^2} = \mathrm{Re}\left\{\mp\, 2\mu\sqrt{i}\,\frac{\partial^2 \Psi}{\partial y^2} - (1+\nu)\,\frac{\partial^3 \Psi}{\partial x \partial y^2}\right\} \quad . \; . \; . \; . \; . \; . \; . \; . \; . \tag{3.4.2}$$

Here again the upper sign must be used if $\Psi$ is a solution of (3.1.2), the lower sign if $\Psi$ is a solution of (3.1.3). From the first equation (2.2.10) follows

$$\frac{\partial \xi}{\partial x} = \mathrm{Re}\left\{\mp\, 2\mu\sqrt{i}\,\frac{\partial \Psi}{\partial x} - (1+\nu)\,\frac{\partial^2 \Psi}{\partial x^2}\right\} \quad . \; . \; . \; . \; . \; . \; . \; . \; . \; . \tag{3.4.3}$$

and, differentiating with respect to $y$,

$$\frac{\partial^2 \xi}{\partial x \partial y} = \mathrm{Re}\left\{\mp\, 2\mu\sqrt{i}\,\frac{\partial^2 \Psi}{\partial x \partial y} - (1+\nu)\,\frac{\partial^3 \Psi}{\partial x^2 \partial y}\right\} \quad . \; . \; . \; . \; . \; . \; . \; . \tag{3.4.4}$$

We are now in a position to determine $\xi$ by integrating. From (3.4.2) and (3.4.4) we find

$$\frac{\partial \xi}{\partial y} = \mathrm{Re}\left\{\mp\, 2\mu\sqrt{i}\,\frac{\partial \Psi}{\partial y} - (1+\nu)\,\frac{\partial^2 \Psi}{\partial x \partial y}\right\} + C_1 \quad . \; . \; . \; . \; . \; . \; . \tag{3.4.5}$$

And from (3.4.3) and (3.4.5)

$$\xi = \mathrm{Re}\left\{\mp\, 2\mu\sqrt{i}\,\Psi - (1+\nu)\,\frac{\partial \Psi}{\partial x}\right\} + C_1 y + C_2 \quad . \; . \; . \; . \; . \tag{3.4.6}$$

So we find that if $\Psi$ is single-valued, also the displacement component in $x$-direction is single-valued.

From the last equation (2.2.10) together with (3.4.5) we find

$$\frac{\partial \eta}{\partial x} = \mathrm{Re}\left\{\pm\, 2\mu\sqrt{i}\,\frac{\partial \Psi}{\partial y} - (1+\nu)\,\frac{\partial^2 \Psi}{\partial x \partial y}\right\} - C_1 \quad . \; . \; . \; . \; . \; . \; . \tag{3.4.7}$$

and from the second equation (2.2.10)

$$\frac{\partial \eta}{\partial y} = \mathrm{Re}\left\{\mp\, 2\mu\sqrt{i}\,\frac{\partial \Psi}{\partial x} - (1+\nu)\,\frac{\partial^2 \Psi}{\partial y^2} - 4\mu^2 i \Psi\right\} \quad . \; . \; . \; . \; . \tag{3.4.8}$$

The condition $\partial^2\eta/\partial x \partial y = \partial^2\eta/\partial y \partial x$ is fulfilled, but in order that the displacement $\eta$ is single-valued it is necessary that

$$\int_c \left\{\frac{\partial \eta}{\partial x}\,\mathrm{d}x + \frac{\partial \eta}{\partial y}\,\mathrm{d}y\right\} = 0 \quad \ldots \ldots \ldots \ldots \ldots \ldots \ldots \quad (3.4.9)$$

where the integration is carried out along any closed contour around the hole. This yields the condition

$$\mathrm{Re}\left[2\mu\sqrt{i}\int_c \left\{\mp \frac{\partial \Psi}{\partial x}\,\mathrm{d}y \pm \frac{\partial \Psi}{\partial y}\,\mathrm{d}x - 2\mu\sqrt{i}\,\Psi\,\mathrm{d}y\right\}\right] = 0 \quad \ldots \quad (3.4.10)$$

And it is clear that, although $\Psi$ is single-valued, the condition (3.4.10) is not always satisfied. We can use only those solutions $\Psi$ that obey this condition.

The expression, whose real part must be zero in order that $\eta$ is single-valued, is the same as the expression occurring in (3.3.15), where we found that the imaginary part is proportional to the moment of the edge load about the $y$-axis.

We shall now substitute the solution $\Psi$ of the basic differential equation in (3.4.10). This will lead us to a relation between the integration constants that must be satisfied in order that the displacements are single-valued.

As we have seen, the general solution consists of the sum of (3.1.15) and (3.1.16). We restrict ourselves first to (3.1.15) and corresponding to that to the upper signs in (3.4.10). The derivative of $\Psi$ with respect to $x$ can be determined, keeping in mind, that the derivative of a function $f$ with respect to $x$, when $f$ is given as a function of $r$ and $\varphi$, must be written

$$\frac{\partial f}{\partial x} = \frac{\partial f}{\partial r}\frac{\partial r}{\partial x} + \frac{\partial f}{\partial \varphi}\frac{\partial \varphi}{\partial x} = \frac{\partial f}{\partial r}\sin\varphi + \frac{\partial f}{\partial \varphi}\frac{\cos\varphi}{r} \quad \ldots \ldots \ldots \quad (3.4.11)$$

We then find

$$\frac{\partial \Psi}{\partial x} = \sum_{n=-\infty}^{+\infty}\left\{\left(-\mu\sqrt{i} + \frac{in\cos\varphi}{r}\right)H_n^{(2)}(\mu r\sqrt{-i}) + \right.$$
$$\left. + \mu\sqrt{-i}\sin\varphi\,\dot{H}_n^{(2)}(\mu r\sqrt{-i})\right\}\tilde{A}_n e^{-\mu x\sqrt{i}} e^{in\varphi} \quad \ldots \ldots \quad (3.4.12)$$

Here $\dot{H}_n^{(2)}(\mu r\sqrt{-i})$ is the derivative of the Hankel function with respect to its argument $\mu r\sqrt{-i}$. Using (3.1.17) we can also write

$$\frac{\partial \Psi}{\partial x} = \sum_{n=-\infty}^{+\infty}\left\{\left(-\mu\sqrt{i} + \frac{in\cos\varphi}{r}\right)H_n^{(2)}(\mu r\sqrt{-i}) + \right.$$
$$\left. + \mu\sqrt{-i}\sin\varphi\,\dot{H}_n^{(2)}(\mu r\sqrt{-i})\right\}\tilde{A}_n \sum_{k=-\infty}^{+\infty} e^{i(k+n)\varphi}(-1)^k J_k(\mu r\sqrt{-i}) \quad (3.4.13)$$

With

$$\frac{\partial f}{\partial y} = \frac{\partial f}{\partial r}\cos\varphi - \frac{\partial f}{\partial \varphi}\frac{\sin\varphi}{r} \quad \ldots \ldots \ldots \ldots \ldots \ldots \quad (3.4.14)$$

we find in a similar manner

$$\frac{\partial \Psi}{\partial y} = \sum_{n=-\infty}^{+\infty} \left\{ - \frac{in \sin \varphi}{r} H_n{}^{(2)}(\mu r \sqrt{-i}) + \right.$$

$$\left. + \mu \sqrt{-i} \cos \varphi \, \dot{H}_n{}^{(2)}(\mu r \sqrt{-i}) \right\} \tilde{A}_n \sum_{k=-\infty}^{+\infty} e^{i(k+n)\varphi} (-1)^k \mathcal{J}_k(\mu r \sqrt{-i}) \quad (3.4.15)$$

And finally $\Psi$ is written, using (3.1.17), as

$$\Psi = \sum_{n=-\infty}^{+\infty} H_n{}^{(2)}(\mu r \sqrt{-i}) \tilde{A}_n \sum_{k=-\infty}^{+\infty} e^{i(k+n)\varphi} (-1)^k \mathcal{J}_k(\mu r \sqrt{-i}) \quad . \quad . \quad (3.4.16)$$

We carry out the integration in (3.4.10) along a circle of radius $r$, $\varphi$ varying from 0 to $2\pi$. An increase $\mathrm{d}\varphi$ corresponds to an increase $\mathrm{d}x$ respectively $\mathrm{d}y$ as follows

$$\left. \begin{aligned} \mathrm{d}x &= r \cos \varphi \, \mathrm{d}\varphi \\ \mathrm{d}y &= -r \sin \varphi \, \mathrm{d}\varphi \end{aligned} \right\} \quad . \quad . \quad . \quad . \quad . \quad . \quad . \quad . \quad . \quad . \quad . \quad . \quad . \quad . \quad . \quad . \quad (3.4.17)$$

This gives

$$\int_c \left\{ - \frac{\partial \Psi}{\partial x} \mathrm{d}y + \frac{\partial \Psi}{\partial y} \mathrm{d}x - 2\mu \sqrt{i} \Psi \, \mathrm{d}y \right\} = \sum_{n=-\infty}^{+\infty} \int_0^{2\pi} \{ \mu \sqrt{i} \, r \sin \varphi \, H_n{}^{(2)}(\mu r \sqrt{-i}) +$$

$$+ \mu \sqrt{-i} \, r \dot{H}_n{}^{(2)}(\mu r \sqrt{-i}) \} \tilde{A}_n \sum_{k=-\infty}^{+\infty} e^{i(k+n)\varphi} (-1)^k \mathcal{J}_k(\mu r \sqrt{-i}) \mathrm{d}\varphi \quad . \quad . \quad . \quad . \quad . \quad (3.4.18)$$

Substituting $e^{i(k+n)\varphi} = \cos(k+n)\varphi + i \sin(k+n)\varphi$, paying attention to the well-known orthogonality properties of trigonometrical functions, and substituting $i\sqrt{i} = -\sqrt{-i}$ in agreement with the choice $\sqrt{-i} = e^{-i\pi/4}$ (cf. p. 21) we now carry out the integration and find

$$\int_c \left\{ - \frac{\partial \Psi}{\partial x} \mathrm{d}y + \frac{\partial \Psi}{\partial y} \mathrm{d}x - 2\mu \sqrt{i} \Psi \, \mathrm{d}y \right\} =$$

$$= \pi \mu \sqrt{-i} \, r \sum_{n=-\infty}^{+\infty} [\mathcal{J}_n(\mu r \sqrt{-i}) H_{n-1}^{(2)}(\mu r \sqrt{-i}) - \mathcal{J}_{n-1}(\mu r \sqrt{-i}) H_n{}^{(2)}(\mu r \sqrt{-i}) +$$

$$+ \mathcal{J}_{n+1}(\mu r \sqrt{-i}) H_n{}^{(2)}(\mu r \sqrt{-i}) - \mathcal{J}_n(\mu r \sqrt{-i}) H_{n+1}^{(2)}(\mu r \sqrt{-i})] \tilde{A}_n \quad . \quad . \quad (3.4.19)$$

Here we made also use of the relation

$$2\dot{H}_n{}^{(2)}(\mu r \sqrt{-i}) = H_{n-1}^{(2)}(\mu r \sqrt{-i}) - H_{n+1}^{(2)}(\mu r \sqrt{-i}) \quad . \quad . \quad . \quad . \quad (3.4.20)$$

We finally can simplify this expression greatly if we use the following property of Bessel functions

$$\mathcal{J}_n(z) H_{n-1}^{(2)}(z) - \mathcal{J}_{n-1}(z) H_n{}^{(2)}(z) = \frac{2}{\pi i z} \quad . \quad . \quad . \quad . \quad . \quad . \quad . \quad . \quad . \quad (3.4.21)$$

This gives

$$\int_c \left\{-\frac{\partial \Psi}{\partial x}\,\mathrm{d}y + \frac{\partial \Psi}{\partial y}\,\mathrm{d}x - 2\mu\sqrt{i}\,\Psi\,\mathrm{d}y\right\} = -4i \sum_{n=-\infty}^{+\infty} \tilde{A}_n \quad . \quad . \quad . \quad . \quad (3.4.22)$$

In a quite analogous way we find if $\Psi$ is a solution of (3.1.3), given by (3.1.16), in which case we must use the lower signs in (3.4.10),

$$\int_c \left\{\frac{\partial \Psi}{\partial x}\,\mathrm{d}y - \frac{\partial \Psi}{\partial y}\,\mathrm{d}x - 2\mu\sqrt{i}\,\Psi\,\mathrm{d}y\right\} = 4i \sum_{n=-\infty}^{+\infty} (-1)^n \tilde{B}_n \quad . \quad . \quad . \quad (3.4.23)$$

From this follows that the displacement component $\eta$ is single-valued if the integration constants in the solution $\Psi$ satisfy the condition

$$\mathrm{Re}\,[\mu\sqrt{-i} \sum_{n=-\infty}^{+\infty} (-\tilde{A}_n + (-1)^n \tilde{B}_n)] = 0 \quad . \quad . \quad . \quad . \quad . \quad . \quad . \quad . \quad . \quad . \quad (3.4.24)$$

It will be shown that in many special cases of symmetric or skew-symmetric loading this condition is automatically satisfied.

Returning to the end of the previous section we find that the resulting moment about the $y$-axis of the edge load is equal to

$$\frac{8E\delta^4}{\{12(1-\nu^2)\}^{3/2}a}\,\mathrm{Im}\,[\mu\sqrt{-i} \sum_{n=-\infty}^{+\infty} (-\tilde{A}_n + (-1)^n \tilde{B}_n)] \quad . \quad . \quad . \quad . \quad . \quad (3.4.25)$$

## 3.5 The stress resultants in polar coordinates

Hitherto in all expressions of the stress resultants we referred to Cartesian coordinates. Since the shell region is bounded by a circle of radius $a$, it is

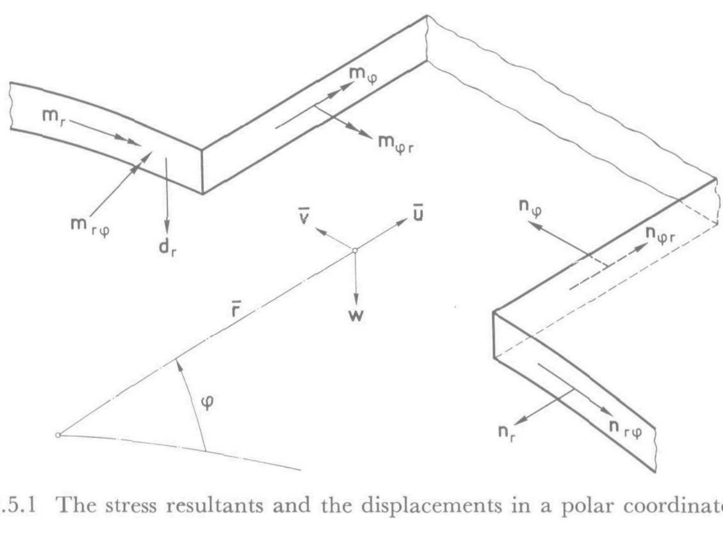


Fig. 3.5.1 The stress resultants and the displacements in a polar coordinate system

convenient, in view of the boundary conditions, to transform to polar coordinates. The corresponding stress resultants are given in Fig. 3.5.1. Here $d_r$ denotes the *reduced* shear force, which appears in the boundary conditions. The expressions in polar coordinates that correspond to the expressions in Cartesian coordinates given in equations (2.2.5), (2.2.6) and (2.2.7) are

$$\left.\begin{aligned}
n_r &= \frac{E\delta^3}{12(1-\nu^2)a^2}\,\mathrm{Re}\left\{\frac{1}{r^2}\frac{\partial^2\Psi}{\partial\varphi^2}+\frac{1}{r}\frac{\partial\Psi}{\partial r}\right\}\\
n_\varphi &= \frac{E\delta^3}{12(1-\nu^2)a^2}\,\mathrm{Re}\left\{\frac{\partial^2\Psi}{\partial r^2}\right\}\\
n_{r\varphi} &= n_{\varphi r} = -\frac{E\delta^3}{12(1-\nu^2)a^2}\,\mathrm{Re}\left\{\frac{\partial}{\partial r}\left(\frac{1}{r}\frac{\partial\Psi}{\partial\varphi}\right)\right\}\\
m_r &= \frac{E\delta^4}{\{12(1-\nu^2)\}^{3/2}a^2}\,\mathrm{Im}\left\{\frac{\partial^2\Psi}{\partial r^2}+\frac{\nu}{r^2}\frac{\partial^2\Psi}{\partial\varphi^2}+\frac{\nu}{r}\frac{\partial\Psi}{\partial r}\right\}\\
m_\varphi &= \frac{E\delta^4}{\{12(1-\nu^2)\}^{3/2}a^2}\,\mathrm{Im}\left\{\frac{1}{r^2}\frac{\partial^2\Psi}{\partial\varphi^2}+\frac{1}{r}\frac{\partial\Psi}{\partial r}+\nu\frac{\partial^2\Psi}{\partial r^2}\right\}\\
d_r &= \frac{E\delta^4}{\{12(1-\nu^2)\}^{3/2}a^3}\,\mathrm{Im}\left\{\frac{\partial^3\Psi}{\partial r^3}+\frac{1}{r}\frac{\partial^2\Psi}{\partial r^2}-\frac{1}{r^2}\frac{\partial\Psi}{\partial r}+\right.\\
&\qquad\left.+\frac{2-\nu}{r^2}\frac{\partial^3\Psi}{\partial r\partial\varphi^2}-\frac{3-\nu}{r^3}\frac{\partial^2\Psi}{\partial\varphi^2}\right\}\\
m_{r\varphi} &= m_{\varphi r} = \frac{E\delta^4}{\{12(1-\nu^2)\}^{3/2}a^2}\,\mathrm{Im}\left\{\frac{1}{r}\frac{\partial^2\Psi}{\partial r\partial\varphi}-\frac{1}{r^2}\frac{\partial\Psi}{\partial\varphi}\right\}
\end{aligned}\right\}\quad\ldots\quad(3.5.1)$$

In the next chapter we shall see how, after substituting the solution $\Psi$, the integration constants $\tilde{A}_n$ and $\tilde{B}_n$ are determined by the boundary conditions.

# CHAPTER 4

# DYNAMIC BOUNDARY CONDITIONS

## 4.1 Introductory remarks

In this chapter we shall demonstrate how in practical cases the complex integration constants $\tilde{A}_n$ and $\tilde{B}_n$ are determined. Once these constants are found all stresses in the shell may be computed after substitution in the formulae (3.5.1). We shall for the present restrict ourselves to dynamic boundary conditions at the edge of the hole. We prescribe the normal stress resultant $n_r$, the tangential shear stress resultant $n_{r\varphi}$, the reduced shear force $d_r$ and the bending moment $m_r$. These stress resultants will be given as Fourier series in $\varphi$. The double series (3.1.19) over $k$ and $n$ expressing the stress function $\Psi$ will be truncated. It will be shown that this procedure is permissible.

As has been said earlier we restricted ourselves already to solutions that give rise to stresses decaying at infinity.

The numerical work to be evaluated is less cumbersome if the boundary conditions have certain aspects of symmetry. In the following sections we shall treat successively the case that the boundary conditions are symmetric with respect to both the $x$- and the $y$-axis and the case that they are skew-symmetric with respect to both axes. In order to restrict ourselves to such particular cases of symmetry we impose certain conditions, to be enunciated in the sequel, on the integration constants $\tilde{A}_n$ and $\tilde{B}_n$. Both cases will be illustrated by an example, viz. the tube in axial tension and the tube in torsion respectively.

## 4.2 Doubly symmetric loading

Let us suppose that the shell is loaded symmetrically with respect to both the $x$- and the $y$-axis. In that case also all stresses and displacements will be doubly symmetric. We can easily restrict ourselves to solutions $\Psi$, given by (3.1.19) that give rise to such stresses and displacements if we impose certain restrictions to the constants $\tilde{A}_n$ and $\tilde{B}_n$. In the first place we must require

$$\left.\begin{aligned} &\tilde{A}_n-\tilde{B}_n = 0 \qquad (\text{for } n = \text{even}) \\ &\tilde{A}_n+\tilde{B}_n = 0 \qquad (\text{for } n = \text{odd}) \end{aligned}\right\} \quad \ldots\ldots\ldots\ldots \quad (4.2.1)$$

and (3.4.24) is then automatically satisfied. Doing so we delete all terms containing a factor $\cos p\varphi$ or $\sin p\varphi$ in which is $p$ is an odd number. For the sake of brevity we introduce new constants $C_n$, equal to $\tilde{A}_n-\tilde{B}_n$ if $n$ is odd and to $\tilde{A}_n + \tilde{B}_n$ if $n$ is even. If furthermore we introduce $l$ given by $2l = k+n$, (3.1.19) can be written

$$\Psi = \sum_{l=-\infty}^{+\infty} \sum_{n=-\infty}^{+\infty} C_n e^{2il\varphi} J_{2l-n}(\mu r \sqrt{-i}) H_n^{(2)}(\mu r \sqrt{-i}) \quad \ldots\ldots \quad (4.2.2)$$

In the second place we delete the terms containing a factor $\sin p\varphi$, if we require

$$C_n = C_{-n} \quad \ldots\ldots \quad (4.2.3)$$

We shall denote the real and imaginary part of each integration constant $C_n$ separately as follows,

$$\left.\begin{aligned} C_n &= {}^1/_2(A_n + iB_n) \\ C_o &= A_o + iB_o \end{aligned}\right\} \quad \ldots\ldots \quad (4.2.4)$$

Here $A_n$ and $B_n$ are real quantities, which must not be confused with the complex constants $\tilde{A}_n$ and $\tilde{B}_n$ that have been used earlier. Using the well-known relation

$$J_{-k}(\mu r \sqrt{-i}) = (-1)^k J_k(\mu r \sqrt{-i}) \quad \ldots\ldots \quad (4.2.5)$$

and a similar relation for the Hankel functions, (4.2.2) can be written as

$$\Psi = \sum_{l=0}^{\infty} \sum_{n=0}^{\infty} (A_n + iB_n) f(l, n, \mu r) \cos 2l\varphi \quad \ldots\ldots \quad (4.2.6)$$

with

$$\left.\begin{aligned} f(o, n, \mu r) &= J_{-n}(\mu r \sqrt{-i}) H_n^{(2)}(\mu r \sqrt{-i}) \\ f(l, n, \mu r) &= \{J_{2l-n}(\mu r \sqrt{-i}) + J_{-2l-n}(\mu r \sqrt{-i})\} H_n^{(2)}(\mu r \sqrt{-i}) \\ & \qquad (l \neq 0) \end{aligned}\right\} \quad (4.2.7)$$

Substituting (4.2.6) in the expressions (3.5.1) gives the stress resultants. The normal displacement $w$ and its derivative $\alpha = \partial w / \partial \bar{r}$ can also immediately be found. We obtain

$$n_r = \frac{E\delta^3 \mu^2}{12(1-\nu^2)a^2} \mathrm{Re}\left[\sum_{l=0}^{\infty} \sum_{n=0}^{\infty} (A_n + iB_n) f_1(l, n, \mu r) \cos 2l\varphi\right] \quad \ldots \quad (4.2.8)$$

where

$$f_1 = \frac{1}{\mu r} f' - \frac{4l^2}{\mu^2 r^2} f \quad \ldots\ldots \quad (4.2.8a)$$

and a prime $'$ denotes differentiation with respect to $\mu r$,

$$n_\varphi = \frac{E\delta^3 \mu^2}{12(1-\nu^2)a^2} \mathrm{Re}\left[\sum_{l=0}^{\infty} \sum_{n=0}^{\infty} (A_n + iB_n) f_2(l, n, \mu r) \cos 2l\varphi\right] \quad \ldots \quad (4.2.9)$$

where

$$f_2 = f'' \quad \ldots\ldots \quad (4.2.9a)$$

$$n_{r\varphi} = \frac{E\delta^3 \mu^2}{12(1-\nu^2)a^2} \mathrm{Re}\left[\sum_{l=0}^{\infty} \sum_{n=0}^{\infty} (A_n + iB_n) f_3(l, n, \mu r) \sin 2l\varphi\right] \quad \ldots \quad (4.2.10)$$

where

$$f_3 = 2l\left(\frac{1}{\mu r}f' - \frac{1}{\mu^2 r^2}f\right) \quad \ldots \ldots \ldots \ldots \quad (4.2.10a)$$

$$d_r = \frac{E\delta^4\mu^3}{\{12(1-\nu^2)\}^{3/2}a^3}\,\mathrm{Im}[\sum_{l=0}^{\infty}\sum_{n=0}^{\infty}(A_n+iB_n)f_4\,(l, n, \mu r)\cos 2l\varphi] \quad (4.2.11)$$

where

$$f_4 = f''' + \frac{1}{\mu r}f'' - \frac{1+8l^2-4\nu l^2}{\mu^2 r^2}f' + \frac{(3-\nu)4l^2}{\mu^3 r^3}f \quad \ldots \quad (4.2.11a)$$

$$m_r = \frac{E\delta^4\mu^2}{\{12(1-\nu^2)\}^{3/2}a^2}\,\mathrm{Im}[\sum_{l=0}^{\infty}\sum_{n=0}^{\infty}(A_n+iB_n)f_5\,(l, n, \mu r)\cos 2l\varphi] \quad (4.2.12)$$

where

$$f_5 = f'' + \frac{\nu}{\mu r}f' - \frac{4\nu l^2}{\mu^2 r^2}f \quad \ldots \ldots \ldots \ldots \quad (4.2.12a)$$

$$m_\varphi = \frac{E\delta^4\mu^2}{\{12(1-\nu^2)\}^{3/2}a^2}\,\mathrm{Im}[\sum_{l=0}^{\infty}\sum_{n=0}^{\infty}(A_n+iB_n)f_6\,(l, n, \mu r)\cos 2l\varphi] \quad (4.2.13)$$

where

$$f_6 = \nu f'' + \frac{1}{\mu r}f' - \frac{4l^2}{\mu^2 r^2}f \quad \ldots \ldots \ldots \ldots \quad (4.2.13a)$$

$$w = \frac{\delta}{\sqrt{12(1-\nu^2)}}\,\mathrm{Im}[\sum_{l=0}^{\infty}\sum_{n=0}^{\infty}(A_n+iB_n)f_7\,(l, n, \mu r)\cos 2l\varphi] \quad . \quad (4.2.14)$$

where

$$f_7 = f \quad \ldots \ldots \ldots \ldots \ldots \ldots \quad (4.2.14a)$$

$$\alpha = \frac{\delta\mu}{\sqrt{12(1-\nu^2)}\,a}\,\mathrm{Im}[\sum_{l=0}^{\infty}\sum_{n=0}^{\infty}(A_n+iB_n)f_8\,(l, n, \mu r)\cos 2l\varphi] \quad (4.2.15)$$

where

$$f_8 = f' \quad \ldots \ldots \ldots \ldots \ldots \ldots \quad (4.2.15a)$$

Let us suppose that the edge load that is prescribed is given as a truncated Fourier series for each of the stress resultants $n_r$, $n_{r\varphi}$, $m_r$ and $d_r$. In the case of a tube in axial tension for example there are only terms that are constant and terms that contain a factor $\cos 2\varphi$. In this case the constants $A_n$ and $B_n$ for large values of $n$ must necessarily be small. This ensues from the following reasoning.

The value of the Bessel functions $\mathcal{J}_k(\mu r\sqrt{-i})$ decreases if $k$ increases. The value of the functions $H_n^{(2)}(\mu r\sqrt{-i})$ on the other hand increases if $n$ increases. This is the more so if $\mu$ is small [1]). Observing (4.2.6) and (4.2.7) it will now

[1]) Cf. N. W. McLachlan [ref. 7, p. 86].

be clear that in the expressions for the stress resultants the coefficients of $A_j$ and $B_j$ are Fourier series of which the dominating terms are the term containing a factor $\cos j\varphi$ or $\cos(j\pm 1)\varphi$ if $j$ is odd and the immediately adjacent terms. The boundary conditions yield an infinite set of linear equations by equating each term of the Fourier series expansion of each of the above-mentioned stress resultants to a prescribed value. If all equations, in which $A_j$ and $B_j$ have large coefficients, have a right-hand side zero it is probable that $A_j$ and $B_j$ are small. This indicates that the summation over $n$ may be truncated at a certain value, say $2N$. Accordingly the summation over $l$ will then be truncated at $N$.

From calculations it has become clear that the truncation of the series is completely justified. This numerical justification a posteriori will be discussed in a following section. Physically it means that, especially if $\mu$ is small, there is only a small coupling between "remote" terms in the Fourier series. This is also clear if we inspect the basic differential equation (2.2.4). If $\Psi$ is given as a Fourier series, the coupling is caused by the second term of the left-hand side. Since this second term contains a second derivative, whereas the first term is a 4th derivative, the second term is small with respect to the first term especially for large $n$ and small $\mu$.

The number of constants to be determined is now $4N+2$. Equating each term of the truncated Fourier series (containing only *even* terms) for $n_r$, $n_{r\varphi}$, $m_r$ and $d_r$ to a prescribed value seems at first sight to give $4N+4$ equations. In the first place, however, the constant term in the Fourier series expansion of $n_{r\varphi}$ does not yield an equation as it is automatically zero (cf. (4.2.10)). In the second place we cannot prescribe arbitrary values of all other terms in view of the requirement of equilibrium of the edge load (cf. Section 3.3). We shall leave out of the boundary conditions the constant term of $d_r$. This brings the total number of equations down to exactly $4N+2$, the number of unknown constants. It may be remarked here already that in all numerical calculations, to be reported later, a constant transverse shear force, which is in equilibrium with the resulting force of the other edge stresses appears automatically.

The double series in the right-hand sides of the expressions (4.2.8) to (4.2.15) are of the shape $\Sigma\Sigma(A_n+iB_n)\, f_i\,(l, n, \mu r)\cos 2l\varphi$. For those values of $\mu r$, one is interested in, one can now tabulate the real and the imaginary parts of the functions $f_i(l, n, \mu r)$ for all combinations $l, n$ $(l = 0 \dots N,\ n = 0 \dots 2N)$. With the aid of these results one can immediately construct the equations from which $A_n$ and $B_n$ must be solved, corresponding to any boundary conditions to be enforced. And once these constants are determined one can immediately calculate the stress resultants and stress couples in the shell with the aid of the tabulated values.

In order to obtain the values of the functions $f_i(l, n, \mu r)$, one must determine the functions $f$ and their derivatives with respect to $\mu r$, viz. (the arguments of the Bessel functions will be omitted in order to save space)

$$\left.\begin{aligned}
f &= \sum{}^{*} \mathcal{J}_p H_n{}^{(2)} \\
f' &= \sum{}^{*} (\dot{\mathcal{J}}_p H_n{}^{(2)} + \mathcal{J}_p \dot{H}_n{}^{(2)}) \sqrt{-i} \\
f'' &= \sum{}^{*} \left\{ \left(2i + \frac{p^2}{\mu^2 r^2} + \frac{n^2}{\mu^2 r^2}\right) \mathcal{J}_p H_n{}^{(2)} + \right. \\
&\qquad \left. - \frac{1}{\mu r} (\dot{\mathcal{J}}_p H_n{}^{(2)} + \mathcal{J}_p \dot{H}_n{}^{(2)}) \sqrt{-i} - 2i \dot{\mathcal{J}}_p \dot{H}_n{}^{(2)} \right\} \\
f''' &= \sum{}_{*} \left\{ - \frac{1}{\mu r} \left(2i + \frac{3p^2}{\mu^2 r^2} + \frac{3n^2}{\mu^2 r^2}\right) \mathcal{J}_p H_n{}^{(2)} + \right. \\
&\qquad + \left(4i + \frac{p^2 + 3n^2 + 2}{\mu^2 r^2}\right) \dot{\mathcal{J}}_p H_n{}^{(2)} \sqrt{-i} + \\
&\qquad \left. + \left(4i + \frac{3p^2 + n^2 + 2}{\mu^2 r^2}\right) \mathcal{J}_p \dot{H}_n{}^{(2)} \sqrt{-i} + \frac{6i}{\mu r} \dot{\mathcal{J}}_p \dot{H}_n{}^{(2)} \right\}
\end{aligned}\right\} \quad (4.2.16)$$

In (4.2.16) the dots denote differentiation of the Bessel functions with respect to their argument $\mu r \sqrt{-i}$ (cf. Section 3.4). The summation $\Sigma^*$ means summation over *two* values of $p$, viz. $p = 2l - n$ and $-2l - n$, but if $l = 0$ only over *one* value of $n$, viz. $p = n$ (cf. (4.2.7)). The tabulated functions $f_i(l, n, \mu r)$ for some value of $\mu r$, say 4, can be used not only to construct the boundary conditions for $\mu = 4$ and to calculate the stress resultants and displacements for $\mu = 4$ at $r = 1$, but also to calculate the stress resultants and displacements for $\mu = 2$ at $r = 2$, for $\mu = 1$ at $r = 4$, etc. (if the integration constants for those cases are known).

The equations following from the boundary conditions are constructed as follows. Suppose that the prescribed edge load is

$$\left.\begin{aligned}
n_r &= \sum_{l=0}^{N} n_r(l) \cos 2l\varphi \\
n_{r\varphi} &= \sum_{l=1}^{N} n_{r\varphi}(l) \sin 2l\varphi \\
d_r &= \sum_{l=1}^{N} d_r(l) \cos 2l\varphi \\
m_r &= \sum_{l=0}^{N} m_r(l) \cos 2l\varphi
\end{aligned}\right\} \quad \ldots\ldots\ldots\ldots \quad (4.2.17)$$

For the sake of convenience we replace the constants $A_n$ and $B_n$ by

$$\left.\begin{aligned} A_n{}^* &= \frac{E\delta^3\mu^2}{12(1-\nu^2)a^2}A_n \\ \text{and}\qquad B_n{}^* &= \frac{E\delta^3\mu^2}{12(1-\nu^2)a^2}B_n \end{aligned}\right\} \quad \ldots\ldots\ldots\ldots \quad (4.2.18)$$

respectively. Then the boundary conditions become

$$\left.\begin{aligned}
&\sum_{n=0}^{2N}\{A_n{}^*\,\mathrm{Re}\,[f_1(l,n,\mu)] - B_n{}^*\,\mathrm{Im}\,[f_1(l,n,\mu)]\} = n_r(l) \\
&\hspace{20em}(l = 0\ldots N) \\
&\sum_{n=0}^{2N}\{A_n{}^*\,\mathrm{Re}\,[f_3(l,n,\mu)] - B_n{}^*\,\mathrm{Im}\,[f_3(l,n,\mu)]\} = n_{r\varphi}(l) \\
&\hspace{20em}(l = 1\ldots N) \\
&\sum_{n=0}^{2N}\{A_n{}^*\,\mathrm{Im}\,[f_4(l,n,\mu)] + B_n{}^*\,\mathrm{Re}\,[f_4(l,n,\mu)]\} = \frac{a\sqrt{12(1-\nu^2)}}{\mu\delta}\,d_r(l) \\
&\hspace{20em}(l = 1\ldots N) \\
&\sum_{n=0}^{2N}\{A_n{}^*\,\mathrm{Im}\,[f_5(l,n,\mu)] + B_n{}^*\,\mathrm{Re}\,[f_5(l,n,\mu)]\} = \frac{\sqrt{12(1-\nu^2)}}{\delta}\,m_r(l) \\
&\hspace{20em}(l = 0\ldots N)
\end{aligned}\right\} \quad (4.2.19)$$

The solutions of these equations may finally be substituted in the equations (4.2.8—15), which give the stress resultants and the normal displacement.

### 4.3 The tube in axial tension

If an unweakened tube is loaded in axial tension by axial normal stress resultants $p$ per unit of length, the stress resultants in our polar coordinate system are

$$\left.\begin{aligned} n_r &= {}^1\!/_2 p(1-\cos 2\varphi) \qquad & d_r &= 0 \\ n_\varphi &= {}^1\!/_2 p(1+\cos 2\varphi) \qquad & m_r &= 0 \\ n_{r\varphi} &= {}^1\!/_2 p \sin 2\varphi \qquad & m_\varphi &= 0 \end{aligned}\right\} \quad \ldots\ldots\ldots \quad (4.3.1)$$

In order to obtain the stress distribution if the tube, loaded by axial stress resultants $p$, is weakened by a circular hole of radius $a$, we must add to the stress distribution of the unweakened shell the stresses arising from a loading at the edge of the hole,

$$\left.\begin{aligned} n_r &= -{}^1\!/_2 p(1-\cos 2\varphi) \qquad & d_r &= 0 \\ n_{r\varphi} &= -{}^1\!/_2 p \sin 2\varphi \qquad & m_r &= 0 \end{aligned}\right\} \quad \ldots\ldots\ldots \quad (4.3.2)$$

while the shell apart from that loading is free.

Applying the method described in the preceding section, we must solve $4N+2$ linear algebraic equations in $A_n$ and $B_n$ ($n = 0 \ldots 2N$), arising from the boundary conditions (4.3.2) at $r = 1$. For the sake of convenience we shall use constants $A_n^*$ and $B_n^*$ instead, obtained from $A_n$ and $B_n$ after multiplying them by $\dfrac{12(1-\nu^2)a^2}{E\delta^3\mu^2}\,\dfrac{p}{2}$.

The boundary conditions then yield the following equations for the constants $A_n^*$ and $B_n^*$.

$$
\left.\begin{aligned}
n_r &= -\frac{p}{2}(1-\cos 2\varphi) \rightarrow \\
&\sum_{n=0}^{2N}\{A_n^*\,\mathrm{Re}\,[f_1(l,n,\mu)] - B_n^*\,\mathrm{Im}\,[f_1(l,n,\mu)]\} = \begin{cases} -1 & (\text{for } l=0) \\ \;\;1 & (\text{for } l=1) \\ \;\;0 & (l=2\ldots N) \end{cases} \\
n_{r\varphi} &= -\frac{p}{2}\sin 2\varphi \rightarrow \\
&\sum_{n=0}^{2N}\{A_n^*\,\mathrm{Re}\,[f_3(l,n,\mu)] - B_n^*\,\mathrm{Im}\,[f_3(l,n,\mu)]\} = \begin{cases} -1 & (\text{for } l=1) \\ \;\;0 & (l=2\ldots N) \end{cases} \\
d_r &= 0 \rightarrow \sum_{n=0}^{2N}\{A_n^*\,\mathrm{Im}\,[f_4(l,n,\mu)] + B_n^*\,\mathrm{Re}\,[f_4(l,n,\mu)]\} = 0 \quad (l = 1\ldots N) \\
m_r &= 0 \rightarrow \sum_{n=0}^{2N}\{A_n^*\,\mathrm{Im}\,[f_5(l,n,\mu)] + B_n^*\,\mathrm{Re}\,[f_5(l,n,\mu)]\} = 0 \quad (l = 0\ldots N)
\end{aligned}\right\}\quad (4.3.3)
$$

When these equations are solved, we may calculate the stress resultants and displacements at $\bar{r} = \lambda a$ as follows

$$
n_r = \frac{p}{2}\sum_{l=0}^{N}\sum_{n=0}^{2N}\{A_n^*\,\mathrm{Re}\,[f_1(l,n,\lambda\mu)] - B_n^*\,\mathrm{Im}\,[f_1(l,n,\lambda\mu)]\}\cos 2l\varphi
$$

and similar expressions for $n_\varphi$ and $n_{r\varphi}$,

$$
m_r = \frac{p\delta}{2\sqrt{12(1-\nu^2)}}\sum_{l=0}^{N}\sum_{n=0}^{2N}\{A_n^*\,\mathrm{Im}\,[f_5(l,n,\lambda\mu)] + B_n^*\,\mathrm{Re}\,[f_5(l,n,\lambda\mu)]\}\cos 2l\varphi
$$

and similar expressions for $m_\varphi$ and $m_{r\varphi}$,

$$
w = \frac{\sqrt{12(1-\nu^2)}\,a^2 p}{2E\delta^2\mu^2}\sum_{l=0}^{N}\sum_{n=0}^{2N}\{A_n^*\,\mathrm{Im}\,[f_7(l,n,\lambda\mu)] + B_n^*\,\mathrm{Re}\,[f_7(l,n,\lambda\mu)]\}\cos 2l\varphi
$$

and a similar expression for $\alpha$. (4.3

Numerical calculations have been carried out, covering the range of values of $\mu$ between zero and 4. In these calculations Poisson's ratio $\nu$ has been assumed to be equal to 0.3. Table 4.3.1 shows the computed values of the constants $A_n{}^*$ and $B_n{}^*$ for four different values of $\mu$. In two cases ($\mu = 1$ and $\mu = 4$) the calculations have been carried out twice, viz. for different values of $N$ in order to gain an insight in the errors of the truncation of the series expansion.

Table 4.3.1

| | $\mu = 0.5$ <br> $N = 3$ | $\mu = 1$ <br> $N = 3$ | $\mu = 1$ <br> $N = 4$ | $\mu = 2$ <br> $N = 3$ | $\mu = 4$ <br> $N = 4$ | $\mu = 4$ <br> $N = 5$ |
|---|---|---|---|---|---|---|
| $A_0{}^*$ | $-0.029282$ | $-0.313850$ | $-0.313850$ | $-3.59929$ | $66.649$ | $66.649$ |
| $B_0{}^*$ | $-0.399280$ | $-1.723207$ | $-1.723207$ | $-10.29920$ | $-131.064$ | $-131.063$ |
| $A_1{}^*$ | $-0.009753$ | $-0.393135$ | $-0.393135$ | $-9.09506$ | $31.557$ | $31.566$ |
| $B_1{}^*$ | $0.848940$ | $3.912743$ | $3.912743$ | $16.44115$ | $-22.401$ | $-22.399$ |
| $A_2{}^*$ | $-0.026258$ | $-0.455282$ | $-0.455282$ | $-6.08537$ | $8.584$ | $8.618$ |
| $B_2{}^*$ | $-0.001463$ | $-0.102263$ | $-0.102263$ | $-5.24652$ | $-33.932$ | $-33.959$ |
| $A_3{}^*$ | $0.000121$ | $0.017755$ | $0.017755$ | $1.89577$ | $-0.786$ | $-0.731$ |
| $B_3{}^*$ | $-0.000315$ | $-0.018793$ | $-0.018793$ | $-0.38374$ | $84.999$ | $84.875$ |
| $A_4{}^*$ | $0.0_3\,0021$ | $0.0_3\,4251$ | $0.0_3\,4252$ | $-0.02728$ | $-64.631$ | $-64.609$ |
| $B_4{}^*$ | $0.0_3\,0016$ | $0.0_3\,8757$ | $0.0_3\,8757$ | $0.31871$ | $6.762$ | $6.486$ |
| $A_5{}^*$ | $-0.0_6\,0095$ | $-0.0_3\,0199$ | $-0.0_3\,0198$ | $-0.02827$ | $-3.819$ | $-3.865$ |
| $B_5{}^*$ | $0.0_6\,0050$ | $0.0_3\,0045$ | $0.0_3\,0045$ | $-0.00515$ | $-21.134$ | $-21.502$ |
| $A_6{}^*$ | $0.0_9\,0138$ | $-0.0_6\,0040$ | $0.0_6\,0093$ | $0.00005$ | $4.482$ | $4.408$ |
| $B_6{}^*$ | $-0.0_9\,0318$ | $-0.0_6\,2627$ | $-0.0_6\,2579$ | $-0.00149$ | $-0.458$ | $-0.767$ |
| $A_7{}^*$ | | | $0.0_6\,0022$ | | $0.114$ | $0.068$ |
| $B_7{}^*$ | | | $0.0_9\,8403$ | | $0.799$ | $0.638$ |
| $A_8{}^*$ | | | $-0.0_9\,0107$ | | $-0.060$ | $-0.0708$ |
| $B_8{}^*$ | | | $0.0_9\,0135$ | | $0.048$ | $-0.00046$ |
| $A_9{}^*$ | | | | | | $0.00011$ |
| $B_9{}^*$ | | | | | | $-0.00686$ |
| $A_{10}{}^*$ | | | | | | $0.00037$ |
| $B_{10}{}^*$ | | | | | | $-0.00017$ |

Comparison shows that the truncation at $N = 3$ for $\mu = 1$ is absolutely correct. This holds also for the truncation at $N = 4$ for $\mu = 4$, be it in a somewhat lesser degree. This is undoubtedly connected with the fact that in the latter case the ratio between the largest constant ($B_0{}^*$) and the smallest one ($B_8{}^*$) is about 2,700, whereas this ratio amounts to 430,000,000 in the case $\mu = 1$, $N = 3$. An impression of the errors introduced by the truncation will now be given in the Tables 4.3.2 and 4.3.3. They show the coefficients of the Fourier series of stress resultants, bending stresses $\sigma_{br} = 6m_r/\delta^2$ and $\sigma_{b\varphi} = 6m_\varphi/\delta^2$ and normal displacement at the edge of the hole in the case $\mu = 4$, caused by the edge load (4.3.2). Table 4.3.2 corresponds to $N = 4$, and a consequence is, that $n_r$, $n_{r\varphi}$, $d_r$ and $m_r$ as far as the terms containing a factor cos $10\varphi$ or sin $10\varphi$ are concerned, do not satisfy even approximately the boundary conditions. Comparison with Table 4.3.3, corresponding to $N = 5$, however, shows that

Table 4.3.2

| $\mu=4$ $N=4$ | $l=0$ | $l=1$ | $l=2$ | $l=3$ | $l=4$ | $l=5$ | multiplied by |
|---|---|---|---|---|---|---|---|
| $n_r$ | $-0.5$ | 0.5 | 0 | 0 | 0 | 0.4407 | $p \quad \cos 2l\varphi$ |
| $n_\varphi$ | 0.8372 | 2.7955 | 2.2748 | 0.2234 | 0.0021 | $-0.3620$ | $p \quad \cos 2l\varphi$ |
| $n_{r\varphi}$ | 0 | $-0.5$ | 0 | 0 | 0 | 0.4166 | $p \quad \sin 2l\varphi$ |
| $d_r$ | 0 | 0 | 0 | 0 | 0 | 0.1127 | $\frac{pa}{R} \cos 2l\varphi$ |
| $\sigma_{br}$ | 0 | 0 | 0 | 0 | 0 | 0.3675 | $\frac{p}{\delta} \cos 2l\varphi$ |
| $\sigma_{b\varphi}$ | 0.3859 | $-2.0068$ | $-0.2768$ | $-0.0564$ | 0.0084 | $-1.1021$ | $\frac{p}{\delta} \cos 2l\varphi$ |
| $w$ | | 18.3044 | 0.4812 | 0.0781 | $-0.0053$ | 0.4368 | $\frac{pR}{E\delta} \cos 2l\varphi$ |

Table 4.3.3

| $\mu=4$ $N=5$ | $l=0$ | $l=1$ | $l=2$ | $l=3$ | $l=4$ | $l=5$ | multiplied by |
|---|---|---|---|---|---|---|---|
| $n_r$ | $-0.5$ | 0.5 | 0 | 0 | 0 | 0 | $p \quad \cos 2l\varphi$ |
| $n_\varphi$ | 0.8372 | 2.7955 | 2.2748 | 0.2332 | 0.0037 | 0.0001 | $p \quad \cos 2l\varphi$ |
| $n_{r\varphi}$ | 0 | $-0.5$ | 0 | 0 | 0 | 0 | $p \quad \sin 2l\varphi$ |
| $d_r$ | 0 | 0 | 0 | 0 | 0 | 0 | $\frac{pa}{R} \cos 2l\varphi$ |
| $\sigma_{br}$ | 0 | 0 | 0 | 0 | 0 | 0 | $\frac{p}{\delta} \cos 2l\varphi$ |
| $\sigma_{b\varphi}$ | 0.3859 | $-2.0067$ | $-0.2769$ | $-0.0557$ | 0.0023 | $-0.0002$ | $\frac{p}{\delta} \cos 2l\varphi$ |
| $w$ | | 18.3043 | 0.4814 | 0.0774 | $-0.0018$ | 0.0001 | $\frac{pR}{E\delta} \cos 2l\varphi$ |

this does not affect the lower terms in the Fourier series expansion appreciably. And this furnishes a numerical justification of the truncation procedure.

To the stress resultants must be added the stress resultants (4.3.1) in order to obtain the actual stress distribution in the shell loaded in tension. We then find at the edge of the hole

$$n_\varphi = \quad 7.145p \quad (\text{at } \varphi = 0), \text{ and } 0.0869p \quad (\text{at } \varphi = \pi/2),$$

$$m_\varphi = -0.325p\delta \ (\text{at } \varphi = 0), \text{ and } 0.362p\delta \ (\text{at } \varphi = \pi/2),$$

which causes bending stresses

$$\sigma_{b\varphi} = -1.951p/\delta \ (\text{at } \varphi = 0), \text{ and } 2.174p/\delta \ (\text{at } \varphi = \pi/2).$$

A *positive* bending stress (corresponding to a positive bending moment) means a *tensile* stress at the outside and a *compressive* stress at the inside of the cylinder. The fact may be recalled that a *positive* $w$ means a normal displacement *inward.*

The stress concentration which is equal to 3 in the case of a flat plate ($\mu = 0$) is apparently increased to more than 7. If the bending stress is also taken into account it is even as high as 9.

It is interesting to note that the constant term in $d_r$ is zero. This was not enforced as a boundary condition but appeared automatically as a result of the fact that the edge load is necessarily self-equilibrating.

Calculations for many other values of $\mu$ between 0 and 4 have been carried

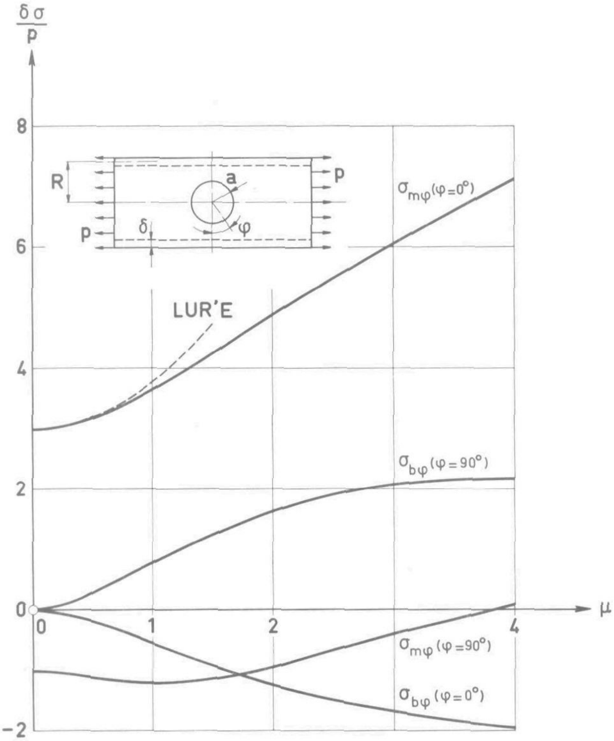


Fig. 4.3.1 Membrane and bending stresses at $\varphi = 0$ and $\varphi = \pi/2$ at the edge of the hole in a tube in axial tension as a function of $\mu$ (positive bending stress means tensile stress at outer surface)

out. They will not be reported in detail. Some significant results are presented in a few graphs.

Fig. 4.3.1 shows the magnitude of the membrane and bending stresses at the edge of the hole for $\varphi = 0$ and $\varphi = \pi/2$ as a function of $\mu$ ($\mu = 0$ represents KIRSCH's solution for a flat plate). For comparison LUR'E's results [1]) for the membrane stresses at $\varphi = 0$ have been given (dashed curve). Attention may be drawn to the relatively large values of the bending stresses (absent if $\mu = 0$) and to the fact that the membrane stress at $\varphi = \pi/2$ which is $-p/\delta$ in the case $\mu = 0$ after a drop to $-1.25p/\delta$ increases and becomes positive at about $\mu = 4$.

Fig. 4.3.2 shows the membrane and bending stresses at the edge of the hole as a function of $\varphi$ for some values of $\mu$. From this graph it appears that the compressive region at $\varphi = \pi/2$ which is vanished at $\mu = 4$ (as followed from Fig. 4.3.1) is shifted towards smaller values of $\varphi$ (and also larger values as is clear from symmetry).

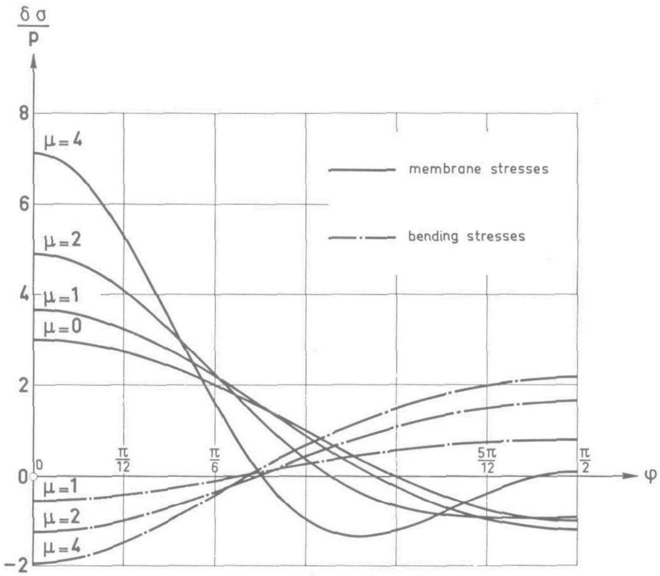


Fig. 4.3.2 Membrane and bending stresses at the edge of the hole in a tube in axial tension as a function of $\varphi$ (positive bending stress means tensile stress at outer surface)

Fig. 4.3.3 shows stresses as a function of $r$ in the special case $\mu = 1.75$. For comparison the case $\mu = 0$ (flat plate) has been given in dashed curves. In the latter case there is no bending. For three values of $\varphi$, viz. $\varphi = 0°$ (curves *a*),

[1]) In LUR'E's original paper the influence of the curvature was overestimated by a factor 2 due to an error in the formal computation.

$\varphi = 45°$ (curves $b$) and $\varphi = 90°$ (curves $c$) the values of the membrane and bending stresses in $\varphi$- and $r$-direction respectively have been given. One fact indicated by these graphs may be mentioned. Looking at the curves $a$ it appears

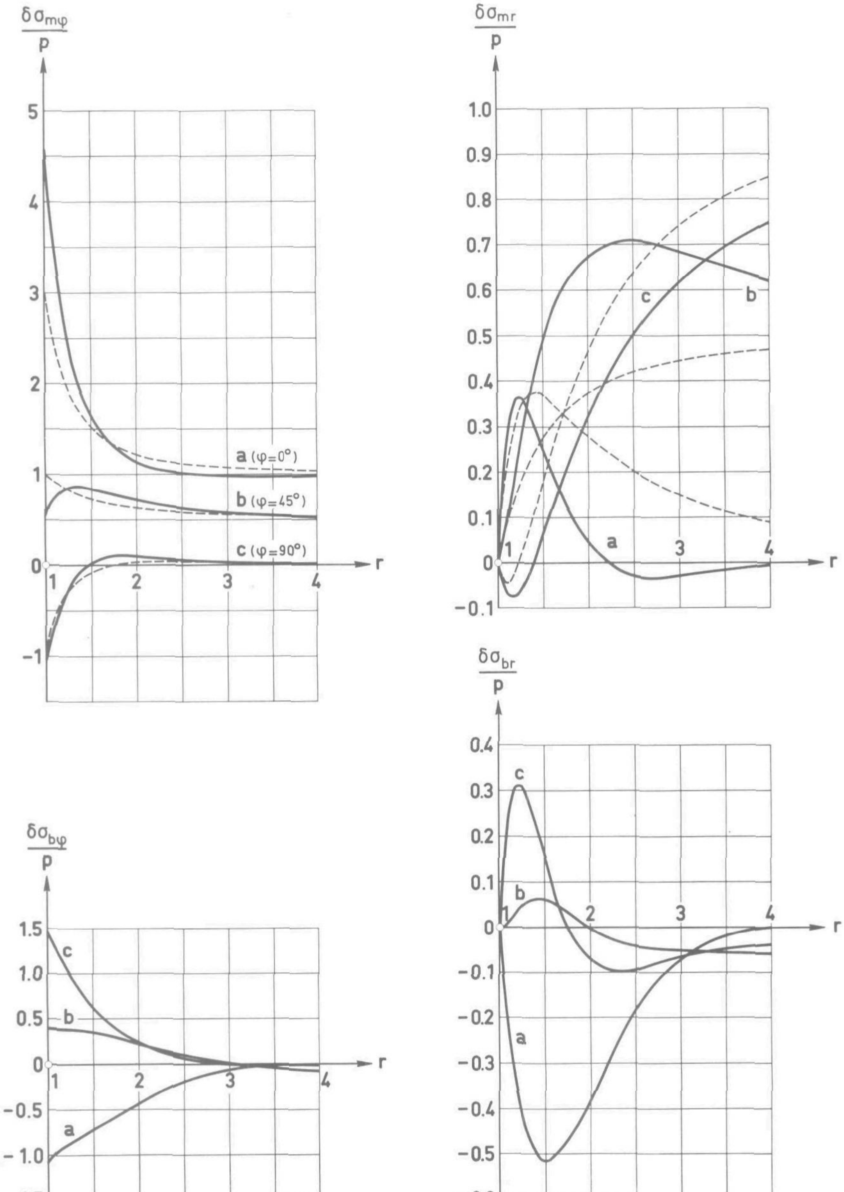


Fig. 4.3.3 Stresses in a tube in axial tension as a function of $r$ in the case $\mu = 1.75$, compared with flat plate solution (positive bending stress means tensile stress at outer surface)

that the disturbance by the presence of the hole in the case $\mu = 1.75$ is more located in the vicinity of the hole than in the case $\mu = 0$, whereas the disturbance along the generator passing through the hole centre (curves $c$) dies out less rapidly for $\mu = 1.75$ than in the case of a flat plate. In Section 6.3 dealing with an investigation of the errors introduced by the spiral shell model we shall return to this feature. More graphs of this type will be given in Chapter 7 where a comparison with experimental results will be discussed.

## 4.4 Doubly skew-symmetric loading

In order to obtain doubly skew-symmetric stresses and displacements we must for similar reasons as in the doubly symmetric case, dealt with in Section 4.2, submit the complex constants $\tilde{A}_n$ and $\tilde{B}_n$ to the requirement (4.2.1). Hence the solution is again written in the form (4.2.2). But instead of (4.2.3) we require next

$$C_n = -C_n, \ (C_o = 0) \quad \ldots \quad (4.4.1)$$

Doing so we retain only the terms containing a factor $\sin p\varphi$ whereas this time the terms with a factor $\cos p\varphi$ are deleted. We introduce real constants $A_n$ and $B_n$ by

$$iC_n = {}^1/_2(A_n + iB_n) \quad \ldots \quad (4.4.2)$$

Substituting in (4.2.2) yields

$$\Psi = \sum_{l=1}^{\infty} \sum_{n=1}^{\infty} (A_n + iB_n) g(l, n, \mu r) \sin 2l\varphi \quad \ldots \quad (4.4.3)$$

where

$$g(l, n, \mu r) = \{\mathcal{J}_{2l-n}(\mu r\sqrt{-i}) - \mathcal{J}_{-2l-n}(\mu r\sqrt{-i})\} H_n^{(2)}(\mu r\sqrt{-i}) \quad (4.4.4)$$

The stress resultants, stress couples, the normal displacement $w$ and its derivative $\alpha = \partial w/\partial \bar{r}$ may be expressed by functions $g_i$ $(i = 1 \ldots 8)$ obtained from the function $g$ and its derivatives with respect to $\mu r$ in the same way as the functions $f_i$ are obtained from $f$ and its derivatives (cf. equations (4.2.8a ... 15a)). The expressions are analogous to the corresponding expressions (4.2.8 ... 15) in the doubly symmetric case. They differ in so far that $\cos 2l\varphi$ must be replaced by $\sin 2l\varphi$ and $\sin 2l\varphi$ by $-\cos 2l\varphi$. We obtain

$$n_r = \frac{E\delta^3\mu^2}{12(1-\nu^2)a^2} \operatorname{Re}\left[\sum_{l=1}^{\infty} \sum_{n=1}^{\infty} (A_n + iB_n) g_1(l, n, \mu r) \sin 2l\varphi\right] \quad \ldots \quad (4.4.5)$$

$$n_\varphi = \frac{E\delta^3\mu^2}{12(1-\nu^2)a^2} \operatorname{Re}\left[\sum_{l=1}^{\infty} \sum_{n=1}^{\infty} (A_n + iB_n) g_2(l, n, \mu r) \sin 2l\varphi\right] \quad \ldots \quad (4.4.6)$$

$$n_{r\varphi} = -\frac{E\delta^3\mu^2}{12(1-\nu^2)a^2} \operatorname{Re}\left[\sum_{l=1}^{\infty} \sum_{n=1}^{\infty} (A_n + iB_n) g_3(l, n, \mu r) \cos 2l\varphi\right] \quad . \quad (4.4.7)$$

$$d_r = \frac{E\delta^4\mu^3}{\{12(1-\nu^2)\}^{3/2}a^3} \operatorname{Im}\left[\sum_{l=1}^{\infty}\sum_{n=1}^{\infty}(A_n+iB_n)g_4(l,n,\mu r)\sin 2l\varphi\right] \quad (4.4.8)$$

$$m_r = \frac{E\delta^4\mu^2}{\{12(1-\nu^2)\}^{3/2}a^2} \operatorname{Im}\left[\sum_{l=1}^{\infty}\sum_{n=1}^{\infty}(A_n+iB_n)g_5(l,n,\mu r)\sin 2l\varphi\right] \quad (4.4.9)$$

$$m_\varphi = \frac{E\delta^4\mu^2}{\{12(1-\nu^2)\}^{3/2}a^2} \operatorname{Im}\left[\sum_{l=1}^{\infty}\sum_{n=1}^{\infty}(A_n+iB_n)g_6(l,n,\mu r)\sin 2l\varphi\right] \quad (4.4.10)$$

$$w = \frac{\delta}{\sqrt{12(1-\nu^2)}} \operatorname{Im}\left[\sum_{l=1}^{\infty}\sum_{n=1}^{\infty}(A_n+iB_n)g_7(l,n,\mu r)\sin 2l\varphi\right] \quad (4.4.11)$$

$$\alpha = \frac{\delta\mu}{\sqrt{12(1-\nu^2)}a} \operatorname{Im}\left[\sum_{l=1}^{\infty}\sum_{n=1}^{\infty}(A_n+iB_n)g_8(l,n,\mu r)\sin 2l\varphi\right] \quad (4.4.12)$$

The treatment of dynamic boundary conditions to be enforced is now quite analogous to the procedure described in Section 4.2. If the series are truncated at $l = N$, there are now only $4N$ constants that must be determined, in view of the absence of $A_0$ and $B_0$. There are also $4N$ boundary conditions, as there are no constant terms of $n_r$ and $m_r$ to be prescribed.

In the next section we shall illustrate this skew-symmetric case with the results bearing on the tube under torsion. It is obvious that we do not need to investigate once more the influence of the truncation of the series. We shall, however, pay attention to the influence of small variations in the value of Poisson's ratio $\nu$.

### 4.5 The tube under torsion

If the tube is loaded by a twisting couple $M_t$, the stress resultants and stress couples in the case that there is no cut-out are, putting $p = M_t/2\pi R^2$,

$$\left.\begin{aligned} n_r &= -p\sin 2\varphi & d_r &= 0 \\ n_\varphi &= p\sin 2\varphi & m_r &= 0 \\ n_{r\varphi} &= -p\cos 2\varphi & m_\varphi &= 0 \end{aligned}\right\} \quad (4.5.1)$$

To this stress distribution we must add the stresses caused by the edge load

$$\left.\begin{aligned} n_r &= p\sin 2\varphi & d_r &= 0 \\ n_{r\varphi} &= p\cos 2\varphi & m_r &= 0 \end{aligned}\right\} \quad (4.5.2)$$

These stresses have been determined for various values of $\mu$. Table 4.5.1 shows the stress resultants and the bending stresses for $\mu = 1$, resulting from the boundary conditions (4.5.2), while Poisson's ratio $\nu$ is assumed to be 0.3. The series have been truncated at $N = 3$.

Table 4.5.1

| | $l = 1$ | $l = 2$ | $l = 3$ | multiplied by |
|---|---|---|---|---|
| $n_r$ | 1.0000 | 0.0000 | 0.0000 | $p \quad \sin 2l\varphi$ |
| $n_\varphi$ | 5.0957 | 0.5159 | 0.0038 | $p \quad \sin 2l\varphi$ |
| $n_{r\varphi}$ | 1.0000 | 0.0000 | 0.0000 | $p \quad \cos 2l\varphi$ |
| $d_r$ | 0.0000 | 0.0000 | 0.0000 | $\frac{pa}{R} \sin 2l\varphi$ |
| $\sigma_{br}$ | 0.0000 | 0.0000 | 0.0000 | $\frac{p}{\delta} \sin 2l\varphi$ |
| $\sigma_{b\varphi}$ | $-2.9432$ | $-0.1344$ | $-0.0002$ | $\frac{p}{\delta} \sin 2l\varphi$ |

In order to have an idea what the influence is of the value of $\nu$, the same calculation has been carried out for $\nu = 0.28$. The results bearing on this case are given by Table 4.5.2. Apparently these results are rather insensitive for small variations in the value of $\nu$.

Table 4.5.2

| | $l = 1$ | $l = 2$ | $l = 3$ | multiplied by |
|---|---|---|---|---|
| $n_r$ | 1.0000 | 0.0000 | 0.0000 | $p \quad \sin 2l\varphi$ |
| $n_\varphi$ | 5.1003 | 0.5117 | 0.0039 | $p \quad \sin 2l\varphi$ |
| $n_{r\varphi}$ | 1.0000 | 0.0000 | 0.0000 | $p \quad \cos 2l\varphi$ |
| $d_r$ | 0.0000 | 0.0000 | 0.0000 | $\frac{pa}{R} \sin 2l\varphi$ |
| $\sigma_{br}$ | 0.0000 | 0.0000 | 0.0000 | $\frac{p}{\delta} \sin 2l\varphi$ |
| $\sigma_{b\varphi}$ | $-2.9093$ | $-0.1363$ | $-0.0002$ | $\frac{p}{\delta} \sin 2l\varphi$ |

In the case of a flat plate with a circular hole that is loaded in a corresponding way, i.e. by shear stresses $p/\delta$ at infinity, the maximum value of the stress resultant $n_\varphi$ is reached at $\varphi = \pi/4$ (and $3\pi/4$, $5\pi/4$ and $7\pi/4$, the second and the fourth value of $\varphi$ giving $n_\varphi$ with opposite sign) where $n_\varphi = 4p$. If $\mu = 1$, it follows from the tables above that the value of $n_\varphi$ at $\varphi = \pi/4$ is increased to about $6.1p$. In virtue of the term containing a factor $\sin 4\varphi$, however, this is no longer the maximum value. Fig. 4.5.1 shows the *maximum* membrane stress and the *maximum* bending stress (in terms of $\tau_\infty$, the shear stress "at infinity") at the edge of the hole as a function of $\mu$. As will be clear from Fig. 4.5.2 the values of $\varphi$ where these maxima are reached do not coincide.

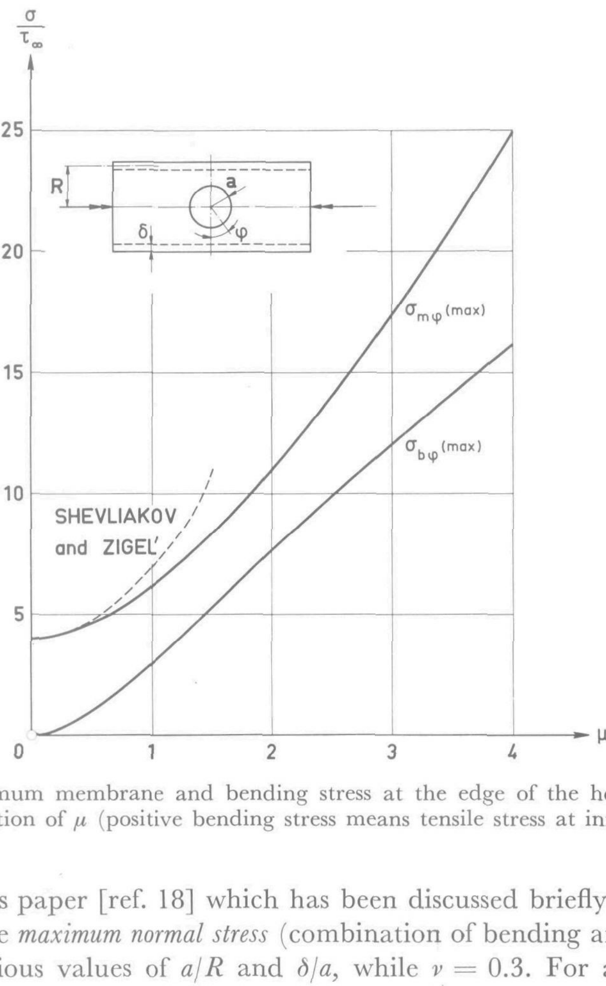


Fig. 4.5.1 Maximum membrane and bending stress at the edge of the hole in a tube in torsion as a function of $\mu$ (positive bending stress means tensile stress at inner surface)

In WITHUM's paper [ref. 18] which has been discussed briefly in Chapter 1 Fig. 8 gives the *maximum normal stress* (combination of bending and membrane stress) for various values of $a/R$ and $\delta/a$, while $\nu = 0.3$. For a given set of values $a/R$ and $\delta/a$, $\mu$ can easily be found. For $\nu = 0.3$ we have $\mu^2 = 0.826a^2/R\delta$. Comparing WITHUM's graph with the present results we find an excellent agreement.

In Fig. 4.5.1 also the results obtained by SHEVLIAKOV and ZIGEL' [ref. 14] are given as a dashed curve. This curve shows the membrane stresses at $\varphi = 45°$, determined by a method that is analogous to LUR'E's method, so these results are valid only for small values of $\mu$.

Fig. 4.5.2 gives the values of the membrane stress $\sigma_{m\varphi} = n_\varphi/\delta$ and the bending stress $\sigma_{b\varphi}$ at the edge of the hole for various values of $\mu$ as a function of $\varphi$. This figure shows clearly the above-mentioned shift of the place where the maximum value of $n_\varphi$ is reached. Fig. 4.5.2 may also be compared with

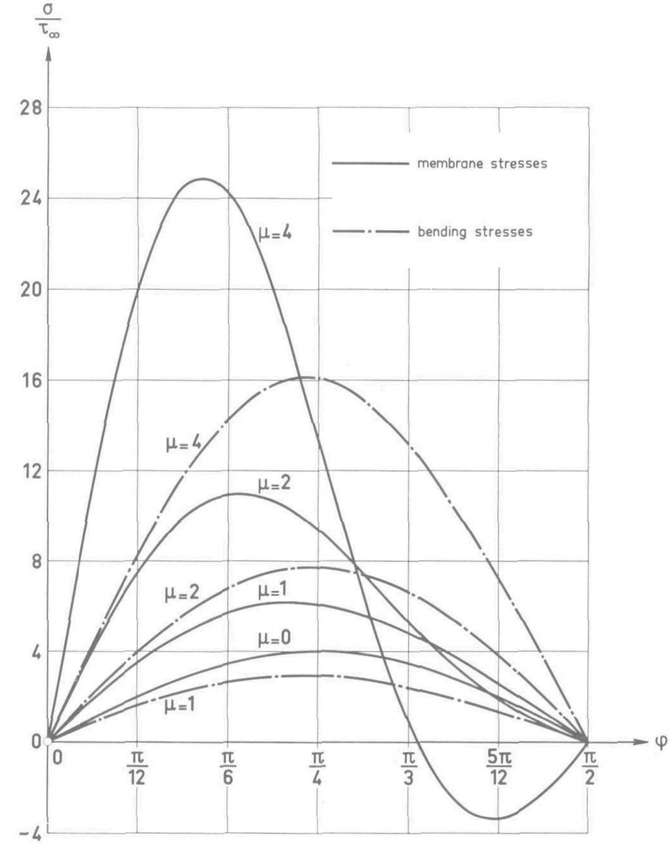


Fig. 4.5.2 Membrane and bending stresses at the edge of the hole in a tube in torsion as a function of $\varphi$ (positive bending stress means tensile stress at inner surface)

Withum's results. In his paper Fig. 7 shows a similar graph of the membrane stresses at the edge of the hole, while $\nu$ is assumed to be 0.3, for various values of $\xi_0$ viz. 0, 1, 2, 3, and 4. Withum's quantity $\xi_0$ corresponds to $\sqrt{2}\mu$ in the present treatise. His results appear to coincide completely with ours. From the graphs 4.5.1 and 4.5.2 we may conclude that large bending stresses occur if $\mu$ increases. Taken as a whole the influence of the curvature is larger in the case of torsion than in the case of axial tension. The stress concentration factor which is 4 if $\mu = 0$ is increased to a value of about 25 if $\mu = 4$, and if the bending stresses are also taken into account even to about 39. In the Figures 4.5.1 and 4.5.2 the sign of the bending stresses has been reversed in order to

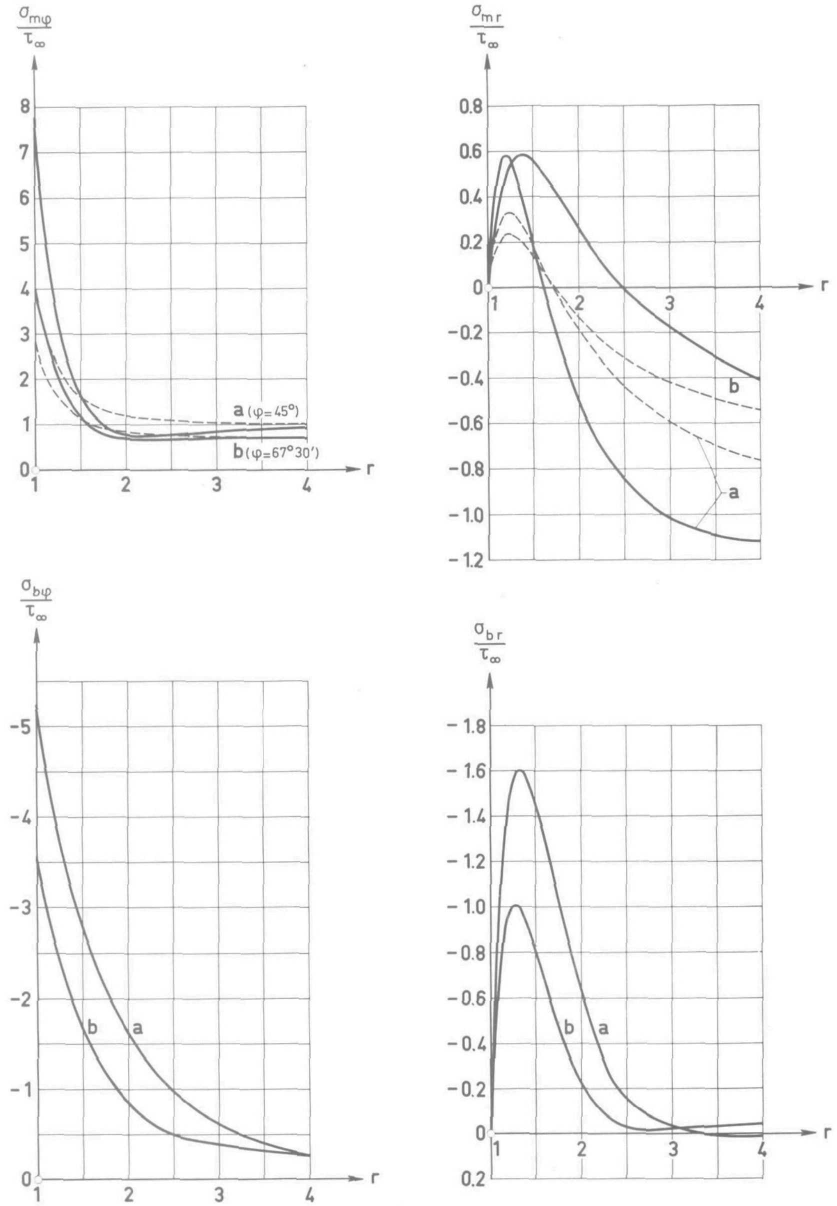


Fig. 4.5.3 Stresses in a tube in torsion as a function of $r$ in the case $\mu = 1.5$, compared with flat plate solution (positive bending stress means tensile stress at outer surface)

be in a position to compare the magnitude of membrane stresses and bending stresses respectively and to get a more compact graph. So in these graphs (in contrast with all other graphs in this chapter) a positive bending stress denotes a tensile stress at the inner surface of the cylinder.

Finally Fig. 4.5.3 shows stresses in the case $\mu = 1.5$ as a function of $r$ for two values of $\varphi$, viz. $\varphi = 45°$ (curves $a$) and $\varphi = 67°30'$ (curves $b$). For comparison also the stresses in a flat plate loaded by shear stresses at infinity have been given. Chapter 7 will also contain some graphs of this type together with experimentally obtained values.

CHAPTER 5

# GEOMETRIC BOUNDARY CONDITIONS

## 5.1 Determination of the tangential displacements

In the previous chapter we described the determination of the stress resultants and the normal displacement (and its derivatives). In order to deal with general boundary conditions, which may be geometric or of mixed type, it is necessary to know also the tangential displacements, $\bar{u}$ in $r$-direction and $\bar{v}$ in $\varphi$-direction.

In this section we shall only treat the doubly symmetric case. The dimensionless displacements

$$\left.\begin{aligned} u &= \frac{12(1-\nu^2)a}{\delta^2}\,\bar{u} \\ v &= \frac{12(1-\nu^2)a}{\delta^2}\,\bar{v} \end{aligned}\right\} \quad \ldots\ldots\ldots \quad (5.1.1)$$

must be calculated from a set of equations, given by application of Hooke's law,

$$\left.\begin{aligned} &\frac{\partial u}{\partial r} = \sum_{l=0}^{N} \bar{f}_l(r)\cos 2l\varphi \\ &\frac{1}{r}\frac{\partial v}{\partial \varphi} + \frac{u}{r} = \sum_{l=0}^{N} \bar{g}_l(r)\cos 2l\varphi \\ &\frac{1}{r}\frac{\partial u}{\partial \varphi} + \frac{\partial v}{\partial r} - \frac{v}{r} = \sum_{l=1}^{N} \bar{h}_l(r)\sin 2l\varphi \end{aligned}\right\} \quad \ldots\ldots\ldots \quad (5.1.2)$$

Here $\bar{f}_l(r)$, $\bar{g}_l(r)$ and $\bar{h}_l(r)$ are rather complicated functions (cf. equation (2.2.10) where stress-strain relations in Cartesian coordinates are given). In the sequel of this section we shall give specific expressions for these functions in terms of the functions $f_i$ $(i = 1 \ldots 8)$ defined in Section 4.2. The form of the equations (5.1.2) indicates that $u$ and $v$ may be written as

$$\left.\begin{aligned} u &= \sum_{l=0}^{N} U_l(r)\cos 2l\varphi \\ v &= \sum_{l=1}^{N} V_l(r)\sin 2l\varphi \end{aligned}\right\} \quad \ldots\ldots\ldots \quad (5.1.3)$$

As far as the coefficients for which $l = k$ is concerned, we must solve $U_k$ and $V_k$ from the equations

$$\left.\begin{aligned} &\frac{\mathrm{d}U_k}{\mathrm{d}r} = \bar{f}_k(r) \\ &\frac{2k}{r} V_k + \frac{1}{r} U_k = \bar{g}_k(r) \\ &-\frac{2k}{r} U_k + \frac{\mathrm{d}V_k}{\mathrm{d}r} - \frac{1}{r} V_k = \bar{h}_k(r) \end{aligned}\right\} \quad \ldots\ldots\ldots \quad (5.1.4)$$

Elimination of $U_k$ and $V_k$ from these equations yields the compatibility equation

$$4k^2\bar{f}_k + r\frac{\mathrm{d}\bar{f}_k}{\mathrm{d}r} - 2r\frac{\mathrm{d}\bar{g}_k}{\mathrm{d}r} - r^2\frac{\mathrm{d}^2\bar{g}_k}{\mathrm{d}r^2} + 2k\bar{h}_k + 2kr\frac{\mathrm{d}\bar{h}_k}{\mathrm{d}r} = 0 \quad . \; . \quad (5.1.5)$$

If this equation is satisfied we can easily solve (5.1.4). The first and the second equation yield

$$2k\frac{\mathrm{d}V_k}{\mathrm{d}r} = \bar{g}_k + r\frac{\mathrm{d}\bar{g}_k}{\mathrm{d}r} - \bar{f}_k$$

The second and the third equation give

$$\frac{4k^2-1}{r} V_k + \frac{\mathrm{d}V_k}{\mathrm{d}r} = 2k\bar{g}_k + \bar{h}_k$$

Elimination of $\mathrm{d}V_k/\mathrm{d}r$ from these equations gives finally

$$V_k = \frac{1}{2k}\left[r\bar{g}_k + \frac{r}{4k^2-1}\left\{\bar{f}_k - r\frac{\mathrm{d}\bar{g}_k}{\mathrm{d}r} + 2k\bar{h}_k\right\}\right] \quad \ldots\ldots \quad (5.1.6)$$

If we substitute this result in the second equation (5.1.4) we obtain

$$U_k = \frac{r}{1-4k^2}\left\{\bar{f}_k - r\frac{\mathrm{d}\bar{g}_k}{\mathrm{d}r} + 2k\bar{h}_k\right\} \quad \ldots\ldots\ldots \quad (5.1.7)$$

The result (5.1.7) is also valid for $k = 0$. The equations (5.1.4) then reduce to

$$\left.\begin{aligned} &\frac{\mathrm{d}U_0}{\mathrm{d}r} = \bar{f}_0(r) \\ &U_0 = r\bar{g}_0(r) \end{aligned}\right\} \quad \ldots\ldots\ldots \quad (5.1.8)$$

The second equation (5.1.8) gives immediately $U_0$. From (5.1.7) we find

$$U_0 = r\left\{\bar{f}_0 - r\frac{\mathrm{d}\bar{g}_0}{\mathrm{d}r}\right\} \quad \ldots\ldots\ldots \quad (5.1.9)$$

These results coincide, as can be seen, using the compatibility equation

$$\bar{g}_0 + r\frac{\mathrm{d}\bar{g}_0}{\mathrm{d}r} - \bar{f}_0 = 0 \quad \ldots\ldots\ldots \quad (5.1.10)$$

which is found if we eliminate $U_0$ from the equations (5.1.8).

Hooke's law is written in polar coordinates (cf. (2.1.4)) as follows.

$$\left.\begin{aligned}
\frac{\partial\bar{u}}{\partial\bar{r}} &= \frac{1}{E\delta}\{n_r - \nu n_\varphi\} + \frac{w}{R}\cos^2\varphi \\
\frac{1}{\bar{r}}\frac{\partial\bar{v}}{\partial\varphi} + \frac{\bar{u}}{\bar{r}} &= \frac{1}{E\delta}\{n_\varphi - \nu n_r\} + \frac{w}{R}\sin^2\varphi \\
\frac{1}{\bar{r}}\frac{\partial\bar{u}}{\partial\varphi} + \frac{\partial\bar{v}}{\partial\bar{r}} - \frac{\bar{v}}{\bar{r}} &= \frac{2(1+\nu)}{E\delta}n_{r\varphi} - 2\frac{w}{R}\sin\varphi\cos\varphi
\end{aligned}\right\} \quad . \; . \; . \; . \; (5.1.11)$$

From (5.1.11) and (4.2.8 . . . 14) the functions $\bar{f}_l(r)$, $\bar{g}_l(r)$ and $\bar{h}_l(r)$ introduced in (5.1.2) are determined. The result is as follows.

$$\left.\begin{aligned}
\bar{f}_0(r) &= \mu^2[\mathrm{Re}\sum_{n=0}^{\infty}(A_n+iB_n)\{f_1(0,n,\mu r) - \nu f_2(0,n,\mu r)\} + \\
&\quad + \mathrm{Im}\sum_{n=0}^{\infty}(A_n+iB_n)\{2f_7(0,n,\mu r) + f_7(1,n,\mu r)\}] \\
\bar{f}_1(r) &= \mu^2[\mathrm{Re}\sum_{n=0}^{\infty}(A_n+iB_n)\{f_1(1,n,\mu r) - \nu f_2(1,n,\mu r)\} + \\
&\quad + \mathrm{Im}\sum_{n=0}^{\infty}(A_n+iB_n)\{2f_7(0,n,\mu r) + 2f_7(1,n,\mu r) + f_7(2,n,\mu r)\}] \\
\bar{f}_l(r) &= \mu^2[\mathrm{Re}\sum_{n=0}^{\infty}(A_n+iB_n)\{f_1(l,n,\mu r) - \nu f_2(l,n,\mu r)\} + \\
&\quad + \mathrm{Im}\sum_{n=0}^{\infty}(A_n+iB_n)\{f_7(l-1,n,\mu r) + 2f_7(l,n,\mu r) + f_7(l+1,n,\mu r)\}] \\
&\qquad (l \geqslant 2)
\end{aligned}\right\} \quad (5.1.12)$$

$$\left.\begin{aligned}
\bar{g}_0(r) &= \mu^2[\mathrm{Re}\sum_{n=0}^{\infty}(A_n+iB_n)\{f_2(0,n,\mu r) - \nu f_1(0,n,\mu r)\} + \\
&\quad + \mathrm{Im}\sum_{n=0}^{\infty}(A_n+iB_n)\{2f_7(0,n,\mu r) - f_7(1,n,\mu r)\}] \\
\bar{g}_1(r) &= \mu^2[\mathrm{Re}\sum_{n=0}^{\infty}(A_n+iB_n)\{f_2(1,n,\mu r) - \nu f_1(1,n,\mu r)\} + \\
&\quad + \mathrm{Im}\sum_{n=0}^{\infty}(A_n+iB_n)\{-2f_7(0,n,\mu r) + 2f_7(1,n,\mu r) - f_7(2,n,\mu r)\}] \\
\bar{g}_l(r) &= \mu^2[\mathrm{Re}\sum_{n=0}^{\infty}(A_n+iB_n)\{f_2(l,n,\mu r) - \nu f_1(l,n,\mu r)\} + \\
&\quad + \mathrm{Im}\sum_{n=0}^{\infty}(A_n+iB_n)\{-f_7(l-1,n,\mu r) + 2f_7(l,n,\mu r) - f_7(l+1,n,\mu r)\}] \\
&\qquad (l \geqslant 2)
\end{aligned}\right\} \quad (5.1.13)$$

$$\left.\begin{aligned}\bar{h}_1(r) &= \mu^2[\mathrm{Re}\sum_{n=0}^{\infty}(A_n+iB_n)2(1+\nu)f_3(1,n,\mu r)+\\ &\quad+\mathrm{Im}\sum_{n=0}^{\infty}(A_n+iB_n)\{-4f_7(0,n,\mu r)+2f_7(2,n,\mu r)\}]\\ \bar{h}_l(r) &= \mu^2[\mathrm{Re}\sum_{n=0}^{\infty}(A_n+iB_n)\,2\,(1+\nu)f_3\,(l,n,\mu r)+\\ &\quad+\mathrm{Im}\sum_{n=0}^{\infty}(A_n+iB_n)\{-2f_7(l-1,n,\mu r)+2f_7(l+1,n,\mu r)\}]\\ &\hspace{20em}(l\geqslant 2)\end{aligned}\right\}\quad(5.1.14)$$

The function $r(\mathrm{d}\bar{g}_l/\mathrm{d}r)$ can be obtained, if we introduce in addition to the formulae (4.2.8a . . . 14a)

$$\left.\begin{aligned} f_9 &= f''-\frac{1+4l^2}{\mu r}f'+\frac{8l^2}{\mu^2r^2}f \qquad &&\left(=\mu r\frac{\partial f_1}{\partial(\mu r)}\right)\\ f_{10} &= \mu r f''' &&\left(=\mu r\frac{\partial f_2}{\partial(\mu r)}\right)\end{aligned}\right\}\quad . \; . \; . \;(5.1.15)$$

Differentiation of (5.1.13) and using (4.2.15) gives

$$\left.\begin{aligned} r\frac{\mathrm{d}\bar{g}_0}{\mathrm{d}r} &= \mu^2[\mathrm{Re}\sum_{n=0}^{\infty}(A_n+iB_n)\{f_{10}(0,n,\mu r)-\nu f_9(0,n,\mu r)\}+\\ &\quad+\mathrm{Im}\sum_{n=0}^{\infty}(A_n+iB_n)\{2\mu r f_8(0,n,\mu r)-\mu r f_8(1,n,\mu r)\}]\\ r\frac{\mathrm{d}\bar{g}_1}{\mathrm{d}r} &= \mu^2[\mathrm{Re}\sum_{n=0}^{\infty}(A_n+iB_n)\{f_{10}(1,n,\mu r)-\nu f_9(1,n,\mu r)\}+\\ &\quad+\mathrm{Im}\sum_{n=0}^{\infty}(A_n+iB_n)\{-2\mu r f_8(0,n,\mu r)+2\mu r f_8(1,n,\mu r)-\mu r f_8(2,n,\mu r)\}]\\ r\frac{\mathrm{d}\bar{g}_l}{\mathrm{d}r} &= \mu^2[\mathrm{Re}\sum_{n=0}^{\infty}(A_n+iB_n)\{f_{10}(l,n,\mu r)-\nu f_9(l,n,\mu r)\}+\\ &\quad+\mathrm{Im}\sum_{n=0}^{\infty}(A_n+iB_n)\{-\mu r f_8(l-1,n,\mu r)+2\mu r f_8(l,n,\mu r)-\mu r f_8(l+1,n,\mu r)\}]\\ &\hspace{26em}(l\geqslant 2)\end{aligned}\right\}\ (5.1.$$

The functions $\bar{f}$, $\bar{g}$ and $\bar{h}$ can now be calculated in a straightforward manner and substituted into (5.1.6) and (5.1.7). Although the calculation is somewhat lengthy, it is very useful in those cases where an integration procedure in order to solve (5.1.2) presents difficulties. Such a method of solution has been described by BIEZENO and GRAMMEL in their textbook "Technische Dynamik" [ref. 1, Chapter VI, 5] but is not appropriate here in view of the complicated character of the right-hand sides of (5.1.2).

## 5.2 Determination of influence matrices

If at the edge of the hole geometric boundary conditions must be satisfied, this may be done most easily if the influence coefficients for suitably chosen unit load systems along the boundary of the hole are known. In this section we shall calculate such influence coefficients for 14 different unit load systems, viz.

$$\left.\begin{aligned}
n_r &= \frac{E\delta^3}{12(1-\nu^2)a^2}\cos 2l\varphi && (l = 0^{1)},\ 1^{1)},\ 2,\ 3)\\
n_{r\varphi} &= \frac{E\delta^3}{12(1-\nu^2)a^2}\sin 2l\varphi && (l = 1^{1)},\ 2,\ 3)\\
d_r &= \frac{E\delta^4}{\{12(1-\nu^2)\}^{3/2}a^3}\cos 2l\varphi && (l = 1,\ 2,\ 3)\\
m_r &= \frac{E\delta^4}{\{12(1-\nu^2)\}^{3/2}a^2}\cos 2l\varphi && (l = 0,\ 1,\ 2,\ 3)
\end{aligned}\right\} \quad . \qquad (5.2.1)$$

For each of the 14 load systems (5.2.1) we solve a set of 14 equations as described in Section 4.2. The solutions enable us to calculate the 14 displacements corresponding to the 14 load systems. In view of the possibility to verify the result with the aid of Betti's theorem we multiply the tangential displacements by $\{12(1-\nu^2)\}a/\delta^2$, the normal displacement by $\sqrt{12(1-\nu^2)}/\delta$ and the slope by $a\sqrt{12(1-\nu^2)}/\delta$. So we determine the constants $A_n$ and $B_n$ from boundary conditions (4.2.19) with right-hand sides given by (5.2.1) and with the aid of these results

$$\left.\begin{aligned}
&U_k(1) \text{ for } k = 0, 1, 2, 3\\
&V_k(1) \text{ for } k = 1, 2, 3\\
W\quad &\operatorname{Im}\sum_{n=0}^{6}\,[(A_n+iB_n)f_7(k,n,\mu)] \text{ for } k = 1, 2, 3 \text{ (cf. (4.2.14))}\\
\alpha\quad &\operatorname{Im}\sum_{n=0}^{6}\,\mu[(A_n+iB_n)f_8(k,n,\mu)] \text{ for } k = 0, 1, 2, 3 \text{ (cf. (4.2.15))}
\end{aligned}\right\} \qquad (5.2.2)$$

We number the load systems consecutively from $i = 1$ to $i = 14$ and the displacement coefficients in (5.2.2) from $j = 1$ to $j = 14$. We then obtain a $14 \times 14$ matrix of influence coefficients $(a_{ij})$. This matrix must show certain symmetry properties in view of Betti's theorem. Let us consider for example the load system $i = 13$, i.e.

$$m_r = \frac{E\delta^4}{\{12(1-\nu^2)\}^{3/2}a^2}\cos 4\varphi \quad . \ . \ . \ . \ . \ . \ . \ . \ . \ . \ . \ . \ . \quad (5.2.3)$$

[1]) In this case the load system includes also a constant shear force in view of the equilibrium of the external load (cf. Section 4.2).

Suppose that among others an influence coefficient $a_{13,4}$ is determined, corresponding to a displacement

$$\bar{u} = \frac{\delta^2}{12(1-\nu^2)a} a_{13,4} \cos 6\varphi \quad \ldots\ldots\ldots\ldots\ldots \quad (5.2.4)$$

And suppose that in the case $i = 4$, i.e. a load

$$n_r = \frac{E\delta^3}{12(1-\nu^2)a^2} \cos 6\varphi \quad \ldots\ldots\ldots\ldots\ldots \quad (5.2.5)$$

an influence coefficient $a_{4,13}$ is found, corresponding to a rotation

$$\alpha = \frac{\delta}{\sqrt{12(1-\nu^2)}\,a} a_{4,13} \cos 4\varphi \quad \ldots\ldots\ldots\ldots\ldots \quad (5.2.6)$$

Applying Betti's theorem yields

$$a_{4,13} = a_{13,4} \quad \ldots\ldots\ldots\ldots\ldots\ldots\ldots\ldots \quad (5.2.7)$$

Observing an influence matrix one has to keep in mind, however, that not always $a_{ij} = a_{ji}$. In the first place they can differ in sign. This is clear, if we take into account the positive directions of the separate stress resultants and displacements as given in Fig. 3.5.1. In the second place they can differ by a factor 2 if we combine a load system that is a constant, e.g. $i = 11$, and a load system that varies as $\cos 2\varphi$, $\cos 4\varphi$ or $\cos 6\varphi$, e.g. $i = 9$. And finally if one applies Betti's theorem for $i = 1$, 2 and 5 one must keep in mind that in these cases also a constant shear force is acting on the edge of the hole.

A numerical example that will be treated in the sequel bears on the case $\mu = 1$. Table 5.2.1 gives the influence coefficients for this value of $\mu$. We may

Table 5.2.1 Influence coefficients $a_{ij}$ for $\mu = 1$ ($\nu = 0{,}3$)

| | $j$ | $i = 1$ | 2 | 3 | 4 | 5 | 6 | 7 |
|---|---|---|---|---|---|---|---|---|
| | 1 | −1.383187 | −0.909804 | 0.033186 | 0.000006 | 0.957075 | −0.033171 | −0.000 |
| | 2 | −0.165547 | −3.189718 | 0.003213 | 0.000348 | 2.766051 | −0.002827 | −0.000 |
| u | 3 | 0.013527 | −0.023209 | −0.607667 | −0.002040 | 0.000438 | 0.345580 | 0.002 |
| | 4 | 0.000026 | 0.000355 | −0.002040 | −0.365063 | −0.000232 | 0.000357 | 0.179 |
| | 5 | 0.180794 | 2.726403 | −0.025985 | −0.000225 | −3.193713 | 0.025713 | 0.000 |
| | 6 | −0.013491 | 0.023598 | 0.345580 | 0.000357 | −0.000712 | −0.605185 | −0.000 |
| V | 7 | −0.000026 | −0.000355 | 0.002045 | 0.179038 | 0.000233 | −0.000360 | −0.3647 |
| | 8 | 0.210417 | 0.215206 | −0.005062 | −0.000016 | −0.220353 | 0.005039 | 0.000 |
| W | 9 | −0.000411 | 0.009257 | 0.011593 | −0.000039 | 0.002538 | −0.011626 | 0.000 |
| | 10 | 0.000006 | −0.000004 | 0.001381 | 0.001966 | −0.000007 | 0.000588 | −0.001 |
| | 11 | −0.563565 | −0.164462 | −0.004497 | 0.000004 | 0.159324 | 0.004497 | −0.000 |
| dw | 12 | −0.045956 | 0.020049 | −0.002988 | 0.000025 | −0.023884 | 0.003012 | −0.000 |
| dr | 13 | −0.001821 | 0.013381 | −0.000586 | −0.000041 | −0.013486 | 0.000546 | 0.000 |
| | 14 | 0.000035 | −0.000026 | 0.001500 | −0.001783 | −0.000041 | −0.003275 | 0.0017 |

$N_r$ $N_{r\varphi}$

summarize the results of this section by giving the formulae that express the displacements of the hole boundary caused by a given load. Let the load be

$$\left.\begin{aligned} n_r &= A_1 + A_2\cos 2\varphi + A_3\cos 4\varphi + A_4\cos 6\varphi \\ n_{r\varphi} &= A_5\sin 2\varphi + A_6\sin 4\varphi + A_7\sin 6\varphi \\ d_r &= A_8\cos 2\varphi + A_9\cos 4\varphi + A_{10}\cos 6\varphi \\ m_r &= a(A_{11} + A_{12}\cos 2\varphi + A_{13}\cos 4\varphi + A_{14}\cos 6\varphi) \end{aligned}\right\} \quad . \; . \qquad (5.2.8)$$

Then the displacement components and the slope are given by

$$\left.\begin{aligned} \bar{u} &= \frac{\delta^2}{12(1-\nu^2)a} \sum_{j=1}^{4} \left[\frac{12(1-\nu^2)a^2}{E\delta^3} \sum_{i=1}^{7} A_i a_{ij} + \frac{\{12(1-\nu^2)\}^{3/2}a^3}{E\delta^4} \sum_{i=8}^{14} A_i a_{ij}\right] \cos 2(j-1)\varphi \\ \bar{v} &= \frac{\delta^2}{12(1-\nu^2)a} \sum_{j=5}^{7} \left[\frac{12(1-\nu^2)a^2}{E\delta^3} \sum_{i=1}^{7} A_i a_{ij} + \frac{\{12(1-\nu^2)\}^{3/2}a^3}{E\delta^4} \sum_{i=8}^{14} A_i a_{ij}\right] \sin 2(j-4)\varphi \\ w &= \frac{\delta}{\sqrt{12(1-\nu^2)}} \sum_{j=8}^{10} \left[\frac{12(1-\nu^2)a^2}{E\delta^3} \sum_{i=1}^{7} A_i a_{ij} + \frac{\{12(1-\nu^2)\}^{3/2}a^3}{E\delta^4} \sum_{i=8}^{14} A_i a_{ij}\right] \cos 2(j-7)\varphi \\ \alpha &= \frac{\delta}{\sqrt{12(1-\nu^2)}a} \sum_{j=11}^{14} \left[\frac{12(1-\nu^2)a^2}{E\delta^3} \sum_{i=1}^{7} A_i a_{ij} + \frac{\{12(1-\nu^2)\}^{3/2}a^3}{E\delta^4} \sum_{i=8}^{14} A_i a_{ij}\right] \cos 2(j-11)\varphi \end{aligned}\right\} \qquad (5.2.9)$$

## 5.3 Influence matrices for the end-section of a transverse pipe

We shall use the influence matrices established in the previous section in the investigation of the stresses and displacements in the neighbourhood of the

$q_r$ $M_r$

| 8 | 9 | 10 | 11 | 12 | 13 | 14 |
|---|---|---|---|---|---|---|
| 0.215806 | 0.000328 | −0.000006 | 0.727612 | 0.202004 | −0.001522 | 0.000038 |
| 0.325804 | −0.009134 | 0.000001 | 0.962252 | 0.245031 | 0.012770 | −0.000005 |
| 0.005062 | −0.011593 | −0.001381 | −0.008994 | −0.002988 | −0.000586 | 0.001500 |
| 0.000016 | 0.000039 | −0.001966 | 0.000008 | 0.000025 | −0.000041 | −0.001783 |
| 0.330951 | −0.002660 | 0.000010 | −0.972529 | −0.248865 | −0.012875 | −0.000062 |
| 0.005039 | 0.011626 | −0.000588 | 0.008994 | 0.003012 | 0.000546 | −0.003275 |
| 0.000016 | −0.000038 | 0.001967 | −0.000008 | −0.000025 | 0.000041 | 0.001782 |
| 0.085211 | −0.000348 | 0.000003 | −0.039954 | 0.059295 | 0.001474 | −0.000017 |
| 0.000348 | 0.011989 | −0.000007 | 0.000404 | −0.000056 | 0.023276 | 0.000041 |
| 0.000003 | −0.000007 | 0.003673 | −0.000003 | −0.000000 | −0.000002 | 0.011962 |
| 0.019977 | −0.000202 | 0.000002 | −0.805220 | −0.045771 | 0.000860 | −0.000009 |
| 0.059295 | 0.000056 | 0.000000 | −0.091541 | −0.357614 | −0.000208 | −0.000002 |
| 0.001474 | −0.023276 | 0.000002 | 0.001720 | −0.000208 | −0.192575 | −0.000009 |
| 0.000017 | −0.000041 | −0.011962 | −0.000019 | −0.000002 | −0.000009 | −0.132296 |

connection of a transverse cylindrical pipe to a cylindrical shell. We shall restrict ourselves to the case that the axis of this pipe passes through the axis of the shell at a right angle. If the radius of the cross-section of the pipe is small with respect to the radius of the shell, the intersection is approximately a geodetic circle in the shell surface. In order to express the requirement that the displacements and slopes of the end-section of the pipe and the edge of the circular hole in the shell coincide it is convenient to determine first influence coefficients for the edge of the pipe for unit loads analogous to those we applied in the previous section.

It is in this case not admissible to make use of shallow shell equations, since the stresses and displacements will in general be such, that they cannot be considered as rapidly changing. Especially an edge load varying as $\cos 2\varphi$ is not capable of analysis by shallow shell theory.

Since we restricted ourselves to cases that the diameter of the pipe is small with respect to that of the shell, the end-section of the pipe is approximately a normal cross-section. The question arises whether a good approximation is obtained if we for sake of simplicity determine influence coefficients for a normal cross-section of a half-infinite pipe. The error introduced will in principle be of the order $a/R$. However, the investigation of VAN DER NEUT [ref. 9] of oblique end-sections warrants the conjecture that the approximation will be even better. It is possible to obtain a rigorous solution for the actual pipe by a laborious calculation, but since this does not lie within the scope of the present treatise, we shall confine ourselves here to the above-mentioned approximation. It will give at least an insight in the solution of the problem under discussion.

The stress resultants $M$, $T$, $D$ and $S$ (Fig. 5.3.1) are considered to be expressed

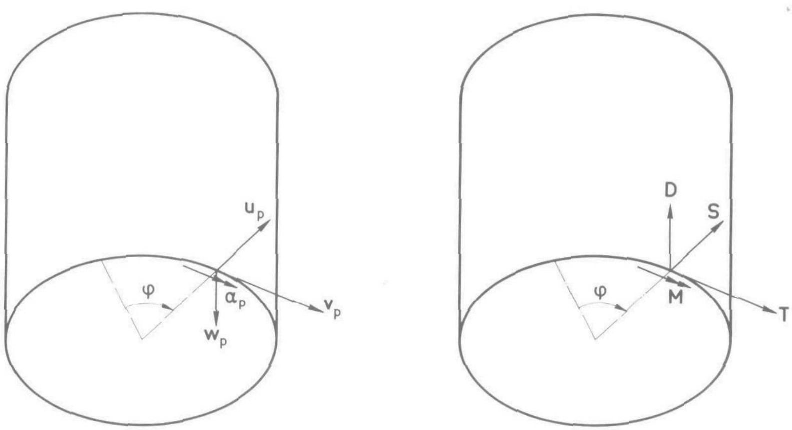


Fig. 5.3.1 Displacements and stress resultants at the end-section of a transverse pipe

as Fourier series in $\varphi$. In the doubly symmetric case they contain only terms of the shape $\cos 2n\varphi$ (for $T$: $\sin 2n\varphi$). The positive direction has been chosen such that $S$ must be set equal to the edge load $n_r$ of the shell (which is only approximately correct in view of the local obliqueness of the end-section), $T$ to $n_{r\varphi}$, $D$ to $d_r$ and $M$ to $m_r$. The displacements are chosen such that they will have to coincide (approximately) with the corresponding displacements of the hole boundary of the shell.

The influence coefficients have been determined following the well-known method described among others in "Technische Dynamik" by BIEZENO and GRAMMEL [ref. 1, Chapter VI, 21]. The wall-thickness of the pipe being $h$, the calculation has been performed for $a/h = 10$ and 20. Poisson's ratio $\nu$ has been assumed to be 0.3. We give here a result corresponding to that in Section 5.2, viz. a $14 \times 14$ matrix $(b_{ij})$. If a load is given by (cf. (5.2.8))

$$\left.\begin{aligned} S &= A_1 + A_2\cos 2\varphi + A_3\cos 4\varphi + A_4\cos 6\varphi \\ T &= A_5\sin 2\varphi + A_6\sin 4\varphi + A_7\sin 6\varphi \\ D &= A_8\cos 2\varphi + A_9\cos 4\varphi + A_{10}\cos 6\varphi \\ M &= a(A_{11} + A_{12}\cos 2\varphi + A_{13}\cos 4\varphi + A_{14}\cos 6\varphi) \end{aligned}\right\} \quad . \; . \quad (5.3.1)$$

the displacement components (cf. Fig. 5.3.1) are

$$\left.\begin{aligned} u_p &= \frac{1}{E}\sum_{j=1}^{4}\sum_{i=1}^{14} A_i b_{ij}\cos 2(j-1)\varphi \\ v_p &= \frac{1}{E}\sum_{j=5}^{7}\sum_{i=1}^{14} A_i b_{ij}\sin 2(j-4)\varphi \\ w_p &= \frac{1}{E}\sum_{j=8}^{10}\sum_{i=1}^{14} A_i b_{ij}\cos 2(j-7)\varphi \\ \alpha_p &= \frac{1}{aE}\sum_{j=11}^{14}\sum_{i=1}^{14} A_i b_{ij}\cos 2(j-11)\varphi \end{aligned}\right\} \quad . \; . \; . \; . \; . \; . \; . \; . \quad (5.3.2)$$

The matrices $(b_{ij})$ are symmetric apart from the sign of $w_p$. They are given in the Tables 5.3.1 and 5.3.2 [1]).

## 5.4 Stresses due to internal pressure

We are now in a position to calculate the stresses in a cylindrical shell to which a transverse pipe is connected, if the loading is such that doubly symmetrical stresses occur. Other cases of symmetry may be dealt with in an analogous way and will not be considered here. An example that will be dealt with in this section is loading by internal pressure.

[1]) p. 62–63

Table 5.3.1 Influence coefficients $b_{ij}$ for a transverse pipe $(a/h = 10)$

| $j$ | $i = 1$ | 2 | 3 | 4 | 5 | 6 | 7 |
|---|---|---|---|---|---|---|---|
| 1 | 81.2963 | – | – | – | – | – | – |
| 2 | – | 1085.23 | – | – | −505.440 | – | – |
| 3 | – | – | 152.154 | – | – | −33.1229 | – |
| 4 | – | – | – | 45.1249 | – | – | − 6.6 |
| 5 | – | −505.440 | – | – | 253.654 | – | – |
| 6 | – | – | − 33.1229 | – | – | 12.6391 | – |
| 7 | – | – | – | − 6.61719 | – | – | 4.3 |
| 8 | – | − 97.7132 | – | – | 48.7159 | – | – |
| 9 | – | – | − 9.45559 | – | – | 3.80134 | – |
| 10 | – | – | – | − 1.99984 | – | – | 1.4 |
| 11 | −330.454 | – | – | – | – | – | – |
| 12 | – | −871.134 | – | – | 296.123 | – | – |
| 13 | – | – | −367.838 | – | – | 60.1838 | – |
| 14 | – | – | – | −171.829 | – | – | 19.4 |

Table 5.3.2 Influence coefficients $b_{ij}$ for a transverse pipe $(a/h = 20)$

| $j$ | $i = 1$ | 2 | 3 | 4 | 5 | 6 | 7 |
|---|---|---|---|---|---|---|---|
| 1 | 229.941 | – | – | – | – | – | – |
| 2 | – | 6095.669 | – | – | −2917.83 | – | – |
| 3 | – | – | 1042.34 | – | – | −228.921 | – |
| 4 | – | – | – | 345.290 | – | – | −49.3 |
| 5 | – | −2917.83 | – | – | 1450.12 | – | – |
| 6 | – | – | − 228.921 | – | – | 63.3168 | – |
| 7 | – | – | – | − 49.3765 | – | – | 14.2 |
| 8 | – | − 422.002 | – | – | 208.126 | – | – |
| 9 | – | – | − 58.8417 | – | – | 16.3967 | – |
| 10 | – | – | – | − 14.2615 | – | – | 4.3 |
| 11 | −1321.82 | – | – | – | – | – | – |
| 12 | – | −3796.67 | – | – | 1279.46 | – | – |
| 13 | – | – | −2342.58 | – | – | 372.285 | – |
| 14 | – | – | – | −1290.09 | – | – | 136.7 |

We first determine the displacements and the slope at the hole boundary if the shell is loaded by an internal pressure of $p$ units of force per unit of area, while the hole boundary is subjected to stress resultants that are the same as would occur in an unweakened shell, viz.

$$\left.\begin{aligned} n_r &= 0.75pR + 0.25pR\cos 2\varphi \\ n_{r\varphi} &= -0.25pR\sin 2\varphi \\ d_r &= 0 \\ m_r &= 0 \end{aligned}\right\} \quad \ldots\ldots\ldots \quad (5.4.1)$$

The displacements and the slope in that case are

| 8 | 9 | 10 | 11 | 12 | 13 | 14 |
|---|---|---|---|---|---|---|
| – | – | – | −330.454 | – | – | – |
| 97.7132 | – | – | – | −871.134 | – | – |
| – | 9.45559 | – | – | – | −367.838 | – |
| – | – | 1.99984 | – | – | – | −171.829 |
| 48.7159 | – | – | – | 296.123 | – | – |
| – | − 3.80134 | – | – | – | 60.1838 | – |
| – | – | − 1.45683 | – | – | – | 19.4421 |
| 22.7280 | – | – | – | 84.6313 | – | – |
| – | − 5.76558 | – | – | – | 22.9485 | – |
| – | – | − 3.44520 | – | – | – | 7.48902 |
| – | – | – | 2686.47 | – | – | – |
| 84.6313 | – | – | – | 2932.55 | – | – |
| – | −22.9485 | – | – | – | 2242.90 | – |
| – | – | − 7.48902 | – | – | – | 1568.28 |

| 8 | 9 | 10 | 11 | 12 | 13 | 14 |
|---|---|---|---|---|---|---|
| – | – | – | − 1321.82 | – | – | – |
| 22.002 | – | – | – | −3796.67 | – | – |
| – | 58.8417 | – | – | – | −2342.58 | – |
| – | – | 14.2615 | – | – | – | −1290.09 |
| 08.126 | – | – | – | 1279.46 | – | – |
| – | − 16.3967 | – | – | – | 372.285 | – |
| – | – | − 4.37075 | – | – | – | 136.752 |
| 65.3498 | – | – | – | 286.974 | – | – |
| – | − 14.4740 | – | – | – | 133.927 | – |
| – | – | − 7.43399 | – | – | – | 53.2896 |
| – | – | – | 15196.97 | – | – | – |
| 86.974 | – | – | – | 16218.32 | – | – |
| – | −133.927 | – | – | – | 15330.5 | – |
| – | – | −53.2896 | – | – | – | 11993.6 |

$$\left.\begin{aligned} u_s &= \frac{apR}{E\delta}\left\{\frac{3(1-\nu)}{4}+\frac{1+\nu}{4}\cos 2\varphi\right\} \\ v_s &= -\frac{apR}{E\delta}\frac{1+\nu}{4}\sin 2\varphi \\ w_s &= \left(1-\frac{\nu}{2}\right)\frac{pR^2}{E\delta} \\ \alpha_s &= 0 \end{aligned}\right\} \quad \ldots\ldots\ldots \quad (5.4.2)$$

Corresponding with the foregoing the transverse pipe (radius $a$, wall thickness $h$) is subjected to internal pressure $p$ and an edge load

$$\left.\begin{aligned} S &= 0.75pR + 0.25pR\cos 2\varphi \\ T &= -0.25pR\sin 2\varphi \\ D &= 0 \\ M &= 0 \end{aligned}\right\} \quad \ldots\ldots\ldots \quad (5.4.3)$$

The displacements and the slope at the end-section of the pipe are (and the nomenclature is analogous to that indicated in Fig. 5.3.1)

$$\left.\begin{aligned} u_e &= \left(1-\frac{\nu}{2}\right)\frac{pa^2}{Eh} + \frac{pR}{E}\{0.75b_{1,1} + 0.25(b_{2,2}-b_{5,2})\cos 2\varphi\} \\ v_e &= 0.25\frac{pR}{E}(b_{2,5}-b_{5,5})\sin 2\varphi \\ w_e &= 0.25\frac{pR}{E}(b_{2,8}-b_{5,8})\cos 2\varphi \\ \alpha_e &= \frac{pR}{aE}\{0.75b_{1,11} + 0.25(b_{2,12}-b_{5,12})\cos 2\varphi\} \end{aligned}\right\} \quad (5.4.4)$$

Obviously (5.4.4) can only be used if the approximation indicated in Section 5.3 is applied. If the influence coefficients of the actual end-section of the pipe are determined more correctly they will in general *all* be different from zero. Apart from the first term of the expression for $u_e$, originating from the internal pressure in the pipe, (5.4.4) must then be replaced by (5.3.2) after identifying (5.3.1) with (5.4.3).

The displacement components (5.4.2) and (5.4.4) do not coincide. In order to achieve compatibility an additional edge load is required. This edge load exerted by the shell upon the pipe and inversely by the pipe upon the shell is a self-equilibrating system. Let it be given by (5.3.1) and (5.2.8) respectively. Then the equations that express the compatibility are

$$\left.\begin{aligned} \bar{u} + u_s &= u_p + u_e \\ \bar{v} + v_s &= v_p + v_e \\ w + w_s &= w_p + w_e \\ \alpha + \alpha_s &= \alpha_p + \alpha_e \end{aligned}\right\} \quad \ldots\ldots\ldots\ldots\ldots \quad (5.4.5)$$

Apparently the constant normal displacement $w_s$ does not play a role and must be ignored.

Since each term of the Fourier series for the displacements and the slope, obtained if we substitute (5.2.9), (5.3.3), (5.4.2) and (5.4.4) in (5.4.5) must vanish, we obtain 14 equations for the 14 unknowns $A_1 \ldots A_{14}$. If these equations are solved, the stresses and displacements in the cylindrical shell may be determined following the method described in Section 4.2.

Table 5.4.1

| | $a/h = 10$, $a/\delta = 6$, $R/a = 4.957$ | $a/h = 20$, $a/\delta = 6$, $R/a = 4.957$ |
|---|---|---|
| $u_s E/pR$ | $3.15 + 1.95 \cos 2\varphi$ | $3.15 + 1.95 \cos 2\varphi$ |
| $u_e E/pR$ | $62.6870 + 397.6675 \cos 2\varphi$ | $175.8854 + 2253.375 \cos 2\varphi$ |
| $v_s E/pR$ | $- 1.95 \sin 2\varphi$ | $- 1.95 \sin 2\varphi$ |
| $v_e E/pR$ | $- 189.7735 \sin 2\varphi$ | $- 1091.9875 \sin 2\varphi$ |
| $w_s E/pR$ | $0$ | $0$ |
| $w_e E/pR$ | $- 36.6073 \cos 2\varphi$ | $- 157.532 \cos 2\varphi$ |
| $\alpha_s aE/pR$ | $0$ | $0$ |
| $\alpha_e aE/pR$ | $-247.8405 - 291.814 \cos 2\varphi$ | $-991.365 - 1269.031 \cos 2\varphi$ |

| | $a/h = 10$, $a/\delta = 12$, $R/a = 9.914$ | $a/h = 20$, $a/\delta = 12$, $R/a = 9.914$ |
|---|---|---|
| $u_s E/pR$ | $6.3 + 3.9 \cos 2\varphi$ | $6.3 + 3.9 \cos 2\varphi$ |
| $u_e E/pR$ | $61.8296 + 397.6675 \cos 2\varphi$ | $174.1706 + 2253.375 \cos 2\varphi$ |
| $v_s E/pR$ | $- 3.9 \sin 2\varphi$ | $- 3.9 \sin 2\varphi$ |
| $v_e E/pR$ | $- 189.7735 \sin 2\varphi$ | $- 1091.9875 \sin 2\varphi$ |
| $w_s E/pR$ | $0$ | $0$ |
| $w_e E/pR$ | $- 36.6073 \cos 2\varphi$ | $- 157.532 \cos 2\varphi$ |
| $\alpha_s aE/pR$ | $0$ | $0$ |
| $\alpha_e aE/pR$ | $-247.8405 - 291.814 \cos 2\varphi$ | $-991.365 - 1269.031 \cos 2\varphi$ |

| | $a/h = 10$, $a/\delta = 18$, $R/a = 14.870$ | $a/h = 20$, $a/\delta = 18$, $R/a = 14.870$ |
|---|---|---|
| $u_s E/pR$ | $9.45 + 5.85 \cos 2\varphi$ | $9.45 + 5.85 \cos 2\varphi$ |
| $u_e E/pR$ | $61.5438 + 397.6675 \cos 2\varphi$ | $173.5990 + 2253.375 \cos 2\varphi$ |
| $v_s E/pR$ | $- 5.85 \sin 2\varphi$ | $- 5.85 \sin 2\varphi$ |
| $v_e E/pR$ | $- 189.7735 \sin 2\varphi$ | $- 1091.9875 \sin 2\varphi$ |
| $w_s E/pR$ | $0$ | $0$ |
| $w_e E/pR$ | $- 36.6073 \cos 2\varphi$ | $- 157.532 \cos 2\varphi$ |
| $\alpha_s aE/pR$ | $0$ | $0$ |
| $\alpha_e aE/pR$ | $-247.8405 - 291.814 \cos 2\varphi$ | $-991.365 - 1269.031 \cos 2\varphi$ |

We shall now illustrate this with some numerical results. They bear on the case $\mu = 1$. The geometry of the shell, being described by two parameters, is not yet determined by $\mu$ alone. We chose three values of $a/\delta$ consecutively, viz. 6, 12 and 18, and in each case two values of the ratio of radius to wall thickness $a/h$ of the transverse pipe, viz. 10 and 20. Table 5.4.1 shows in each of these 6 cases the values of the displacements (5.4.2) of the hole boundary of the shell and (5.4.4) of the end-section of the pipe. Table 5.4.2 shows the solutions $A_1 \ldots A_{14}$ of the equations (5.4.5) in each case. The Fourier series are truncated at cos $6\varphi$ and sin $6\varphi$ and the numerical values obtained indicate that the truncation procedure is again completely justified.

The Tables 5.4.3 ... 8 show the stress resultants, stress couples and displacements of the shell at the hole boundary. These are the final values, i.e. the forces, couples and displacements as indicated by (5.4.1) and (5.4.2) combined with those arising from the edge loads corresponding to the solutions that are given in Table 5.4.2 [1]).

In order to estimate the stiffening influence of the transverse pipe we calculated also the stresses in the case that there is no reinforcing by a pipe and the shell is loaded by internal pressure. Of course in this case there is a transverse shear force acting on the edge of the hole in order to ensure the equilibrium. Apart from this shear force the hole boundary is free. This problem has also been dealt with by LUR'E [refs. 5 and 6]. The results obtained, viz. the stress resultants, stress couples and displacements at the hole boundary in the three cases $a/\delta = 6$, 12 and 18 are given in the Tables 5.4.9 ... 11 [1]).

Table 5.4.2

| | $a/h = 10$<br>$a/\delta = 6$<br>$R/a = 4.957$ | $a/h = 10$<br>$a/\delta = 12$<br>$R/a = 9.914$ | $a/h = 10$<br>$a/\delta = 18$<br>$R/a = 14.87$ | $a/h = 20$<br>$a/\delta = 6$<br>$R/a = 4.957$ | $a/h = 20$<br>$a/\delta = 12$<br>$R/a = 9.914$ | $a/h = 20$<br>$a/\delta = 18$<br>$R/a = 14.87$ |
|---|---|---|---|---|---|---|
| $A_1/pR$ | −0.563502 | −0.505614 | −0.455043 | −0.670704 | −0.602549 | −0.583279 |
| $A_2/pR$ | −0.368925 | −0.401486 | −0.408346 | −0.299404 | −0.351146 | −0.368369 |
| $A_3/pR$ | −0.003428 | −0.005820 | −0.004980 | −0.001122 | −0.003185 | −0.433268 |
| $A_4/pR$ | −0.000003 | −0.000009 | −0.000008 | 0.000009 | −0.000021 | −0.000013 |
| $A_5/pR$ | 0.025266 | −0.065771 | −0.102848 | −0.166340 | 0.056452 | 0.015651 |
| $A_6/pR$ | −0.003170 | −0.007658 | −0.008173 | −0.001566 | −0.006785 | −0.009678 |
| $A_7/pR$ | 0.000109 | 0.000123 | 0.000129 | 0.000074 | 0.000123 | 0.000119 |
| $A_8/pR$ | 0.124891 | 0.067304 | 0.062529 | 0.122700 | 0.073449 | 0.051505 |
| $A_9/pR$ | 0.014595 | 0.011878 | 0.013295 | 0.008553 | 0.008146 | 0.006893 |
| $A_{10}/pR$ | 0.000065 | 0.000083 | 0.000077 | 0.000024 | 0.000043 | 0.000045 |
| $A_{11}/pR$ | 0.024932 | 0.015627 | 0.009354 | 0.009647 | 0.013947 | 0.011028 |
| $A_{12}/pR$ | −0.012500 | −0.013126 | −0.008775 | −0.003323 | −0.009248 | −0.009570 |
| $A_{13}/pR$ | 0.000878 | −0.001639 | −0.001415 | −0.000149 | −0.000583 | −0.000859 |
| $A_{14}/pR$ | −0.000000 | −0.000002 | −0.000001 | 0.000000 | 0.000001 | 0.000000 |

[1]) In these tables the quantities $u$ and $v$ devote the final *dimensional* displacements $\bar{u}+u_s$ and $\bar{v}+v_s$ respectively.

Table 5.4.3

| $a/h = 10$ $\quad a/\delta = 6$ | | | | | |
|---|---|---|---|---|---|
| | $l = 0$ | $l = 1$ | $l = 2$ | $l = 3$ | multiplied by |
| $n_r$ | 0.186498 | − 0.118925 | −0.003428 | 0.000003 | $pR$ cos $2l\varphi$ |
| $n_\varphi$ | 1.822995 | − 1.293492 | −0.042543 | −0.000423 | $pR$ cos $2l\varphi$ |
| $n_{r\varphi}$ | 0 | − 0.224734 | −0.003170 | 0.000109 | $pR$ sin $2l\varphi$ |
| $d_r$ | −0.076722 | 0.124891 | 0.014595 | 0.000065 | $pR$ cos $2l\varphi$ |
| $m_r$ | 0.149591 | − 0.074999 | −0.005270 | 0.000002 | $pR\delta$ cos $2l\varphi$ |
| $m_\varphi$ | 0.059130 | − 0.016201 | −0.001330 | 0.000006 | $pR\delta$ cos $2l\varphi$ |
| $w$ | | − 3.2240 | −0.0839 | 0.0000 | $(pR/E)$ cos $2l\varphi$ |
| $\alpha$ | 5.3491 | −10.1752 | −1.2349 | −0.0001 | $(pR/aE)$ cos $2l\varphi$ |
| $u$ | 8.6376 | 7.6215 | 0.0445 | −0.0005 | $(pR/E)$ cos $2l\varphi$ |
| $v$ | | − 6.6810 | −0.0349 | 0.0004 | $(pR/E)$ sin $2l\varphi$ |

Table 5.4.4

| $a/h = 10$ $\quad a/\delta = 12$ | | | | | |
|---|---|---|---|---|---|
| | $l = 0$ | $l = 1$ | $l = 2$ | $l = 3$ | multiplied by |
| $n_r$ | 0.244386 | − 0.151486 | −0.005820 | −0.000009 | $pR$ cos $2l\varphi$ |
| $n_\varphi$ | 1.577112 | − 0.926934 | −0.016720 | −0.000012 | $pR$ cos $2l\varphi$ |
| $n_{r\varphi}$ | 0 | − 0.315771 | −0.007658 | 0.000123 | $pR$ sin $2l\varphi$ |
| $d_r$ | − 0.033967 | 0.067304 | 0.011878 | 0.000083 | $pR$ cos $2l\varphi$ |
| $m_r$ | 0.187520 | − 0.157513 | −0.019672 | −0.000027 | $pR\delta$ cos $2l\varphi$ |
| $m_\varphi$ | 0.033815 | − 0.043113 | −0.006473 | −0.000006 | $pR\delta$ cos $2l\varphi$ |
| $w$ | | − 3.2215 | −0.0802 | −0.0001 | $(pR/E)$ cos $2l\varphi$ |
| $\alpha$ | −38.7778 | − 5.7311 | −2.2696 | −0.0001 | $(pR/aE)$ cos $2l\varphi$ |
| $u$ | 15.5612 | 13.2176 | 0.0888 | −0.0007 | $(pR/E)$ cos $2l\varphi$ |
| $v$ | | −10.6952 | −0.0478 | 0.0004 | $(pR/E)$ sin $2l\varphi$ |

Table 5.4.5

| $a/h = 10$ $\quad a/\delta = 18$ | | | | | |
|---|---|---|---|---|---|
| | $l = 0$ | $l = 1$ | $l = 2$ | $l = 3$ | multiplied by |
| $n_r$ | 0.294957 | − 0.158346 | −0.004980 | −0.000008 | $pR$ cos $2l\varphi$ |
| $n_\varphi$ | 1.493285 | − 0.811106 | −0.010745 | 0.000055 | $pR$ cos $2l\varphi$ |
| $n_{r\varphi}$ | 0 | − 0.352848 | −0.008173 | 0.000129 | $pR$ sin $2l\varphi$ |
| $d_r$ | − 0.030654 | 0.062529 | 0.013295 | 0.000077 | $pR$ cos $2l\varphi$ |
| $m_r$ | 0.168370 | − 0.157947 | −0.025468 | −0.000020 | $pR\delta$ cos $2l\varphi$ |
| $m_\varphi$ | 0.031905 | − 0.042801 | −0.007886 | −0.000006 | $pR\delta$ cos $2l\varphi$ |
| $w$ | | − 3.4069 | −0.0676 | 0.0000 | $(pR/E)$ cos $2l\varphi$ |
| $\alpha$ | −72.3410 | 4.1936 | −2.0371 | 0.0017 | $(pR/aE)$ cos $2l\varphi$ |
| $u$ | 21.4595 | 18.2182 | 0.1173 | −0.0009 | $(pR/E)$ cos $2l\varphi$ |
| $v$ | | −14.0961 | −0.0572 | 0.0005 | $(pR/E)$ sin $2l\varphi$ |

Table 5.4.6

| $a/h = 20 \quad a/\delta = 6$ | | | | | |
|---|---|---|---|---|---|
| | $l = 0$ | $l = 1$ | $l = 2$ | $l = 3$ | multiplied by |
| $n_r$ | 0.079296 | − 0.049404 | −0.001122 | 0.000009 | $pR \cos 2l\varphi$ |
| $n_\varphi$ | 2.283982 | − 1.836676 | −0.063576 | −0.000426 | $pR \cos 2l\varphi$ |
| $n_{r\varphi}$ | 0 | − 0.083660 | −0.001566 | 0.000074 | $pR \sin 2l\varphi$ |
| $d_r$ | − 0.091145 | 0.122700 | 0.008553 | 0.000024 | $pR \cos 2l\varphi$ |
| $m_r$ | 0.057882 | − 0.019937 | −0.000895 | 0.000002 | $pR\delta \cos 2l\varphi$ |
| $m_\varphi$ | 0.114102 | 0.012955 | 0.000354 | −0.000001 | $pR\delta \cos 2l\varphi$ |
| $w$ | | − 5.5351 | −0.1034 | 0.0000 | $(pR/E) \cos 2l\varphi$ |
| $\alpha$ | 41.7904 | −13.9598 | −1.3857 | 0.0006 | $(pR/aE) \cos 2l\varphi$ |
| $u$ | 8.9114 | 7.3491 | 0.0415 | −0.0006 | $(pR/E) \cos 2l\varphi$ |
| $v$ | | − 6.9522 | −0.0380 | 0.0005 | $(pR/E) \sin 2l\varphi$ |

Table 5.4.7

| $a/h = 20 \quad a/\delta = 12$ | | | | | |
|---|---|---|---|---|---|
| | $l = 0$ | $l = 1$ | $l = 2$ | $l = 3$ | multiplied by |
| $n_r$ | 0.147451 | − 0.101146 | −0.003185 | 0.000021 | $pR \cos 2l\varphi$ |
| $n_\varphi$ | 1.866441 | − 1.328952 | −0.021349 | 0.000012 | $pR \cos 2l\varphi$ |
| $n_{r\varphi}$ | 0 | − 0.193548 | −0.006785 | 0.000123 | $pR \sin 2l\varphi$ |
| $d_r$ | − 0.040669 | 0.073449 | 0.008146 | 0.000043 | $pR \cos 2l\varphi$ |
| $m_r$ | 0.167368 | − 0.110972 | −0.006993 | 0.000014 | $pR\delta \cos 2l\varphi$ |
| $m_\varphi$ | 0.060080 | − 0.041665 | −0.003934 | 0.000005 | $pR\delta \cos 2l\varphi$ |
| $w$ | | − 5.0522 | −0.1198 | 0.0000 | $(pR/E) \cos 2l\varphi$ |
| $\alpha$ | 17.0542 | −34.6778 | −5.0904 | 0.0013 | $(pR/aE) \cos 2l\varphi$ |
| $u$ | 17.1839 | 14.2936 | 0.0809 | −0.0010 | $(pR/E) \cos 2l\varphi$ |
| $v$ | | −12.6594 | −0.0511 | 0.0007 | $(pR/E) \sin 2l\varphi$ |

Table 5.4.8

| $a/h = 20 \quad a/\delta = 18$ | | | | | |
|---|---|---|---|---|---|
| | $l = 0$ | $l = 1$ | $l = 2$ | $l = 3$ | multiplied by |
| $n_r$ | 0.166721 | − 0.118369 | −0.004333 | 0.000013 | $pR \cos 2l\varphi$ |
| $n_\varphi$ | 1.739714 | − 1.143627 | −0.011109 | 0.000123 | $pR \cos 2l\varphi$ |
| $n_{r\varphi}$ | 0 | − 0.234349 | −0.009678 | 0.000119 | $pR \sin 2l\varphi$ |
| $d_r$ | − 0.026068 | 0.051505 | 0.006893 | 0.000045 | $pR \cos 2l\varphi$ |
| $m_r$ | 0.198504 | − 0.172258 | −0.015466 | 0.000007 | $pR\delta \cos 2l\varphi$ |
| $m_\varphi$ | 0.045975 | − 0.051853 | −0.006093 | 0.000003 | $pR\delta \cos 2l\varphi$ |
| $w$ | | − 4.9344 | −0.1186 | 0.0000 | $(pR/E) \cos 2l\varphi$ |
| $\alpha$ | −52.7824 | −20.4222 | −7.5484 | 0.0023 | $(pR/aE) \cos 2l\varphi$ |
| $u$ | 24.9021 | 20.3228 | 0.1177 | −0.0014 | $(pR/E) \cos 2l\varphi$ |
| $v$ | | −17.4187 | −0.0538 | 0.0009 | $(pR/E) \sin 2l\varphi$ |

Table 5.4.9

| no pipe | $a/\delta = 6$ | | | | |
|---|---|---|---|---|---|
| | $l = 0$ | $l = 1$ | $l = 2$ | $l = 3$ | multiplied by |
| $n_\varphi$ | 2.640900 | $-$ 2.289606 | $-0.252035$ | $-0.000527$ | $pR \cos 2l\varphi$ |
| $d_r$ | $-$ 0.100871 | 0 | 0 | 0 | $pR \cos 2l\varphi$ |
| $m_\varphi$ | 0.138686 | 0.300243 | 0.004568 | 0.000043 | $pR\delta \cos 2l\varphi$ |
| $w$ | | $-31.72782$ | $-0.16312$ | $-0.00061$ | $(pR/E) \cos 2l\varphi$ |
| $\alpha$ | 59.91239 | 2.79373 | 0.63654 | $-0.00356$ | $(pR/aE) \cos 2l\varphi$ |
| $u$ | 12.17466 | 11.62861 | $-0.02540$ | $-0.00100$ | $(pR/E) \cos 2l\varphi$ |
| $v$ | | $-11.64375$ | 0.02424 | 0.00100 | $(pR/E) \sin 2l\varphi$ |

Table 5.4.10

| no pipe | $a/\delta = 12$ | | | | |
|---|---|---|---|---|---|
| | $l = 0$ | $l = 1$ | $l = 2$ | $l = 3$ | multiplied by |
| $n_\varphi$ | 2.640900 | $-$ 2.289606 | $-0.252035$ | $-0.000527$ | $pR \cos 2l\varphi$ |
| $d_r$ | $-$ 0.050436 | 0 | 0 | 0 | $pR \cos 2l\varphi$ |
| $m_\varphi$ | 0.138686 | 0.300243 | 0.004568 | 0.000043 | $pR\delta \cos 2l\varphi$ |
| $w$ | | $-126.91128$ | $-0.65249$ | $-0.00244$ | $(pR/E) \cos 2l\varphi$ |
| $\alpha$ | 239.64955 | 11.17492 | $-2.54614$ | $-0.01422$ | $(pR/aE) \cos 2l\varphi$ |
| $u$ | 24.34932 | 23.25722 | $-0.05080$ | $-0.00199$ | $(pR/E) \cos 2l\varphi$ |
| $v$ | | $-23.28749$ | 0.04849 | 0.00200 | $(pR/E) \sin 2l\varphi$ |

Table 5.4.11

| no pipe | $a/\delta = 18$ | | | | |
|---|---|---|---|---|---|
| | $l = 0$ | $l = 1$ | $l = 2$ | $l = 3$ | multiplied by |
| $n_\varphi$ | 2.640900 | $-$ 2.289606 | $-0.252035$ | $-0.000527$ | $pR \cos 2l\varphi$ |
| $d_r$ | $-0.033624$ | 0 | 0 | 0 | $pR \cos 2l\varphi$ |
| $m_\varphi$ | 0.138686 | 0.300243 | 0.004568 | 0.000043 | $pR\delta \cos 2l\varphi$ |
| $w$ | | $-285.55038$ | $-1.46810$ | $-0.00548$ | $(pR/E) \cos 2l\varphi$ |
| $\alpha$ | 539.21150 | 25.14358 | $-5.72882$ | $-0.03201$ | $(pR/aE) \cos 2l\varphi$ |
| $u$ | 36.52398 | 34.88584 | $-0.07620$ | $-0.00299$ | $(pR/E) \cos 2l\varphi$ |
| $v$ | | $-34.93124$ | 0.07274 | 0.00300 | $(pR/E) \sin 2l\varphi$ |

In Table 5.4.12 some interesting results are collected illustrating the influence of the transverse pipe. For each of the cases investigated this table gives the *maximum value* of the membrane stresses $\sigma_{mr}$ $(= n_r/\delta)$ and $\sigma_{m\varphi}$ $(= n_\varphi/\delta)$, the bending stresses $\sigma_{br}$ $(= 6m_r/\delta^2)$ and $\sigma_{b\varphi}$ $(= 6m_\varphi/\delta^2)$, the normal displacement component $w$ (the non-essential constant term has been omitted) and the tangential displacement component $u$. These maximum values have been determined using the data given in the Tables 5.4.3 ... 11 and for more detailed information these tables must be consulted. It may be remarked, for example, that the place where a membrane stress reaches its maximum value does not always coincide with the place where the corresponding bending stress reaches its maximum value. But this may be investigated in each separate case by means of the Tables 5.4.3 ... 11. From Table 5.4.12 we see that in particular $w$ is reduced considerably by the presence of the pipe, whereas $u$ is affected less. This is plausible since the pipe offers less resistance against displacements perpendicular to its surface than against axial displacements. The maximum value of $\sigma_{m\varphi}$ in the case that there is no pipe is found to be $4.68pR/\delta$. We may compare this result with LUR'E's whose analysis yields a maximum value of $4.82pR/\delta$, which is only 3% too high, or maybe it is more appropriate to say that LUR'E overestimates the influence of the curvature by 6%. At larger values of $\mu$ the inaccuracy of LUR'E's analysis will obviously be larger.

Table 5.4.12

| | $a/\delta = 6$ | | | $a/\delta = 12$ | | | $a/\delta = 18$ | | | |
|---|---|---|---|---|---|---|---|---|---|---|
| | no pipe | $a/h=20$ | $a/h=10$ | no pipe | $a/h=20$ | $a/h=10$ | no pipe | $a/h=20$ | $a/h=10$ | |
| max. of $\sigma_{mr}$ | 0 | 0.13 | 0.30 | 0 | 0.25 | 0.39 | 0 | 0.28 | 0.45 | $pR/\delta$ |
| max. of $\sigma_{m\varphi}$ | 4.68 | 4.06 | 3.07 | 4.68 | 3.17 | 2.49 | 4.68 | 2.87 | 2.29 | $pR/\delta$ |
| max. of $\sigma_{br}$ | 0 | 0.48 | 1.32 | 0 | 1.63 | 1.95 | 0 | 2.13 | 1.81 | $pR/\delta$ |
| max. of $\sigma_{b\varphi}$ | 2.66 | 0.77 | 0.43 | 2.66 | 0.59 | 0.42 | 2.66 | 0.55 | 0.40 | $pR/\delta$ |
| max. of $w$ | 31.9 | 5.6 | 3.3 | 127.6 | 5.2 | 3.3 | 287.0 | 5.0 | 3.5 | $pR/E$ |
| max. of $u$[1]) | 23.8 | 16.3 | 16.3 | 47.6 | 31.6 | 28.9 | 71.3 | 45.3 | 39.8 | $pR/E$ |

The presence of a transverse pipe evidently reduces the stress concentration factor appreciably. In order to assess the effect of the curvature in this case, we have to compare the results collected in Table 5.4.12 (evaluated for $\mu = 1$) with the similar results for a flat plate of thickness $\delta$, weakened by a circular hole of radius $a$ to which a transverse pipe of thickness $h$ is attached. The plate is stretched at infinity in the direction $\varphi = 0$ by forces $pR$ per unit length and in the direction $\varphi = \pi/2$ by forces $^1/_2 pR$ per unit length. Table 5.4.13 shows the membrane stresses, bending stresses, normal displacement component $w$ and radial displacement component $u$ (normal to the surface of the transverse pipe) at the edge of the hole.

If no pipe is present no bending stresses occur. It is clear that if the pipe is rigid, i.e. if the plate is clamped at the hole boundary there will be no bending

[1]) Cf. note on p. 66.

either. This fact explains the phenomenon that the magnitude of the bending stresses, *increasing* if the wall thickness of the pipe increases from $a/20$ to $a/10$ in the case that the plate thickness is relatively large ($a/\delta = 6$), *decreases* if the plate thickness is smaller ($a/\delta = 12$ and 18).

Table 5.4.13

| | $a/\delta = 6$ | | | $a/\delta = 12$ | | | $a/\delta = 18$ | | | |
|---|---|---|---|---|---|---|---|---|---|---|
| | no pipe | $a/h=20$ | $a/h=10$ | no pipe | $a/h=20$ | $a/h=10$ | no pipe | $a/h=20$ | $a/h=10$ | |
| max. of $\sigma_{mr}$ | 0 | 0.11 | 0.21 | 0 | 0.15 | 0.31 | 0 | 0.20 | 0.40 | $pR/\delta$ |
| max. of $\sigma_{m\varphi}$ | 2.5 | 2.30 | 2.09 | 2.5 | 2.20 | 1.90 | 2.5 | 2.12 | 1.73 | $pR/\delta$ |
| max. of $\sigma_{br}$ | 0 | 0.27 | 0.48 | 0 | 0.44 | 0.33 | 0 | 0.39 | 0.20 | $pR/\delta$ |
| max. of $\sigma_{b\varphi}$ | 0 | 0.22 | 0.32 | 0 | 0.23 | 0.19 | 0 | 0.18 | 0.12 | $pR/\delta$ |
| max. of $w$ | 0 | 0.004 | 0.005 | 0 | 0.001 | 0.001 | 0 | 0.000 | 0.000 | $pR/E$ |
| max. of $u$ [1]) | 14.1 | 13.4 | 12.7 | 28.2 | 26.2 | 23.8 | 42.3 | 38.4 | 33.5 | $pR/E$ |

[1]) Cf. note on p. 66.

# CHAPTER 6

# INACCURACIES DUE TO THE APPROXIMATIVE CHARACTER OF THE THEORY

## 6.1 Introductory remarks

The analysis developed in the preceding chapters is of an approximate character. In this chapter we shall investigate whether any *essential* errors in the results, i.e. errors that do not vanish if the ratios $a/R$ and $\delta/a$ tend to zero, must be anticipated. These investigations will at the same time give an insight in the accuracy obtained, if these ratios are finite. The following causes of inaccuracies will be discussed.

A. The analysis is based on shallow shell theory, and it is a well-known fact that the validity of the shallow shell equations depends both on the geometry of the shell and on the type of loading. In the next section we shall investigate the resulting inaccuracy by determining qualitatively the influence of the terms that have been neglected in FLÜGGE's general equations.

B. The replacement of the actual cylindrical shell by a spiral shell model introduces errors. In order to study these errors, we may close the shell along the generator opposite to the hole centre, i.e. the line for which the circumferential angle $\vartheta$ (cf. Fig. 2.1.2) is equal to $\pi$ or $-\pi$, and determine the stresses originating therefrom. The inaccuracies due to the spiral shell model will be admissible if along this generator stresses and displacements are present that are small to a degree to be specified. This will be discussed in Section 6.3.

Anticipating the results of the following sections we mention here already that neither the use of shallow shell equations nor the application of the spiral shell model introduces essential errors.

We may finally note here, that it cannot be expected that the analysis is accurate if stresses or displacements appear to change very rapidly, that is if the wave-length of the deformation pattern is of the order of magnitude of the wall thickness. In fact such a state of stress can never be described by the conventional shell theories. It may be shown, however, that each solution found has a meaning within any desired accuracy if $\delta/a$ is sufficiently small. In this connection it should be remembered that the geometry of the shell is described by two parameters, the ratios $\delta/a$ and $a/R$. So we have one of these ratios at our free disposal, if $\mu$ is given. And since a solution found, for some value of $\mu$, yields stresses and displacements that depend on the non-dimensional coordinates, we can always choose $\delta/a$ sufficiently small in order to obtain a shell geometry for which the solution is correct within any desired accuracy.

## 6.2 Inaccuracy due to shallow shell theory

In the system of equilibrium equations for cylindrical shells given by FLÜGGE [ref. 2, p. 219, eq. (13a–c)] a number of terms must be neglected, in order to obtain a system that corresponds with shallow shell theory. Our solution of the shallow shell equations may now also be regarded as a solution of FLÜGGE's more complete equations provided that additional surface loads are applied equivalent to FLÜGGE's additional terms in his equations, evaluated for our solution. The accuracy of our solution based on shallow shell theory may now be assessed by estimating the stresses due to a "corrective" load opposite to the additional surface loads to be removed.

The equilibrium equations that are equivalent to the shallow shell equations are the unnumbered equations following equation (14) [ref. 2, p. 219]. These equations have been established using the approximate expressions (12a–f) on page 217 for the stress resultants and stress couples, which are equivalent to those that have been applied in the present analysis (cf. (2.1.1), (2.1.4) and (2.1.8)). This may easily be seen, using Table 6.2.1 [1]) which gives the transcription from the quantities used by FLÜGGE to the quantities used here.

This table enables us also to establish the expressions for the components $\bar{p}_x$, $\bar{p}_y$ and $\bar{p}_n$ in $x$-, $y$- and normal direction respectively of the corrective load.

$$\left.\begin{aligned}
\bar{p}_x &= \frac{E\delta^3}{12(1-\nu^2)R^4}\left[\frac{1-\nu}{2}\frac{R^2}{a^2}\frac{\partial^2\bar{\xi}}{\partial y^2}+\frac{R^3}{a^3}\frac{\partial^3 w}{\partial x^3}-\frac{1-\nu}{2}\frac{R^3}{a^3}\frac{\partial^3 w}{\partial x\partial y^2}\right]\\
\bar{p}_y &= \frac{E\delta^3}{12(1-\nu^2)R^4}\left[\frac{3(1-\nu)}{2}\frac{R^2}{a^2}\frac{\partial^2\bar{\eta}}{\partial x^2}+\frac{1-\nu}{2}\frac{R^3}{a^3}\frac{\partial^3 w}{\partial x^2\partial y}-\frac{R^3}{a^3}\frac{\partial^3 w}{\partial y^3}\right]\\
\bar{p}_n &= \frac{E\delta^3}{12(1-\nu^2)R^4}\left[\frac{1-\nu}{2}\frac{R^3}{a^3}\frac{\partial^3\bar{\xi}}{\partial x\partial y^2}-\frac{R^3}{a^3}\frac{\partial^3\bar{\xi}}{\partial x^3}+\right.\\
&\qquad\left.-\frac{3-\nu}{2}\frac{R^3}{a^3}\frac{\partial^3\bar{\eta}}{\partial x^2\partial y}-2\frac{R^2}{a^2}\frac{\partial^2 w}{\partial y^2}-w\right]
\end{aligned}\right\}\quad(6.2.1)$$

We shall first estimate the magnitude of these loads expressed in terms of the order of magnitude of the membrane and bending stresses, previously calculated. Let $\sigma$ denote the latter order of magnitude, given by $E\delta^2/a^2$ multiplied by a second derivative of $\Psi$ (cf. (2.2.5) and (2.2.6)).

From (4.2.6), (4.2.7) and (4.2.16), the latter formulae giving derivatives with respect to $\mu r$, it follows that by differentiation of $\Psi$ with respect to $x$, $y$ or $r$ the order of magnitude is multiplied by $\mu$. If, however, $\mu$ is small the order

[1]) p. 74.

Table 6.2.1

| FLÜGGE's notation | Present notation |
|---|---|
| $a$ | $R$ |
| $t$ | $\delta$ |
| $u$ | $\bar{\xi}$ |
| $v$ | $\bar{\eta}$ |
| $w$ | $-w$ |
| $(\ )'$ | $R\dfrac{\partial}{\partial\bar{x}} = \dfrac{R}{a}\,\dfrac{\partial}{\partial x}$ |
| $(\ )^{\cdot}$ | $R\dfrac{\partial}{\partial\bar{y}} = \dfrac{R}{a}\,\dfrac{\partial}{\partial y}$ |

of magnitude is unaltered. So we must in the following discussion distinguish between two cases, viz. $\mu$ is large and $\mu$ is not large. We have

$$\partial\Psi/\partial x,\ \partial\Psi/\partial y = \left\{\begin{array}{ll} O\{\mu\Psi\} & \text{(if } \mu \text{ is large)} \\ O\{\Psi\} & \text{(if } \mu \text{ is not large)} \end{array}\right\} \quad . \quad . \quad . \quad . \quad (6.2.2)$$

The dominating terms in the expressions for $\bar{\bar{p}}_x$ and $\bar{\bar{p}}_y$ are those that originate from third derivatives of $w$. Their order of magnitude is $E\delta^4/a^3R$ multiplied by a third derivative of $\Psi$. So

$$\bar{\bar{p}}_x,\ \bar{\bar{p}}_y = \left\{\begin{array}{ll} O\{\delta^2\mu\sigma/aR\} & \text{(if } \mu \text{ is large)} \\ O\{\delta^2\sigma/aR\} & \text{(if } \mu \text{ is not large)} \end{array}\right\} \quad . \quad . \quad . \quad . \quad (6.2.3)$$

The leading three terms of $\bar{\bar{p}}_n$ are of the order of magnitude of $E\delta^5/a^4R$ multiplied by a fourth derivative of $\Psi$. As compared with $\sigma$ this is $O\{\delta^3\mu^2\sigma/a^2R\} = O\{\delta^2\sigma/R^2\}$, if $\mu$ is large, and $O\{\delta^3\sigma/a^2R\}$ if $\mu$ is not large. The fourth term of the expression for $\bar{\bar{p}}_n$ is of order of magnitude $E\delta^4/a^2R^2$ multiplied by a second derivative of $\Psi$, and hence $O\{\delta^2\sigma/R^2\}$. This is the same result as we obtained for the leading three terms if $\mu$ is large. If $\mu$ is not large these three terms are dominating over the fourth one. The fifth (last) term of the expression is of a smaller order of magnitude, and we may conclude

$$\bar{\bar{p}}_n = \left\{\begin{array}{ll} O\{\delta^2\sigma/R^2\} & \text{(if } \mu \text{ is large)} \\ O\{\delta^3\sigma/a^2R\} & \text{(if } \mu \text{ is not large)} \end{array}\right\} \quad . \quad . \quad . \quad . \quad (6.2.4)$$

The distribution of this corrective load depends on the non-dimensional coordinates $x$ and $y$. Let us assume that it has no resultant force or that at least the resultant force is completely canceled by the boundary loads at the edge $\bar{r} = a$, if we use FLÜGGE's expressions for the stress resultants at the edge. We shall return to this assumption later. A consequence is that this load causes membrane stresses and bending stresses that decay at infinity.

The order of magnitude of the stresses due to the corrective load may be

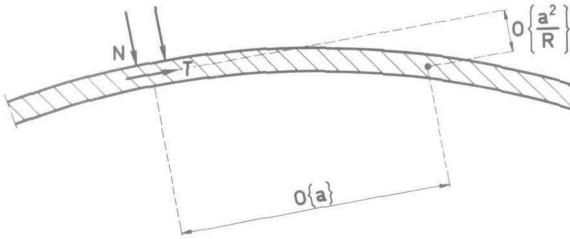

Fig. 6.2.1 Order of magnitude of loads and distances

estimated as follows. On a finite part of the shell surface we have a load that has a normal component $N$ and a tangential component $T$ that are of the order of magnitude of $a^2\bar{p}_n$ and $a^2\bar{p}_x$ or $a^2\bar{p}_y$ respectively. $N$ and $T$ cause bending stresses that are of the order of magnitude of $Na/\delta^2 a$ and $Ta^2/R\delta^2 a$ respectively and membrane stresses that are of the order of magnitude $(NR/a)/\delta a$ and $T/\delta a$ respectively.

We may now construct Table 6.2.2 which gives the order of magnitude of these stresses in both cases $\mu$ is large and $\mu$ is not large.

Table 6.2.2

| | $\mu$ is large | $\mu$ is not large |
|---|---|---|
| bending stresses caused by $N$ | $O\left\{\frac{a^2}{R^2}\sigma\right\}$ | $O\left\{\frac{\delta}{R}\sigma\right\}$ |
| bending stresses caused by $T$ | $O\left\{\frac{a^2}{R^2}\mu\sigma\right\}$ | $O\left\{\frac{a^2}{R^2}\sigma\right\} = O\left\{\frac{\delta}{R}\mu^2\sigma\right\}$ |
| membrane stresses caused by $N$ | $O\left\{\frac{\delta}{R}\sigma\right\}$ | $O\left\{\frac{\delta^2}{a^2}\sigma\right\}$ |
| membrane stresses caused by $T$ | $O\left\{\frac{\delta}{R}\mu\sigma\right\}$ | $O\left\{\frac{\delta}{R}\sigma\right\}$ |

The stresses that are of the order of magnitude of $\delta\sigma/R$ do not introduce errors that are larger than those introduced by Flügge's equations. Hence if $\mu$ is not large (that is of the order of magnitude of 1 or smaller) the inaccuracies do not exceed those of Flügge's equations. If $\mu$ is large, however, the neglections made correspond to the neglection of $\mu a^2/R^2$ with respect to 1, and we must as a consequence require that $a/R$ is small.

There may still be some doubt that the corrective load at large distance from the hole causes stresses in the vicinity of the origin that exceed those we just investigated. We shall therefore estimate the magnitudes of the resultant forces and moments of the corrective load acting of the part $x \geqslant x_0$ of the shell, where $x_0$ is positive and large.

The axial resultant force of the loads $\bar{p}_x$ in the region $x \geqslant x_0$ is equal to the resultant of the membrane forces $n_x$ along the arc $x = x_0$ if we write these membrane forces according to FLÜGGE's expressions in the form

$$n_x = \frac{E\delta^3}{12(1-\nu^2)a^2} \operatorname{Re} \frac{\partial^2 \Psi}{\partial y^2} + \frac{E\delta^3}{12(1-\nu^2)a^2 R} \frac{\partial^2 w}{\partial x^2} \quad \ldots \ldots \quad (6.2.5)$$

Only the second term contributes to the resultant since the first term is the expression used in the present analysis. This second term is of the order $\delta^2\sigma_0/R$ and so the axial resultant of these forces causes membrane stresses in the vicinity of the hole that are at most of order $\delta\sigma_0/R$, where $\sigma_0$ is the order of magnitude of the stresses at $x = x_0$. In a similar way we may estimate the stresses originating from the resulting moment about the axis of the cylinder. This moment is due to the loads $\bar{p}_y$ and the corrective stresses are again at most of order $\delta\sigma_0/R$.

The remaining resulting forces and moments decay even exponentially if $x_0$ increases. The way in which this may be shown will be illustrated by the determination of the resulting force in the direction of the normal to the shell surface in the origin.

The solution $\Psi$ of our basic equation tends to zero exponentially if $r$ tends to infinity, except in a region along the $x$-axis, where $\Psi$ tends to zero as $r^{-1/2}$. If $x$ is large and positive we may write (cf. (3.1.13))

$$\Psi = e^{\mu x \sqrt{i}} \Sigma \, \tilde{B}_n e^{in\varphi} \sqrt{2/\pi\mu r} \, e^{-i\{\mu r \sqrt{(-i)} - (3/8 + n/2)\pi\}} \quad \ldots \ldots \quad (6.2.6)$$

We may briefly note some properties of this function. If $x$ (large) is held constant, the function decreases with increasing $|y|$, and if the order of magnitude of $|y|$ exceeds $O\{\sqrt{x}\}$, it decreases even exponentially. Differentiation with respect to $x$ means multiplication by $\mu\sqrt{i}\,(1 - \sin\varphi)$, or somewhat more precisely

$$\frac{\partial \Psi}{\partial x} = \mu\sqrt{i}\,(1 - \sin\varphi)\, \Psi + O\{\Psi/r\} \quad \ldots \ldots \quad (6.2.7)$$

Differentiation with respect to $y$ gives

$$\frac{\partial \Psi}{\partial y} = \mu\sqrt{i}\,(\cos\varphi)\, \Psi + O\{\Psi/r\} \quad \ldots \ldots \quad (6.2.8)$$

We shall now determine the resultant in the direction of the normal to the shell surface in the origin of the corrective load *on a strip of width* d$x$. This resultant is

$$a^2\, \mathrm{d}x \int_{-\infty}^{+\infty} \left\{ \bar{p}_n \cos\left(\frac{ay}{R}\right) + \bar{p}_y \sin\left(\frac{ay}{R}\right) \right\} \mathrm{d}y \quad \ldots \ldots \quad (6.2.9)$$

The contribution of the regions, for which $O\{|y|\} > O\{\sqrt{x}\}$, tends exponentially to zero with increasing $x$. In the region $O\{|y|\} \leqslant O\{\sqrt{x}\}$ we have $|y| \ll x$, so the deviation of $\varphi$ from $\pi/2$ tends to zero with increasing $x$, and we may conclude that the dominating term in (6.2.9) originates from the last term in the expression for $\bar{\bar{p}}_n$ (6.2.1), all other terms containing derivatives of $\Psi$. We shall show that its contribution tends to zero *exponentially*. Therefore we must show that $\int_0^\infty \Psi \cos(ay/R)\mathrm{d}y$ tends to zero exponentially if $x$ increases. We substitute (6.2.6), keeping in mind that in the region $O\{|y|\} \leqslant O\{\sqrt{x}\}$ the change in value of $\varphi$ and $\sqrt{r}$ is negligible. So

$$\left.\begin{aligned} &\int_0^\infty \Psi \cos\left(\frac{ay}{R}\right)\mathrm{d}y = \\ &= \sum \left\{\tilde{B}_n e^{in\pi/2} \sqrt{\frac{2}{\pi\mu x}}\, e^{i(3/8+n/2)\pi}\right\} \int_0^\infty e^{-1/2\mu\sqrt{i}y^2/x} \cos\left(\frac{ay}{R}\right)\mathrm{d}y = \\ &= \sum \{\tilde{B}_n e^{in\pi}\}\, e^{i\pi/4}\, \frac{1}{\mu}\, e^{-a^2x/2R^2\mu\sqrt{i}} \end{aligned}\right\} \quad (6.2.10)$$

Here we made use of an integral that is known in the theory of Fourier transforms,

$$\int_0^\infty e^{-bu^2}\cos(ut)\mathrm{d}u = {}^1/_2 \sqrt{\frac{\pi}{b}}\, e^{-t^2/4b} \;\; ^{1)} \quad \ldots\ldots\ldots\ldots \quad (6.2.11)$$

The factor $\sin(ay/R)$ instead of $\cos(ay/R)$ in the second term of the integrand in (6.2.9) does not disturb this proof since we have the similar integral

$$\int_0^\infty e^{-bu^2}\sin(ut)\mathrm{d}u = -\frac{i}{2}\sqrt{\frac{\pi}{b}}\, e^{-t^2/4b}\, \mathrm{Erf}\left(\frac{i}{2}\, t\sqrt{b}\right) \quad \ldots\ldots \quad (6.2.12)$$

from which follows

$$\left.\begin{aligned} &\int_0^\infty \Psi \sin\left(\frac{ay}{R}\right)\mathrm{d}y = \\ &= \sum \{\tilde{B}_n e^{in\pi}\} e^{i\pi/4}\, \frac{1}{\mu}\, e^{-a^2x/2R^2\mu\sqrt{i}}\, \mathrm{Erf}\left(\frac{i^{5/4}}{2\sqrt{2}}\, \frac{a\sqrt{\mu}}{R\sqrt{x}}\right) \end{aligned}\right\} \quad (6.2.13)$$

Integration with respect to $x$ from $x_0$ to $\infty$ does not affect the exponential character.

In this way it may be shown that the resulting forces directed perpendicular

---

1) Cf. e.g. TITCHMARSH [ref. 16, p. 177-178].

to the $x$-axis as well as the resulting moments with vectors that are perpendicular to the $x$-axis originating from the corrective load in the region $x \geqslant x_0$ tend to zero exponentially if $x_0$ increases. They will as a consequence cause stresses in the neighbourhood of the hole that are negligibly small.

A similar result is obtained for the loads in the region $x \leqslant x_0$ where $x_0$ is negative. In this case the integration constants $\tilde{A}_n$ appear in the expressions instead of the constants $\tilde{B}_n$. The loads in the regions for which $|x|$ is small and $|y|$ is large need not be considered since in these regions $\Psi$ decays exponentially.

We must finally verify the assumption made that the corrective load as a whole has no resultant force. In the doubly skew-symmetric case (cf. Chapter 4) there is indeed no such resultant force in virtue of the absence of constant terms in the Fourier series. In the doubly symmetric case such a resultant is not excluded a priori. But at closer inspection it appears that there are no resultant forces in $x$- and $y$-direction in view of the symmetry. Only a resultant force in the direction of the normal to the shell surface in the origin is still possible. We may determine it by investigating the resultant force of the stresses along a contour at infinity enclosing the hole. If this resultant force is zero we know that the normal resultant of the corrective load, if it exists, is cancelled by the boundary stresses at the edge $\bar{r} = a$.

A part of a contour surrounding the hole has been given by Fig. 3.3.1. The forces $Da\,\mathrm{d}s$ and $p_y a\,\mathrm{d}s$ contribute to the resultant force in normal direction. They are given by (cf. (3.3.1)).

$$\left.\begin{aligned} Da\,\mathrm{d}s &= d_y a\,\mathrm{d}x - d_x a\,\mathrm{d}y \\ p_y a\,\mathrm{d}s &= n_y a\,\mathrm{d}x - n_{xy} a\,\mathrm{d}y \end{aligned}\right\} \quad \ldots\ldots\ldots\ldots \quad (6.2.14)$$

For the stress resultants in the right-hand sides we must now use the expressions of FLÜGGE (loc. cit.). As for the transverse shear forces we may use the equations (2.1.6) and (2.1.8), in the latter formulae, however, retaining the underlined terms. This leads to

$$\left.\begin{aligned} Da\,\mathrm{d}s = {} & \frac{E\delta^4}{\{12(1-\nu^2)\}^{3/2}a^2}\,\mathrm{Im}\left\{\frac{\partial}{\partial y}\Delta\Psi\,\mathrm{d}x - \frac{\partial}{\partial x}\Delta\Psi\,\mathrm{d}y + \right. \\ & \left. + \frac{a^2}{R^2}\left[\frac{\partial\Psi}{\partial y}\mathrm{d}x + \frac{3-\nu}{2}\frac{\partial\Psi}{\partial x}\mathrm{d}y\right]\right\} + \\ & - \frac{E\delta^5(1-\nu)}{2\{12(1-\nu^2)\}^2a^2R}\,\mathrm{Re}\left\{3\frac{\partial^3\Psi}{\partial x^3}\mathrm{d}y + 2(2+\nu)\frac{\partial^3\Psi}{\partial x^2\partial y}\mathrm{d}x + \right. \\ & \left. + 3(2+\nu)\frac{\partial^3\Psi}{\partial x\partial y^2}\mathrm{d}y + 2\frac{\partial^3\Psi}{\partial y^3}\mathrm{d}x\right\} \end{aligned}\right\} \quad (6.2.15)$$

In order to express $p_y a\,\mathrm{d}s$ we do not use (2.2.5) but the more accurate expressions (corresponding with FLÜGGE's expressions)

$$
\left.\begin{aligned}
n_y &= \frac{E\delta^3}{12(1-\nu^2)a^2}\,\mathrm{Re}\,\frac{\partial^2\Psi}{\partial x^2} - \frac{E\delta^3}{12(1-\nu^2)R^3}\left\{w + \frac{R^2}{a^2}\,\frac{\partial^2 w}{\partial y^2}\right\} \\
n_{xy} &= -\frac{E\delta^3}{12(1-\nu^2)a^2}\,\mathrm{Re}\,\frac{\partial^2\Psi}{\partial x\partial y} + \frac{E\delta^3}{12(1-\nu^2)R^3}\left\{\frac{1-\nu}{2}\left(\frac{R}{a}\,\frac{\partial\bar{\eta}}{\partial x} + \frac{R^2}{a^2}\,\frac{\partial^2 w}{\partial x\partial y}\right)\right\}
\end{aligned}\right\} \quad (6.2.16)
$$

Substituting in (6.2.14) we obtain

$$
\left.\begin{aligned}
p_y a\,\mathrm{d}s = {} & \frac{E\delta^3}{12(1-\nu^2)a}\,\mathrm{Re}\left\{\frac{\partial^2\Psi}{\partial x^2}\,\mathrm{d}x + \frac{\partial^2\Psi}{\partial x\partial y}\,\mathrm{d}y + \right. \\
& \left. + \frac{\delta^2}{24(1+\nu)R^2}\left[\mp 2\mu\sqrt{i}\,\frac{\partial\Psi}{\partial y} + (1+\nu)\,\frac{\partial^2\Psi}{\partial x\partial y}\right]\mathrm{d}y\right\} + \\
& - \frac{E\delta^4}{\{12(1-\nu^2)\}^{3/2}aR}\,\mathrm{Im}\left\{\left(\frac{\partial^2\Psi}{\partial y^2} + \frac{a^2}{R^2}\,\Psi\right)\mathrm{d}x + \frac{\partial^2\Psi}{\partial x\partial y}\,\mathrm{d}y\right\}
\end{aligned}\right\} \quad (6.2.17)
$$

Here again the upper sign must be used if $\Psi$ is a solution of (3.1.2), the lower sign if it is a solution of (3.1.3).

The resultant force $F_r$ in the direction of the normal in the origin is equal to

$$
F_r = a\int_c \left\{p_y \sin\left(\frac{ay}{R}\right) - D\cos\left(\frac{ay}{R}\right)\right\}\mathrm{d}s \quad \ldots\ldots\ldots\ldots \quad (6.2.18)
$$

where the integral is taken along a closed contour at infinity surrounding the

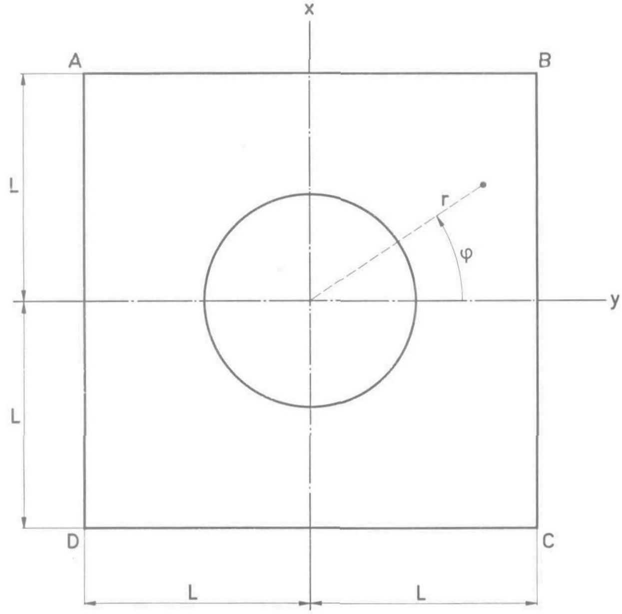


Fig. 6.2.2 Square contour in the developed shell surface

hole. We choose a contour that is a square with sides $2L$ in the developed shell surface (Fig. 6.2.2). If $L$ is large, it is immediately clear that the sides BC and DA do not contribute since the function $\Psi$ and its derivatives decay exponentially if $y$ tends to infinity. Although the behaviour of $\Psi$ is not exponential if $x$ tends to infinity and $y$ is kept constant it may be proved that the stress resultants along the sides AB and CD have a resultant force in normal direction that tends to zero exponentially. This may be shown in a way analogous to the way in which we established that the resultant of the corrective load on a strip of width d$x$ decays exponentially. And this fact finally justifies our assumption, that the corrective load has no resultant force.

## 6.3 Inaccuracy of spiral shell model

The value of the function $\Psi$ along the generators $\vartheta = \pm \pi$ decays exponentially, with increasing value of $R/a$, as long as $O\{|x|\} < O\{\mu\pi^2 R^2/a^2\}$, as is clear from the previous section. If $|x|$ is larger, the order of magnitude of $\Psi$ is given by

$$\Psi = O\{\Psi_v/\sqrt{\mu r}\} = O\{\Psi_v a/\mu R\} \quad \ldots \quad (6.3.1)$$

where $\Psi_v$ denotes the order of magnitude of $\Psi$ in the vicinity of the hole. In this case we have furthermore

$$\left.\begin{aligned} &1 - \sin\varphi \leqslant O\{a^2/\mu^2 R^2\} \\ &\cos\varphi \leqslant O\{a/\mu R\} \end{aligned}\right\} \quad \ldots \quad (6.3.2)$$

So from (6.2.7) and (6.2.8) we may conclude that differentiation in an arbitrary direction means lowering of the order of magnitude by at least a factor $a/R$ (in the region for which $O\{|x|\} \geqslant O\{\mu\pi^2 R^2/a^2\}$).

The closing of the shell along the generators $\vartheta = \pm \pi$, mentioned in Section 6.1, consists in removing the transverse shear forces $d_y$ and the membrane shear forces $n_{yx}$ along that generator, together with the displacements $\bar{\eta}$ and the rotations $\partial w/\partial \bar{y}$. This requires additional bending moments $m_y$ and direct stress resultants $n_y$ along the generators $\vartheta = \pm \pi$. It is evident that the part of the generator where $\Psi$ tends to zero exponentially if $R/a$ tends to infinity does not cause *essential* errors. We can restrict our investigation to the closing of that part of the generator for which $|x|$ is large. The stresses in the shell caused thereby will be compared with the order of magnitude $\sigma$ of the stresses calculated previously. As follows from the preceding section we have

$$\sigma = O\left\{\frac{E\delta^2}{a^2}\,\mu^2\Psi_v\right\} \quad \ldots \quad (6.3.3)$$

From (2.2.7) and (6.3.1) follows

$$d_y \leqslant O\left\{\frac{E\delta^4}{a^3}\,\frac{a^4\Psi_v}{\mu R^4}\right\} \quad \text{(along the generators } \vartheta = \pm \pi) \quad \ldots \quad (6.3.4)$$

These forces introduce bending stresses that are of order of magnitude $O\{E\delta^2 a\Psi_v/\mu R^3\}$, or, comparing them with the stresses calculated, of order $O\{a^3\sigma/\mu^3 R^3\}$. They cause additional tangential displacements $\bar{\eta}$ that are of order $O\{\delta a\Psi_v/R\}$ and rotations $\partial w/\partial\bar{y}$ that are of order $O\{\delta a\Psi_v/R^2\}$. These additional displacement quantities are of the same order of magnitude as those already present. This will be clear from (6.3.1) and, as far as $\bar{\eta}$ is concerned, from Section 5.1, and, as far as $\partial w/\partial\bar{y}$ is concerned, from (4.2.15). Their suppression requires stresses of the same order $O\{a^3\sigma/\mu^3 R^3\}$.

We must finally remove the load $n_{yx}$. From (6.3.1) and (2.2.5) follows

$$n_{yx} \leqslant O\{E\delta^3 a\Psi_v/\mu R^3\} \quad \text{(along the generators } \vartheta = \pm\,\pi) \quad . \qquad (6.3.5)$$

Such shear loads along a straight edge produce membrane and bending stresses that decay exponentially at large distance from the edge [1]). So the removal of the stress resultants (6.3.5) introduces stresses in the vicinity of the hole that tend to zero exponentially if $a/R$ tends to zero, while $\mu$ is held constant. If $a/R$ is held constant but $\mu$ increases (so the shell is made thinner) the distance of the hole to the edge $\vartheta = \pi$ (or $\vartheta = -\pi$) remains unaltered. The bending moments resulting from the edge load (6.3.5) are zero at the edge, reach a maximum, and then decay exponentially. The maximum, however, may be reached in the vicinity of the hole. Its magnitude may be estimated from equation (60), p. 256, of FLÜGGE's treatise [2]). We find after some computation that it is of order $O\{a^2\sigma/\mu R^2\}$. If the load $-n_{yx}$ is applied to the edge there will again be produced displacements $\bar{\eta}$ and rotations $\partial w/\partial\bar{y}$. Their removal requires stresses that are of the same order of magnitude, $O\{a^2\sigma/\mu R^2\}$.

Hence we have established the result that the order of magnitude of the stresses in the neighbourhood of the hole caused by the closing of the shell along the generators $\vartheta = \pm\,\pi$ is $a^2\sigma/\mu R^2$. The error introduced for a given value of $a/R$ apparently becomes small if $\mu$ is large. From the Figures 4.3.3 and 7.3.1 . . . 2 it follows indeed that for large values of $\mu$ the disturbance in the stress distribution by the presence of the hole is concentrated in a smaller region than for small values of $\mu$. It may be conjectured after the results of this section (and this prediction seems plausible) that in a shell with a fixed value $a/R$ and a thickness tending to zero the presence of the hole causes large bending stresses in a narrow zone along the edge, and a strip along the $x$-axis of width comparable with the diameter of the hole.

[1]) Cf. FLÜGGE [ref. 2, Chapter 5.4.3].
[2]) In the right-hand side of this equation a factor $\lambda$ is missing.

# CHAPTER 7

# EXPERIMENTAL RESULTS

## 7.1 Introduction

Since the numerical results obtained are of an approximative character for reasons outlined in the previous chapter, it appeared desirable to test the reliability of the analysis with experiments.

Experimental results available are those of HOUGHTON and ROTHWELL [ref. 3]. They investigated among others the stress concentration around circular holes in cylindrical tubes made of araldite, applying photoelastic methods. In the case of axial tension no influence of the curvature was found. In the case of torsion the influence found was two third of that predicted by the present theoretical results. It was verified that the position of the maximum stress changes with increase in hole diameter. HOUGHTON and ROTHWELL made also experiments bearing on the case of axial tension, on aluminium curved panels, making use of electric resistance strain gauges. These experiments yielded the results, shown in Table 7.1.1 (taken from a graph, viz. fig. 12 of the paper mentioned).

Table 7.1.1

| $\mu$ | Stress concentration factor | |
|---|---|---|
| | HOUGHTON and ROTHWELL (experimental) | Present analysis ($\nu = 0.3$) |
| 1 | 3.03 | 3.66 |
| 2 | 3.46 | 4.89 |

The large discrepancy between the theoretical values and these test results seems to be due to the fact that the curved panels were provided with special end plates, which were designed to minimize bending effects. Of course bending of the panel as a whole had to be avoided, but the stiff end plates may also have suppressed secondary bending effects originating from the presence of the hole. These effects, however, are essential and are closely related to the influence of the curvature upon the stress concentration factor.

In order to obtain some more reliable experimental data, careful tests bearing on the cases axial tension and torsion of a circular cylindrical tube weakened by a circular hole have been carried out in the laboratory of engineering mechanics of the Technological University of Delft. Several values of the parameter $\mu$ have been dealt with successively by enlarging the hole each time after the completion of an experiment both on axial tension and torsion. Since the hole was machined by a boring machine the boundary was not exactly a circle in the *developed* shell surface. For small values of the ratio $a/R$ the deviation has obviously been small.

The scope of the experimental investigation has been a verification of the analysis. There is not the pretention of a complete experimental stress analysis. At some points of the tube the direct membrane stresses and the bending stresses have been determined, and compared with the corresponding computed stresses. In view of the general agreement within test accuracy the analysis may be assumed to be reliable.

## 7.2 Description of test-arrangement

The test-piece (Fig. 7.2.1) was a tube made of mild steel ($E = 2{,}100{,}000$ kgf/cm$^2$, $\nu = 0.28$) with the following principal dimensions.

Radius of middle surface, $R = 25$ cm.
Wall thickness, $\delta = 0.48$ cm.
Length between front plates, $l = 180$ cm.

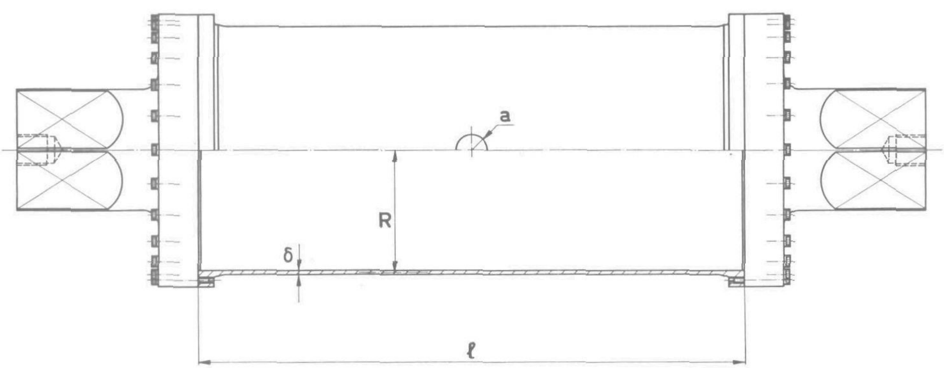


Fig. 7.2.1 The test-piece

The following hole radii have been dealt with consecutively [1]:

$a = 1$ cm (corresponding to $\mu = 0.263$)
$a = 2$ cm (corresponding to $\mu = 0.526$)
$a = 2.85$ cm (corresponding to $\mu = 0.75$)
$a = 3.8$ cm (corresponding to $\mu = 1$)

[1]) After the completion of this thesis the experiments are being continued for larger values of the hole radius, but the results obtained so far are adequate for comparison between theoretical and experimental results.

Each time a number of electric resistance strain gauges have been attached both to the rim of the hole in order to determine the membrane stresses $\sigma_{m\varphi}$ at $r = 1$ ($\bar{r} = a$) and on the inner and outer wall of the tube outside the hole in order to measure strains at larger values of $r$. As an example Fig. 7.2.2 shows the places (on the developed shell surface) where strain gauges have been applied in the case $\mu = 1$. The strain gauges along the lines $\varphi = 0°$, $45°$, $90°$ and $112°30'$ are directed radially, in order to measure the strains in radial direction, $\varepsilon_r$. Along the lines $\varphi = 180°$, $225°$, $270°$ and $292°30'$ we measured the strains in $\varphi$-direction, $\varepsilon_\varphi$.

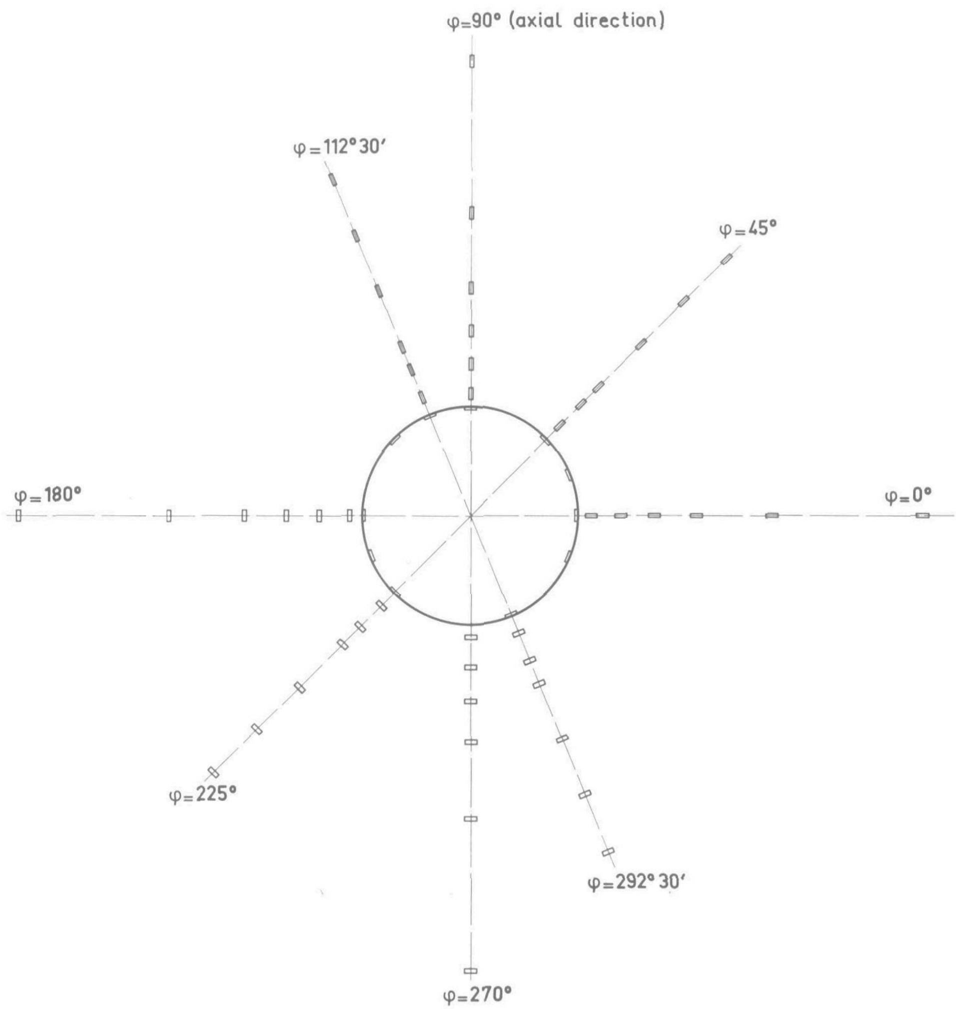


Fig. 7.2.2 Strain gauges on developed shell surface in the case $\mu = 1$

Along each of these lines strain gauges have been attached at several distances $\bar{r}$ from the hole centre. It may be assumed that in the doubly symmetric case of loading in axial tension as well as in the doubly skew-symmetric case of loading in torsion, points that are opposite with respect to the hole centre are in the same state of stress. This is the case for example for the points $\bar{r} = 7.5$ cm, $\varphi = 0°$ and $\bar{r} = 7.5$ cm, $\varphi = 180°$. The two radial strains $\varepsilon_r$ at the inside and at the outside at $\bar{r} = 7.5$ cm, $\varphi = 0°$ together with the two tangential strains $\varepsilon_\varphi$ at $\bar{r} = 7.5$ cm, $\varphi = 180°$ yield after a simple computation, taking into account the lateral contraction, the membrane stress resultants $n_r$ and $n_\varphi$, and the bending moments $m_r$ and $m_\varphi$. In this way the direct membrane stresses and bending stresses along the lines indicated in Fig. 7.2.2 have been determined.

In the case of torsion only the lines $\varphi = 45°$ (and $225°$) and $112°30'$ (and $292°30'$) have been investigated, as the lines $\varphi = 0°$ and $\varphi = 90°$ are lines of zero strains $\varepsilon_r$ and $\varepsilon_\varphi$ in view of the symmetry. In the case of axial tension the lines $\varphi = 0°$ (and $180°$), $\varphi = 45°$ (and $225°$) and $\varphi = 90°$ (and $270°$) have been investigated.

In the case of torsion the twisting moment was applied with the aid of the rectangular extremities (Fig. 7.2.1), part of the front plates of the tube. In the case of axial tension the tube was suspended horizontally and stretched axially. The load was applied through two slender bars made of high alloyed steel, in order to avoid bending of the tube as a whole due to a possible misalignment

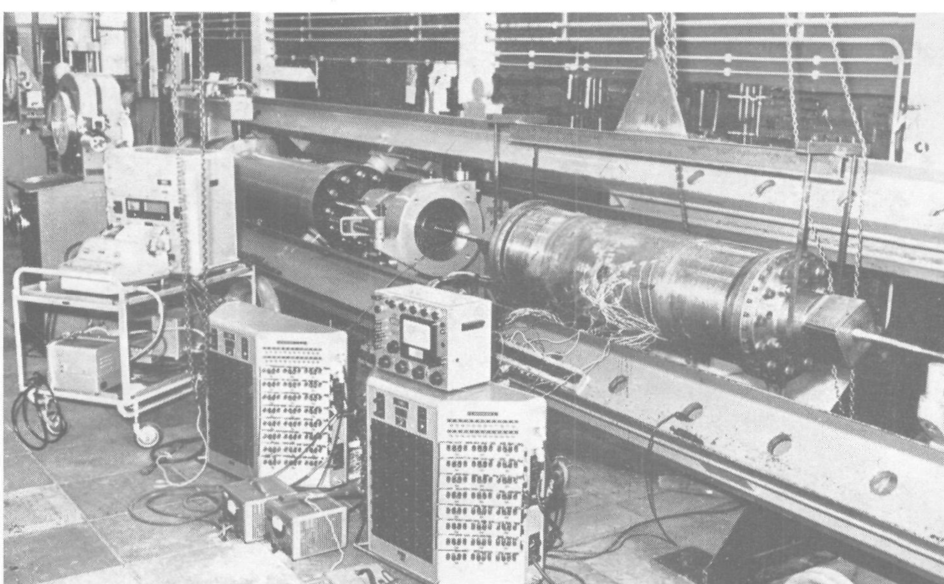

Fig. 7.2.3 Test-arrangement in the case of axial tension

of the wedge grips. Fig. 7.2.3 shows the arrangement in this case. On this photograph also one of the rectangular extremities by means of which the torsional moment is applied is clearly visible. The magnitude of the tensile force was measured by strain gauges attached to one of the slender bars, which has been calibrated.

After applying a prescribed load the change of the electric resistance of each strain gauge was measured consecutively and printed by a typewriter and at the same time punched by a 5-channel tape puncher. The punched tape could then be fed into an electronic digital computer in order to calculate the membrane and bending stresses following the method indicated above. Corrections for the transverse sensitivity of the strain gauges have been taken into account.

### 7.3 Test results and discussion

We shall in this section give the results obtained in the cases $\mu = 0.75$ and $\mu = 1$. For smaller values of $\mu$ there is only a small deviation from the flat plate solution since the stresses due to the curvature are initially proportional to $\mu^2$. In order to compare the results with the results predicted by the theory developed we calculated the stress distribution in the shell, following the method described in Section 4.3 for axial tension and in Section 4.5 for torsion. In the Figures 7.3.1. . . . 4, which may be compared with the Figures 4.3.3 and 4.5.3, the distribution of membrane and bending stresses, both in $\varphi$- and $r$-direction along the lines where the strain gauges have been attached (cf. Section 7.2) is shown. In these graphs the experimental values are indicated by dots. These values are in general *mean values* of the results of a number of experiments carried out on consecutive days in order to be influenced as little as possible by disturbing circumstances, such as sudden changes in temperature.

At each test a load (tension or torsion) was applied and enlarged stepwise after measuring the strains. After reaching the maximum admissible load it was reduced again stepwise. In the case of torsion both positive and negative load cycli were performed. In the case of tension, for practical reasons, only tensile forces were applied as compressive forces would have required a modified test-equipment. At each step the strains were measured, and from these data the membrane and bending stresses per unit load increase were computed.

The agreement between theoretical and experimental results is surprisingly good. Apart from a few points where relatively large deviations occur, which are obviously due to incidental disturbances and will be discussed below, all deviations are within test accuracy. An error of 1–1.5% of the measured strains must be taken into account because the gauge factor of the strain gauges is known only with that accuracy. An error of about 0.25% is due to the fact that the transverse sensitivity of the strain gauges is not known accurately.

An error of about 0.5% of *the maximum strain measured* is due to the inaccuracy of the test apparatus, mainly in view of round off errors. The magnitude of the load was known very accurately. Finally, errors were introduced by the fact that the wall thickness was not exactly constant. In a circular region of radius 18 cm, concentric with the hole, it varied from 0.476 cm to 0.484 cm.

We shall have a closer look at some results that show obvious errors.

*In the case of axial tension*, $\mu = 0.75$ (cf. Fig. 7.3.1), we measured at $\varphi = 0°$ (curve *a*) and $r = 1.23$ a bending stress $\sigma_{b\varphi}$ of magnitude $-0.42p/\delta$ whereas the theoretical value is $-0.31p/\delta$. In order to obtain this experimental result we had to subtract two strains at the inner and the outer wall that are large, the membrane stress $\sigma_{m\varphi}$ at that point being about $2.35p/\delta$. A maximum error in each of these strains may introduce an error of $0.1p/\delta$ in the bending stress. Because moreover on the same theoretical curve four other experimental points have been found very accurately it is evident that the experimental value at $r = 1.23$ cannot be trusted.

The experimentally determined membrane stresses $\sigma_{mr}$ at $\varphi = 0°$ and $r = 1.23$ and $r = 1.40$ are both about $0.04p/\delta$ larger than the theoretical values. The theoretical curve reaches a maximum in the neighbourhood of these points and it may be remarked that this maximum value has been calculated very accurately. These errors must be blamed to the fact that the membrane stresses $\sigma_{m\varphi}$ are about five times as large and must be taken into account in view of lateral contraction and transverse sensitivity. Relatively small errors in the measured values of the tangential strains $\varepsilon_{\varphi}$ introduce errors in $\sigma_{mr}$ that are relatively large.

The bending stress $\sigma_{br}$ for $\varphi = 45°$ and $r = 1.82$ ($\bar{r} = 5.2$ cm) is $0.05p/\delta$ too large whereas $\sigma_{br}$ for $\varphi = 45°$ and $r = 2.11$ ($\bar{r} = 6$ cm) is $0.03p/\delta$ too small. It may again be conjectured that these errors are due to the large membrane stresses occurring at the same points. It is interesting to see what stresses are obtained from the same strain gauges in the case $\mu = 1$. Since the transition from $\mu = 0.75$ to $\mu = 1$ was obtained by enlarging the radius of the hole from 2.85 cm to 3.8 cm, the non-dimensional coordinates $r = 1.82$ and $r = 2.11$ in the case $\mu = 0.75$ became $r = 1.37$ and $r = 1.58$ (corresponding again to $\bar{r} = 5.2$ cm and $\bar{r} = 6$ cm respectively) in the case $\mu = 1$. In Fig. 7.3.2 it may be seen that the bending stresses obtained show the same deviations as in the case $\mu = 0.75$. Obviously these deviations must be attributed mainly to inaccurate gauge factors.

In the graphs bearing on *the case of loading in torsion* the largest deviation is the radial membrane stress $\sigma_{mr}$ measured at $\varphi = 45°$, $r = 1.12$ in the case $\mu = 0.75$ (Fig. 7.3.3). Obviously this error may again be blamed on the fact that the stress $\sigma_{m\varphi}$ in the same point is ten times as large.

In general we may conclude that the experiments support the analytical

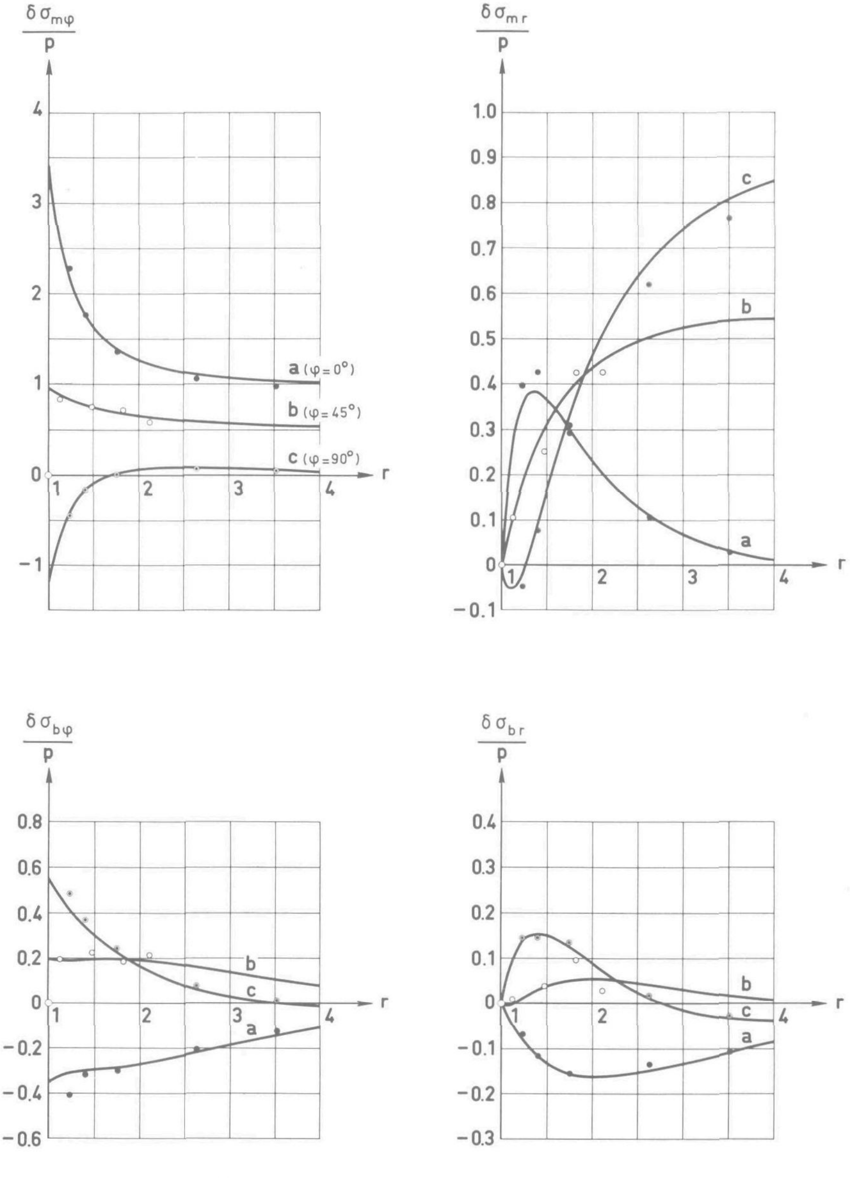


Fig. 7.3.1 Stresses in a tube in axial tension as a function of $r$ and experimental results

$$\left(\mu = \frac{\sqrt[4]{12(1-\nu^2)}}{2}\,\frac{a}{\sqrt{\delta R}} = 0.75\right)$$

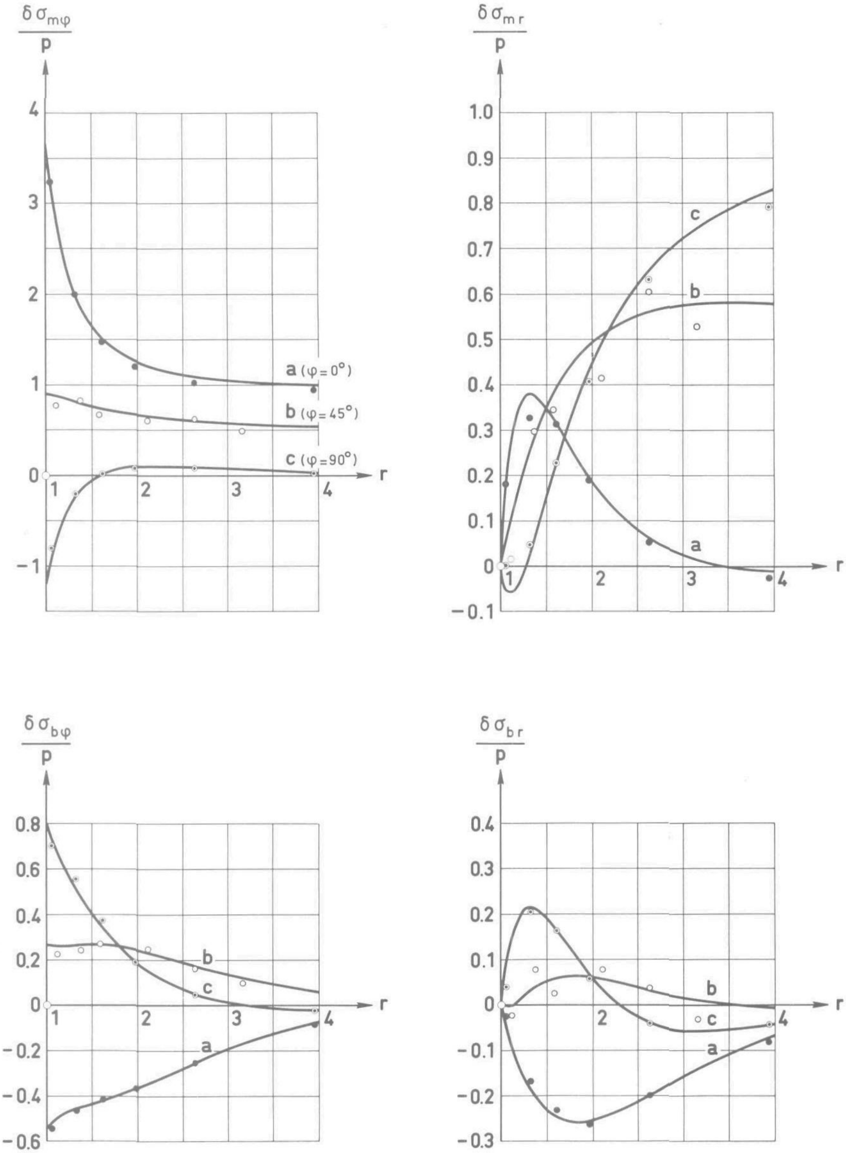


Fig. 7.3.2 Stresses in a tube in axial tension as a function of $r$ and experimental results

$$\left(\mu = \frac{\sqrt[4]{12(1-\nu^2)}}{2}\,\frac{a}{\sqrt{\delta R}} = 1\right)$$

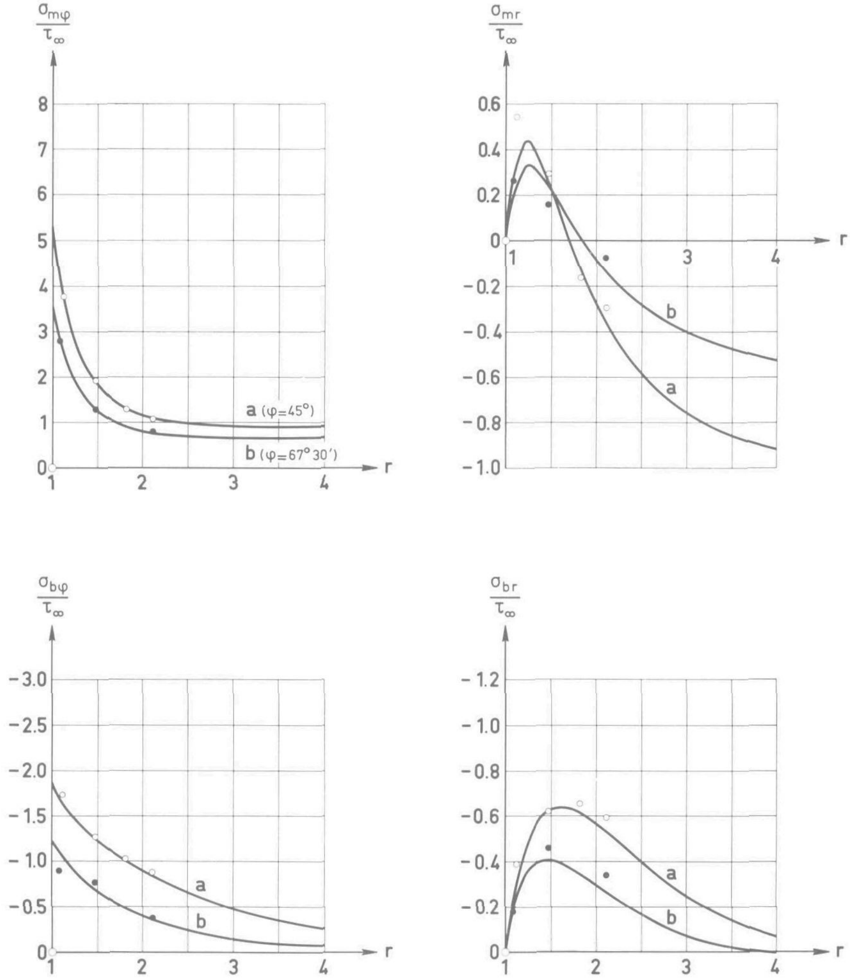


Fig. 7.3.3 Stresses in a tube in torsion as a function of $r$ and experimental results

$$\left(\mu = \frac{\sqrt[4]{12(1-\nu^2)}}{2} \frac{a}{\sqrt{\delta R}} = 0.75\right)$$

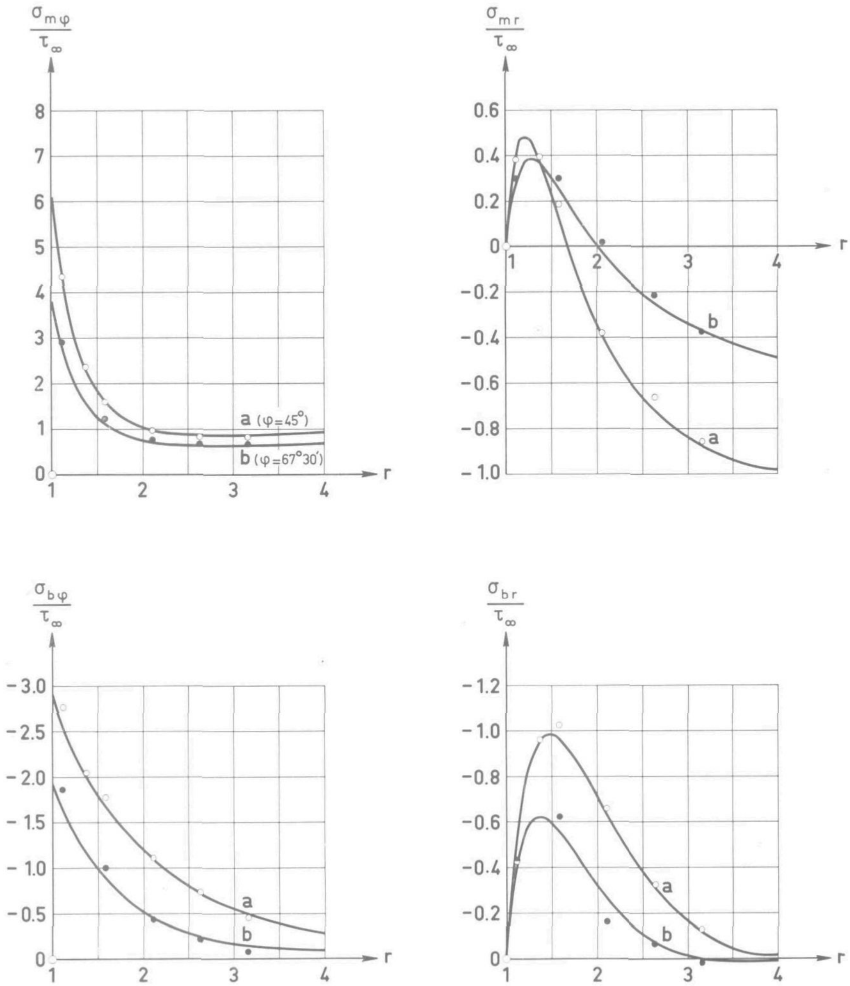


Fig. 7.3.4 Stresses in a tube in torsion as a function of $r$ and experimental results

$$\left(\mu = \frac{\sqrt[4]{12(1-\nu^2)}}{2} \frac{a}{\sqrt{\delta R}} = 1\right)$$

results. There is furthermore no indication whatsoever that in the case $\mu = 1$ the radius of the hole, which is then about one seventh of the radius of the cylinder, has already reached a value such as to make the analysis less accurate in view of the approximations studied in Chapter 6.

As explained in Section 7.2 we have also attempted to measure the membrane stress $\sigma_{m\varphi}$ at the hole boundary. The results obtained were not entirely satisfactory, probably due to the difficulty of placing the strain gauges exactly in the middle of the comparatively small wall thickness. This difficulty is more pronounced for smaller hole diameters. We shall therefore restrict our discussion to the case $\mu = 1$, $a = 3.8$ cm, for which the results are collected in Table 7.3.1. The strain gauge at $\varphi = 225°$ which in the case of torsion indicated a membrane stress of 5.70 times the shear stress at infinity has been replaced and the second strain gauge indicated a stress of 6.21 times the shear stress at infinity, as compared with a theoretical value 6.09. Since there is a bending stress of about $-3\tau_\infty$, the stress varies over the wall thickness from about $3\tau_\infty$ at the outside to about $9\tau_\infty$ at the inside. The difference in the results of these two strain gauges may therefore be due to a different location in the thickness direction of no more than 0.04 cm. Hence the deviations found are indeed likely to be due to small errors in the location of the filament of the strain gauges. In view of the fact that the width of the hole was only 7.6 cm and the wall thickness only 0.48 cm it is quite understandable that such errors have been made.

Table 7.3.1

| $\varphi$ | Axial tension, $\sigma/\sigma_\infty$ | | Torsion, $\sigma/\tau_\infty$ | |
|---|---|---|---|---|
| | experimental value | theoretical value | experimental value | theoretical value |
| 0° | 3.61 | 3.66 | −0.04 | 0 |
| 22°30′ | 2.62 | 2.78 | 4.90 | 4.83 |
| 45° | | | 6.08 | 6.09 |
| 90° | −1.27 | −1.20 | 0.05 | 0 |
| 112°30′ | | | −3.73 | −3.80 |
| 135° | 0.87 | 0.91 | −5.69 | −6.09 |
| 180° | 3.70 | 3.66 | 0.18 | 0 |
| 202°30′ | | | 5.02 | 4.83 |
| 225° | 0.67 | 0.91 | 5.70 / 6.21 | 6.09 |
| 292°30′ | −0.59 | −0.65 | −3.78 | −3.80 |
| 337°30′ | | | −5.02 | −4.83 |

The influence of the fact that the wall thickness was not exactly constant may also be estimated from this table. The values measured at $\varphi = 0°$, 90° and 180° must necessarily originate from this reason since at these points both the membrane and the bending stresses are zero in view of the symmetry. The largest stress (at $\varphi = 180°$) is almost 3% of the maximum stress present.

Taken as a whole, however, the results in Table 7.3.1 agree reasonably well with the analytical results. For example the theoretical prediction that the maximum stress in the case of torsion does not occur at $\varphi = 45°, 135°, 225°$ and $315°$ is fully confirmed by the experiment, and the computed value of the maximum stress is in fair agreement with the experimental values.

# REFERENCES


1. BIEZENO, C. B. und R. GRAMMEL, Technische Dynamik, 2. Auflage, Springer-Verlag, Berlin/Göttingen/Heidelberg (1953).
2. FLÜGGE, W., Stresses in shells, 2nd printing, Springer-Verlag, Berlin/Göttingen/Heidelberg (1962).
3. HOUGHTON, D. S. and A. ROTHWELL, The effect of the curvature on the stress concentrations around holes in shells, The College of Aeronautics, Cranfield, Report No. 156 (1962).
4. KIRSCH, G., Die Theorie der Elastizität und die Bedürfnisse der Festigkeitslehre, Z.V.D.I. **42** (1898), 797.
5. LUR'E, A. I., Statics of thin-walled elastic shells, State Publishing House of Technical and Theoretical Literature, Moscow/Leningrad, Chapter 4, Art. 9 (1947).
6. LUR'E, A. I., Concentration of stresses in the vicinity of an aperture in the surface of a circular cylinder, Prik. Mat. i. Mekh., **10** (1946), 397–406 (English transl. by N. Brunswick, New York University, Inst. of Math. Sc., (1960)).
7. MCLACHLAN, N. W., Bessel functions for engineers, 2nd ed., Oxford (1955).
8. MYINT, T., J. R. M. RADOK and MARIE WOLFSON, Numerical solution of shell intersection problems, Österreichisches Ingenieur-Archiv, XVI, Heft 3 (1962), 253–270.
9. VAN DER NEUT, A., *Bending at the oblique end-section of cylindrical shells*, Proc. I.U.T.A.M. Symposium on the theory of thin elastic shells, Delft, North-Holland Publ. Cy, Amsterdam (1959), 247–269.
10. NOVOZHILOV, V. V., The theory of thin shells, Groningen (1959).
11. PIROGOV, I. M., Stress concentrations in the region of a rigid ring on the surface of a circular cylinder (in Russian), Sb. statei Vsesoiuzn. Zaochn. politekhn. in-ta **16** (1957), 65–71.
12. PIROGOV, I. M., The stress distribution around a hole in a cylindrical shell under the influence of concentrated forces (in Russian), Izv. Ak. Nauk S.S.S.R., Otd. tekhn. n. mekhan. i mashinostr. (1959), 146–147.
13. REIDELBACH, W., Der Spannungszustand im Übergangsgebiet einer rechtwinkligen Rohrabzweigung, Ingenieur-Archiv XXX (1961), 293–316.
14. SHEVLIAKOV, JU. A. and F. S. ZIGEL', Torsion of a cylinder with a hole in the lateral surface (in Ukrainian), Dopovidi Akademii Nauk Ukrainsjkoi R.S.R. (1954), 41–44.
15. SHEVLIAKOV, JU. A. and F. S. ZIGEL', Stress concentration in a cylindrical shell with a circular hole in the lateral surface (in Ukrainian), Dopovidi Akademii Nauk Ukrainsjkoi R.S.R. (1955), 123–125.
16. TITCHMARSH, E. C., Introduction to the theory of Fourier integrals, 2nd ed., Oxford (1948).
17. WATSON, G. N., A treatise on the theory of Bessel functions, Cambridge (1952).
18. WITHUM, D., Die Kreiszylinderschale mit kreisförmigem Ausschnitt unter Schubbeanspruchung, Ingenieur-Archiv, XXVI (1958), 435–446.
19. YUAN, SHAO WEN, Thin cylindrical shells subjected to concentrated loads, Quarterly of Appl. Math., **4** (1946), 13–26.

# SAMENVATTING

Het onderwerp van deze dissertatie is de bepaling van de spanningen en de verplaatsingen in een dunwandige cirkelcilindrische buis, verzwakt door een gat dat in het ontwikkelde schaaloppervlak cirkelvormig is. De buis is onderworpen aan belastende krachten en er wordt uitgegaan van de veronderstelling dat de spanningen en verplaatsingen die ten gevolge van de belasting zouden optreden in het geval van een onverzwakte buis bekend zijn. De oplossing van het gestelde vraagstuk wordt verkregen door de gatrand spanningsvrij te maken en de daarbij optredende inwendige spanningen en verplaatsingen op te tellen bij de reeds bekende. Dit spanningsvrij maken van de gatrand geschiedt door een evenwichtsbelasting, en het is dit laatste vraagstuk dat in de dissertatie wordt behandeld.

De ontwikkelde theorie is in tweeërlei opzicht van een benaderend karakter. In de eerste plaats worden de vergelijkingen der flauw gekromde schalen er aan ten grondslag gelegd, en in de tweede plaats wordt de werkelijke cilinderschaal vervangen door een model in de vorm van een spiraalschaal, waarin de omtrekshoek zich uitstrekt van $-\infty$ tot $+\infty$. De laatste vereenvoudiging lijkt aanvaardbaar omdat kan worden verwacht dat de spanningen op grote afstand van het gat klein zullen zijn. Beide vereenvoudigingen beperken de geldigheid van de theorie tot waarden van de gatstraal die betrekkelijk klein zijn ten opzichte van de straal van de buis, bijvoorbeeld niet groter dan $^1/_4$.

Het eerst is dit probleem aangevat door LUR'E [lit. 5 en 6], die een oplossing geeft in de vorm van de eerste term van reeksen in een krommingsparameter $a^2/R\delta$ ($a$ = gatstraal, $R$ = straal van cilinderschaal, $\delta$ = wanddikte). Een nadeel van LUR'E's theorie is dat de resultaten alleen nauwkeurig zijn voor kleine waarden van deze parameter.

De thans ontwikkelde theorie heeft deze beperking niet. In navolging van LUR'E wordt het probleem herleid tot de bepaling van een complexe functie $\Psi$, waarvan het reële deel een spanningsfunctie voor de membraanspanningen en het imaginaire deel de normale verplaatsing voorstelt. Deze functie $\Psi$ voldoet aan een differentiaalvergelijking van de vierde orde waarvan de oplossingen worden gezocht in de vorm van een fourierontwikkeling in de hoek $\varphi$ van een poolcoördinatensysteem $(r, \varphi)$ in het ontwikkelde schaaloppervlak. De oorsprong van dit coördinatensysteem valt samen met het middelpunt van het gat. De coëfficiënten van de fourierreeksen zijn functies van de radiale coördinaat $r$. Het blijkt mogelijk te zijn op in principe eenvoudige wijze te voldoen aan dynamische en geometrische randvoorwaarden.

Enkele theoretische aspecten die niet aan de orde zijn gekomen in tot dusverre verschenen publikaties worden mede behandeld, te weten:

De volledigheid van de oplossing (hoofdstuk 3.2).

De eventuele mogelijkheid, een gatrandbelasting te behandelen, die een resulterende kracht of een resulterend koppel heeft. Het blijkt evenwel, dat de theorie alleen toestaat een gatrandbelasting te behandelen, die een evenwichtssysteem vormt. Hierbij dient echter een uitzondering vermeld te worden. Het blijkt namelijk, dat één component van de momentvector (de component die raakt aan de cilindermantel en loodrecht staat op de as van de cilinder) niet identiek nul is (hoofdstuk 3.3).

De ondubbelzinnigheid van de verplaatsingen in het tweevoudig samenhangend gebied, gevormd door de spiraalschaal (hoofdstuk 3.4).

De onnauwkeurigheid veroorzaakt door het benaderend karakter van de theorie (hoofdstuk 6).

Als voorbeelden ter illustratie worden enige belastingsgevallen behandeld, en voor een aantal waarden van de geometrische parameters numeriek uitgewerkt. Zij betreffen de gevallen belasting door trekkrachten in axiale richting en door wringende momenten uitgeoefend op de verzwakte buis, welke behandeld worden in hoofdstuk 4, en belasting door inwendige overdruk van een buis waaraan een dwarspijp is bevestigd, behandeld in hoofdstuk 5. Het laatste geval is een voorbeeld van een probleem met gemengde randvoorwaarden. Voor de behandeling van dergelijke problemen wordt gebruik gemaakt van invloedsgetallen voor geschikt gekozen eenheidsbelastingen langs de gatrand. Voor een groot aantal waarden van de krommingsparameter zijn deze invloedsgetallen bepaald, en voor de waarde, welke betrekking heeft op het behandelde numerieke voorbeeld, in dit proefschrift vermeld (tabel 5.2.1). In alle behandelde voorbeelden wordt uitvoerig stilgestaan bij de invloed welke de kromming blijkt te hebben op de numerieke waarde der spanningsconcentraties. In vele gevallen is deze invloed zeer groot.

Bij gebrek aan meer gegevens zijn LUR'E's resultaten wel eens toegepast voor grote waarden van de krommingsparameter. De daarbij gevonden spanningsconcentratie, bijvoorbeeld in het geval van axiale trek, blijken nu aanzienlijk te groot te zijn.

Mede op grond van de door HOUGHTON naar aanleiding van zijn proefresultaten uitgesproken twijfel aan een merkbare invloed van de kromming zijn in het laboratorium voor technische mechanica spanningsmetingen verricht aan buizen verzwakt door cirkelvormige gaten, en belast door axiale trekkrachten en door wringende momenten. De resultaten worden in hoofdstuk 7 besproken en ondersteunen de theoretische voorspellingen ten volle.

# LEVENSBERICHT

De schrijver van dit proefschrift werd op 16 november 1927 geboren te Veldhuizen. Na in 1947 aan het Christelijk Gymnasium te Utrecht het diploma $\beta$ te hebben behaald, ving hij de studie voor werktuigkundig ingenieur aan de Technische Hogeschool te Delft aan. Hij was van januari 1951 tot september 1952 als student-assistent verbonden aan het laboratorium voor technische mechanica en van september 1952 tot september 1953 als leraar aan de Academie Minerva te Groningen. In juli 1953 behaalde hij het diploma werktuigkundig ingenieur. Sinds september 1953 is hij in verschillende functies, eerst als grafostatica-assistent en vanaf september 1956 als instructeur, verbonden aan het laboratorium voor technische mechanica te Delft. Vanaf september 1963 wordt door hem een leeropdracht vervuld voor het geven van de colleges Toegepaste Mechanica ten behoeve van de afdelingen der elektrotechniek en der mijnbouwkunde en de tussenafdeling der metaalkunde van de Technische Hogeschool te Delft.

# STELLINGEN

1

De door HOUGHTON gedane uitspraak, dat voor waarden van de in deze dissertatie door formule (2.2.3) gedefinieerde krommingsparameter $\mu$, kleiner dan 1, de theorie voor vlakke platen toereikend zou zijn voor het bepalen van de spanningstoestand in op axiale trek belaste, doorboorde cilinderschalen, moet worden verworpen.

HOUGHTON, D. S., Journal of the Royal Aeronautical Society, **65** (1961), 201–204.

2

Sommige numerieke voorbeelden in de literatuur betreffende spanningsconcentraties rond gaten in schalen zijn gebaseerd op de theorie der flauw gekromde schalen, doch hebben betrekking op constructies waarvoor de geldigheid van deze theorie twijfelachtig is.

REIDELBACH, W., Ingenieur - Archiv. XXX (1961) 293–316.
VAINBERG, D. V. and A. L. SINIAVSKII, Problems of Continuum Mechanics, Philadelphia (1961), 570–581.

3

Een voor de hand liggende methode om langs iteratieve weg de oplossing van de in dit proefschrift voorkomende vergelijkingen voor de flauw gekromde schalen (2.1.5) en (2.1.10) te bepalen, bijvoorbeeld voor het behandelde geval van trek in axiale richting, is de volgende. De spanningsfunctie $\Phi$, die geldt voor het geval van een vlakke plaat, wordt gesubstitueerd in het rechterlid van (2.1.10). De oplossing van deze vergelijking, een eerste benadering van $w$, wordt op haar beurt gesubstitueerd in het rechterlid van (2.1.5), hetgeen een tweede benadering van $\Phi$ oplevert, waarna het proces naar believen herhaald wordt. Deze methode is onbruikbaar, daar het proces niet convergeert.

4

De vergelijkingen, gebaseerd op het principe van virtuele verplaatsingen door KOLLBRUNNER en MEISTER ten grondslag gelegd aan het probleem van het uitknikken van in hun vlak belaste platen, zijn onjuist ten gevolge van een verkeerde formulering van het variatieprobleem.

KOLLBRUNNER, C. F. und M. MEISTER, Ausbeulen, Springer-Verlag (1958).

5

Bij het bereiken van de kniklast van Euler van een in zijn uiteinden scharnierend ondersteunde op druk belaste balk is het evenwicht in het kritieke punt, zoals bekend, nog stabiel. De kniklast wordt verhoogd door het aanbrengen van een lineaire verende bedding in de zin van Winkler, waarbij de beddingreactie per eenheid van booglengte evenredig is met de plaatselijke doorbuiging van de balk. Het evenwicht in het kritieke punt is dan echter meestal instabiel.

Lekkerkerker, J. G., Proc. Kon. Ned. Ak. v. Wet. Series B, **65** (1962), 190–197.

6

De door Capurso aanbevolen wijziging van de methode van Ritz ter bepaling van de doorbuiging van een plaat, welke daarop neerkomt dat van de aangenomen functies lineaire combinaties worden gevormd die orthogonaal zijn, levert geen vereenvoudiging op. De door de schrijver geuite bewering, dat een betere benadering wordt verkregen, is onjuist.

Capurso, Michele, Città di Siracusa, Celebr. Archimed. Sec. XX, 11–16 Aprile 1961, Vol. **3**, Simpos. Mecc. Mat. appl. 107–111 (1962).

7

De door Jacobs voor een bepaald vleugelprofiel berekende afstand tussen het dwarskrachtmiddelpunt van Trefftz en het dwarskrachtmiddelpunt dat gedefinieerd is met het nul zijn van de gemiddelde specifieke wringhoek, namelijk 8,3% van de lengte der koorde, is onjuist. Deze afstand bedraagt slechts 1,2% van de lengte der koorde.

Jacobs, J. A., Journal of the Royal Aeronautical Society, **57** (1953), 235–237.
Zie ook: Koiter, W. T., Journal of the Royal Aeronautical Society, **58** (1964), 64–65.

8

De proeven van Brown en Hall ter bepaling van insteekdiepten van balken met cirkelvormige doorsnede zijn weinig betrouwbaar. Een belangrijk bezwaar is, dat niet met zekerheid kan worden gezegd, dat parasitaire verplaatsingen, ten gevolge van de vervorming van de constructie waarin het proefstuk is bevestigd, de meetresultaten niet hebben beinvloed.

Brown, J. M. and A. S. Hall, Journal of Applied Mechanics, **29** (1962), 86–90.

9

Bij schepen met een niet achterin geplaatste hoofdmotor verdient het aanbeveling, het verhoogde niveau van de tanktop in de machinekamer over een afstand van enkele spanten onder de schroefastunnel te handhaven, teneinde een continue stijfheid van de ondersteunende constructie voor schroefas en motor te waarborgen.

10

De invloed van de vervorming door dwarskrachten op de trillingen van schepen wordt onvoldoende in rekening gebracht met de door PROHASKA aangegeven correctiefactor.

PROHASKA, C. W., Lodrette Skibssvingninger med to Knuder, København (1941).

PROHASKA, C. W., Bulletin de l'Association Technique Maritime et Aéronautique, **46** (1947), 171–215.

11

Het verdient aanbeveling, de schriftelijke eindexamenopgaven voor de basisvakken aan de Hogere Technische Scholen landelijk centraal te redigeren.